EFFECTIVENESS OF SEISMIC BEARINGS ON A TYPICAL ISOLATED TWO-COLUMN RC BRIDGE PIER LOCATED IN NORTH MISSISSIPPI

Hemant Raj Joshi
University of Mississippi

EFFECTIVENESS OF SEISMIC BEARINGS ON A TYPICAL ISOLATED TWO-COLUMN RC BRIDGE PIER LOCATED IN NORTH MISSISSIPPI

A Thesis

Presented for the Degree

Master of Science in Engineering Science with Emphasis in Civil Engineering

The University of Mississippi

Hemant Raj Joshi

May, 2021

ABSTRACT

The 2020 ASCE infrastructure report card has assigned a letter grade of D- for bridges in Mississippi based on poor to fair condition ratings with many approaching the end of their useful service lives. Bridges in northern Mississippi lie up to 100 miles from the New Madrid Fault and fall into the Region 3 Seismic Performance Category defined by AASHTO. The primary objective of this study is to evaluate the performance of commercially available bridge bearings on a common bridge pier type used in northern MS under the combined action of superstructure gravity and lateral seismic loads. The use of bearings as seismic isolation devices to limit the inelastic deformations in bridge substructures is a common practice in high seismic regions (Region 4) but their benefits in moderate ones (Region 3) have not been fully explored in MS. Analytical formulations under lateral load at the bearing levels are first used in the study to characterize modal characteristics and response of the bearing/pier subsystem idealized as a 2DOF oscillator. Effective linear properties of the bearing/pier system defined based on AASHTO provisions are used to determine expected overall behavior.

Non-linear pushover analysis is then performed of an existing two-column pier recently designed to satisfy AASHTO criteria. The pier is modeled as a frame using beam and link elements available in a commercial finite element software (SAP2000). The analysis is used to capture the plastic hinge formation sequence, damage limit states in potential hinge locations, and the overall frame response up to the formation of a collapse mechanism. Lastly, non-linear time history analysis is performed using the software to obtain lateral deck/pier displacement histories in the transverse direction. The effectiveness of two common isolation bearings

(laminated rubber and disc type) in isolating the pier from the deck motion and reducing the base shear is then demonstrated.

DEDICATION

This thesis is dedicated to my family.

ACKNOWLEDGEMENTS

I would like to thank my academic and thesis advisor Dr. Christopher Mullen for his continuous support, advice, and encouragement throughout the project in every possible way. I am grateful to my thesis committee members Dr. Ahmed Al Ostaz and Dr. Hakan Yasarer for their valuable suggestions and time. I am equally thankful to Dr. Yacoub Najjar, the Chairman of the Civil Engineering Department for the financial support throughout my Master's program and to the Mississippi Department of Transportation for providing design drawings used in the study as well as their expertise in a UM course I took on Bridge Engineering.. I pay my sincere gratitude to Mr. Pratap Bohara from Geology and Geological Department and Mrs. Swornima Singh Thakuri, who are also my roommates, for their assistance throughout the semester including this project. Finally, I extend my thanks to all my friends at Ole Miss and those unnamed individuals who helped me directly or indirectly in the accomplishment of my degree and this thesis.

TABLE OF CONTENTS

LIST OF FIGURES

LIST OF TABLES

CHAPTER I

INTRODUCTION

1.1.Background, Motivation, and Objectives

There has been an extensive study on bridge bearings; their performance as the load transferring mechanism and the seismic isolation devices. The early studies on bearings were experimental investigations leading to numerical analysis and finite element analysis (FEA) in recent years. The modern progress in computational power has enhanced the simulation-driven contemporary research on bridge bearings. The primary objective of this study is to simplify the simulation procedure to evaluate the performance of commercially used bridge bearings under the superstructure loads and the seismic loads. The results from the simplified model can be validated with an example from the literature. The simplified model not only expedites the simulation but also yields and checks the critical displacement-based parameters in the dead load and seismic load transfer mechanism from the superstructure to the substructure.

The field investigation after the 2011 Great East Japan Earthquake identified the damage of bearings as the causes of the most bridge failures, second only after the subsidence of backfill soil of abutments as the bridges were also hit by the Tsunami. The excessive movement of bearings and the breakage of side blocks of steel bearings were seen often in the damage scene. The advantage of the elastomeric bearing as compared to conventional steel bearings is due to its relatively greater cross-sectional area which supports the girder even after losing the lateral resisting capacity (Takahashi, 2012).

1.1.1. Seismic Vulnerability of Bridges in Mississippi

The infrastructure report card published by ASCE in 2020 has assigned a letter grade of D- for the bridges in Mississippi established on their poor to fair conditions; many of which are approaching the end of their life service. A strong risk of failure is accessed based on the deteriorated condition and reduced capacity. According to the Federal Highway Agency (FHWA) report, there are a total of 17,071 bridges in Mississippi in 2018. About 9% (1603) of these bridges are in poor condition and 28% (4757) of those are in fair conditions. (Black et al., 2021) The spatial map of all the major bridges in Mississippi is shown in *Figure 1*.

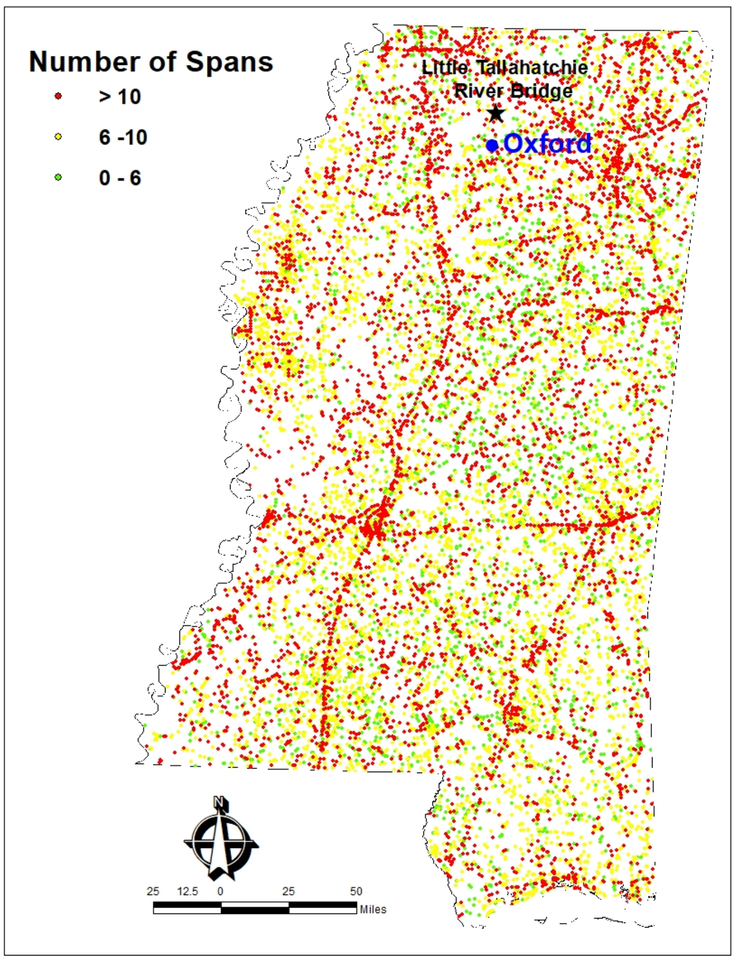

Figure 1: Major Bridges in Mississippi

The northern Mississippi is not more than 100 miles away from the New Madrid Fault Line. The New Madrid Seismic Zone is defined as Region 3 for the seismic loading and seismic design purpose by AASHTO. The AASHTO LRFD Bridge Design Specification recommends the earthquake ground motions that have a 7% probability of exceedance in 75 years at a period of 1.0-second(AASHTO, 2010). The USGS Seismic Hazard Map (2014) shown in *Figure 2* provides the color contour of the horizontal peak ground acceleration (PGA) values for 0.2- and 1.0-second periods with probabilities of excedence of 10% in 50 years and 2% in 50 years.

The use of the USGS Seismic Hazard Map is a relevant and conservative approach for design against Maximum Considered Earthquake (MCE_R) ground motions when compared to the ASSHTO recommendation. A simulated M7.7 earthquake using the software made available by the United States Geological Survey (USGS) that generates peak ground acceleration (PGA) value has been previously used for the study of "Seismic vulnerability of critical bridges in North Mississippi" (Mullen, 2011). The Little Tallahatchie River Bridge (Lat. 34°32′31" Long. 89°29′67") lies within the New Madrid Seismic Zone. Therefore the color contour map for the multi-state region defined around the New Madrid Seismic Zone for use in the state of emergency management plans has been used to interpolate PGA values. The time history function from the aforementioned study has been scaled using USGS guidelines and the Seismo Signal tool generates the time history function applicable at the site of Little Tallahatchie River Bridge. The Seismic Design Maps tool developed by the Structural Engineers Association of California (SEAOC) is first verified and utilized to obtain all the seismic design parameters including site factors and response coefficients based on the ASCE7-16 design standard.

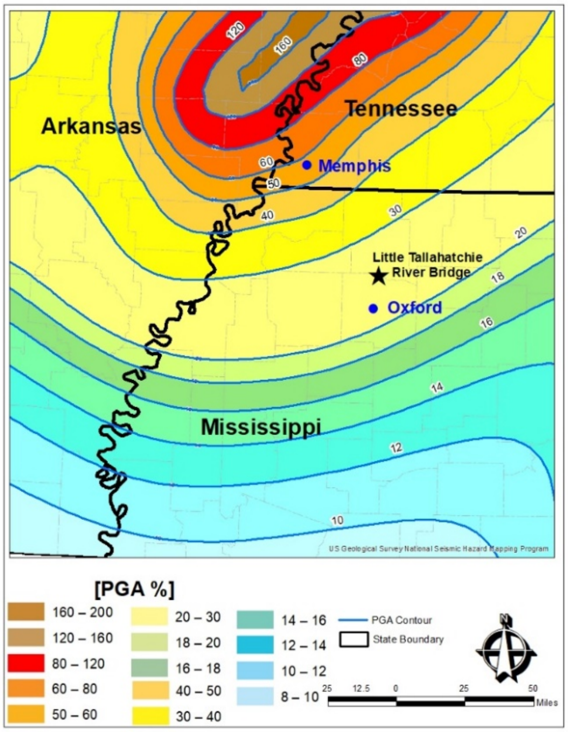

Figure 2: PGA (%g) contour map for North MS

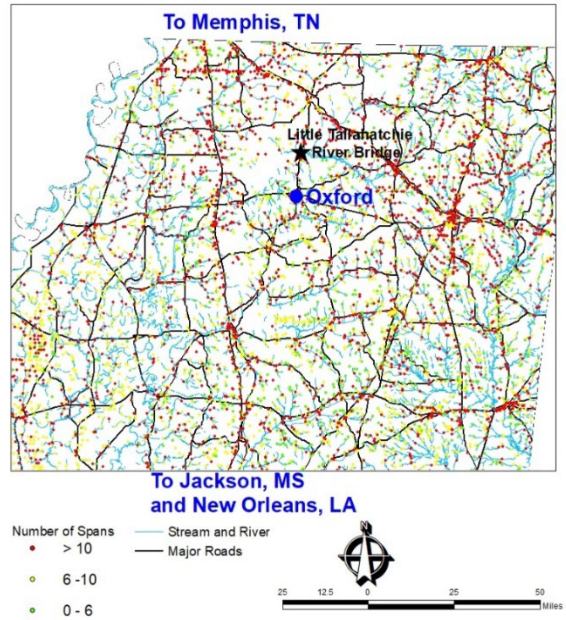

Figure 3: Major Roads and Bridges in North MS

1.2.Literature Review

Steel-concrete composite structures are widely used in a variety of structural systems, from buildings to bridges. A numerical model to simulate the non-linear behavior of composite structures under vertical load, and horizontal earthquake action uses the suitable material constitutive models. This experimentally and numerically validated model captures the interaction between the reinforcement steel and the concrete in circular CFST analogous to the circular concrete pier in bridges. (Qiang et al., 2018)

A parametric study emphasized the performance of bearing in a typically isolated bridge under seismic loading outlines a three-dimensional finite element model (FEM) where the piers are modeled by linear elastic frame elements with cracked effective stiffness properties. The effective cracked stiffness is 50% of the gross stiffness and it is described in the model by reducing the second moment of area of the transverse pier section. (Tubaldi et al., 2016)

An equivalent SDOF system for the pier to evaluate the structural behavior can be modeled as a cantilever having a distributed mass along with the height and lumped mass, equivalent to the mass of the pier cap and the deck, at the top. The application point of the mass depends on the direction of analysis (transverse or longitudinal). The analysis can be simplified by neglecting the interaction between the superstructure, and the foundation with an assumption that the pier is fully restrained at the base. (Raffaele et al., 2014)

The period of vibration is longer in a transverse direction because the rigidity of the superstructure is much smaller in the transverse direction than longitudinal direction. In a SAP2000 model of the bridge structure, the piers can be modeled using 3D frame elements with mass lumped at discrete points, and elastomeric bearings using elastic link elements. The first phase in the study of the seismic response of a bridge is the evaluation of its dynamic characteristics under free vibrations followed by the linear time history analysis including the elastomeric bearings. (Ghosh et al., 2011)

Seismic isolation is based on the principle of decoupling the motion of the ground from the structure by the application of a horizontal disconnection between a fixed substructure and a superstructure; allowing the transfer of vertical load through isolation bearing with high vertical stiffness. The natural period of the structure and the damping capacity required to reduce the seismic effects on the superstructure are computed for the design of the isolation system; followed by the evaluation of the dynamic behavior of the whole structure. The goal of the seismic isolation is to reduce the shear forces and to limit the seismic displacements using the isolators with high damping, low horizontal stiffness, and hysteretic cycle with high energy dissipation. The commonly used isolators exhibit the non-linear behavior making their effective secant horizontal stiffness a function of displacement. In an initial or a retrofitting seismic isolation design, the most efficient design approach would be through the simplified single-degree-of-freedom (SDOF) model. The SDOF model offers flexibility and the possibility to manage the main parameters. (Lo Monte et al., 2018)

An isolated bridge system can be treated as SDOF if the displacements are checked within a prescribed magnitude. This SDOF consideration for the preliminary design of seismic isolation requires the computation of the key parameters such as loadings and dynamics of structures. The foremost step is the calculation of the weight (the permanent dead load) of the bridge per unit length according to the code provisions. The selection of type and number per support of bearings used as seismic isolation device based on its cross-section, total height and shear modulus of elastomer is a sequential task. The subsequent steps are calculations of the total effective stiffness of the isolated system, the effective period of the bridge (using the total mass), and the seismic displacement of the deck in the direction of seismic excitation. The knowledge-based decision-making system for the design of seismically isolated bridges extracts the user input relevant data: bearings, bridge structure, and seismic hazard. The database compiled based on the available literature and experimentally tested elastomeric bearings is the reference for the bearings' properties like shear stiffness, shape, rubber and steel plate thickness, height and width, overall dimensions, and area. The bridge structure system is characterized by the total length, length of middle and central span, the mass per unit length, and the initial configuration of the bearings based on the preliminary design. The design seismic acceleration, soil type, and the importance factor of the bridge are the parameter that designates the seismic hazard. This analysis is based on the assumption that the rigid deck model has a mass of piers less than 20% of the total mass of the system. The analysis is also limited to the bridges that are straight or have small curvature in the plan, small longitudinal inclination, and have bearings with effective damping not larger than 6%. (George C. Manos et al., 2012)

The experimental investigation of elastomeric bridge bearings, designed for thermal expansion, under seismic loadings conditions shows that they perform beyond the 50% limit proposed by current design guidelines for non-seismic conditions. The experimental results demonstrate that the shear strain at the failure exceeds 400% while the allowable shear strain by AASHTO is only 50%, making the provisions excessively conservative. The formula $K_H = \frac{GA}{t_r}$ is used to calculate the horizontal stiffness of bonded bearings where G is the shear modulus, A is the plan area of the bearing, and t_r is the total thickness of the rubber. (Konstantinidis et al., 2009)

The value of the effective damping ratio (ξ_{eff}) for low damping bearings is less than 6% and that for high damping bearings is between 10% and 20%.(Naeim & Kelly, 1999)

The isolation system allows the decoupling of the superstructure motion from the piers motion during seismic events. It decreases the inertial forces, the energy is dissipated in the isolators, and thus acceleration transmitted to the superstructure is reduced. The experimental study demonstrates that the increment in the compressive stress level decreases effective shear stiffness decreases but increases the effective damping ratio value. (G. C. Manos et al., 2007)

The horizontal shear stiffness of an elastomeric bearing depends on the total thickness of the rubber, and the larger vertical shear stiffness depends on the close spacing of the intermediate shim plates. The vertical stiffness of elastomeric bearings at a given lateral displacement can be empirically derived using the two-spring model proposed by Koh and Kelly (1987).

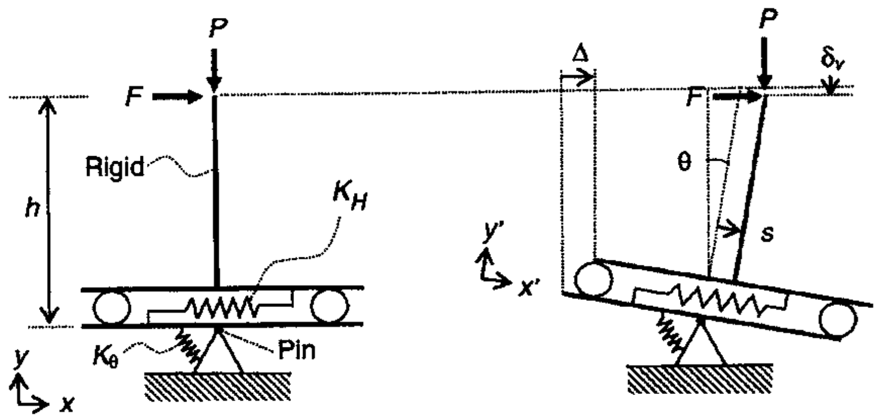

Figure 4: Two-spring model in undeformed and deformed configurations

The two-spring model for predicting vertical stiffness of elastomeric bearings developed by Koh and Kelly (1987) in the undeformed and deformed configuration is shown in Figure 4. The model has a total height of (h) supported by two friction-less rollers, and a rigid tee supported by a pin. The two springs in the system are: linear spring with the stiffness (K_H) and the rotational spring with the stiffness (K_θ). The effects of lateral load (F) and the axial load (P) are the lateral displacements at the top (Δ), rotation about the pin (θ), reduction in height (δ_v), and deformation of linear spring (s). The initial vertical deformation under axial load as well as the reduction in height due to combined axial load and lateral deformation contribute to the total vertical displacement.

The relations between the local deformations (s and θ) and the global deformation (Δ and δ_v) based on the compatibility and the geometry are defined by Equation 1.2.1 and Equation 1.2.2.

$$\Delta = s + h\theta \qquad \textit{Equation 1.2.1}$$

$$\delta_v = s\theta + \frac{h\theta^2}{2} \qquad \textit{Equation 1.2.2}$$

The vertical stiffness (K_v) incorporates the integration of the vertical displacement and the mechanical properties (Shear modulus G, and Compression modulusE_c) of an elastomeric bearing subjected to combined lateral and vertical loading.

The normalized vertical stiffness (K_v/K_{vo}) depends on the lateral displacement and the radius (R) of the bearing as shown in Equation 1.2.3.

$$\frac{K_v}{K_{vo}} = \frac{1}{\left[1 + \frac{12}{\pi^2}\left(\frac{\Delta}{R}\right)^2\right]} \qquad \textit{Equation 1.2.3}$$

The normalized form can be simplified to the expression shown in Equation 1.2.4 using the concept based on a column with a reduced area where A_r is the overlapping area, and A_b is the bonded rubber area.

$$\frac{K_v}{K_{vo}} = \left(\frac{A_r}{A_b}\right) \qquad \textit{Equation 1.2.4}$$

The normalized form can be defined as a linear function assuming that the vertical stiffness decreases linearly with increasing lateral displacement up to $\Delta = 2R$ and then remains constant as shown in Equation 1.2.5.

$$\frac{K_v}{K_{vo}} = \begin{cases} 1 - 0.4\left(\frac{\Delta}{R}\right) & for\ \Delta\backslash R\ \leq 2 \\ 0.2 & for\ \Delta\backslash R > 2 \end{cases} \qquad \textit{Equation 1.2.5}$$

The empirical formulation and the experimental validation for the influence of lateral displacement on the vertical stiffness of elastomeric bearing conclude that the vertical stiffness of the low damping rubber (LDR) bearing decreased with increasing lateral displacement. (Warn et al., 2007)

A mechanical model, aiming to improvise the two-spring model by incorporating the effects of varying vertical load on a bearing under seismic loading, comprises shear and axial springs, and two series of axial springs at the top and bottom boundaries. The comparison of results with the experimental and the simulation output validates that this mechanical can successfully predict a variety of complex bearing force-displacement relationships under a wide range of vertical load conditions. This model also simplifies the nonlinear time-history analysis of isolated structures where the vertical loads are expected to vary due to overturning forces during seismic loads. (Yamamoto et al., 2009)

The linear two-spring model is usually extended to include non-linear behavior also representing the axial-load effects in lead-rubber bearings. The response of isolation bearings is affected by the axial forces which are correlated with the lateral stiffness. The non-linearity can be accounted for in the two-spring model by incorporating various constitutive models: (i) Coupled linear model with linear shear spring, (ii) Coupled nonlinear constant strength model with a shear spring that shows bilinear force-deformation behavior, and (iii) Coupled nonlinear variable-strength model with varying yield strength. (Ryan et al., 2005)

The reduction in horizontal stiffness under increasing axial load and increasing lateral displacements causes instability in elastomeric bearings. The stability performance of bearing involves an evaluation of the critical load capacity under combined loading. The dynamic stability tests demonstrate that elastomeric bearings can perform well and recover from excursions beyond the stability limit without vivid negative impacts on the structural system. (Sanchez et al., 2013)

The new mathematical models of LDR and LR bearings considering the effects of lateral displacement and cyclic vertical and horizontal loadings extend the study to shear and compression. The variation of critical buckling load capacity with lateral displacement is evaluated using the bilinear area reduction method. A bidirectional hysteretic model in horizontal shear for the elastomeric bearing is shown in *Figure 5*. This mathematical model is based on the Bouc-Wen model extended for the analysis of seismic isolators under bidirectional motion. The basic parameters in this force vs. displacement curve comprise of initial elastic stiffness (K_{el}), characteristic strength (Q_d), yield strength (F_Y), yield displacement (Y), and post-elastic stiffness (K_d).

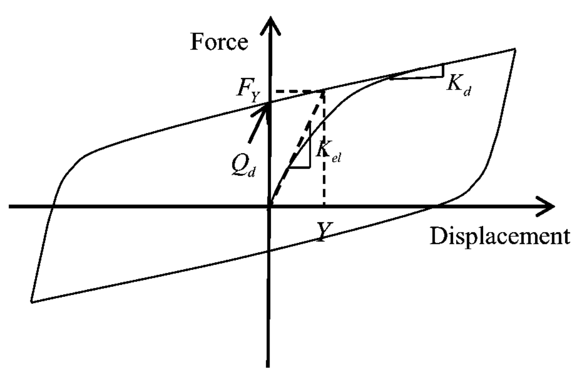

Figure 5: Mathematical Model in Shear

The force vs. displacement curve in shear is idealized in *Figure 6.* The guidelines and equations from the AASHTO Guide Specifications for Seismic Isolation Design and ASCE 7-10 are used to compute the effective period (T_{eff}), stiffness (K_{eff}), and damping (ξ_{eff}) of IS due to seismic loading using the following equations where D is the horizontal displacement, and EDC is the energy dissipated per cycle at displacement (D).

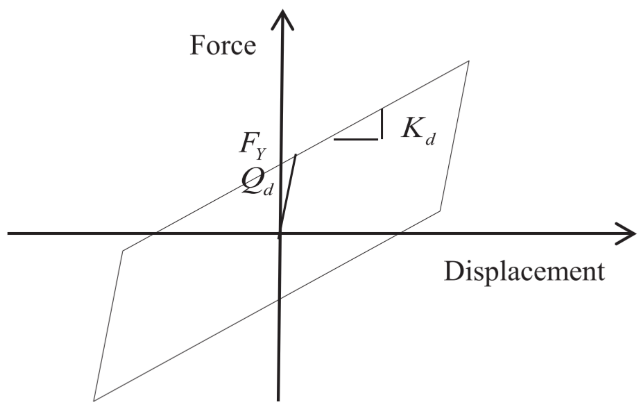

Figure 6: Idealized behavior in shear

$$T_{eff} = 2\pi\sqrt{\frac{W}{K_{eff}g}} \qquad \textit{Equation 1.2.6}$$

$$K_{eff} = K_d + \frac{Q_d}{D} \qquad \textit{Equation 1.2.7}$$

$$\xi_{eff} = \frac{1}{2\pi}\left[\frac{EDC}{K_{eff}D^2}\right] \qquad \textit{Equation 1.2.8}$$

$$Q_d \geq \frac{\pi}{2} \times \xi_{eff} \times K_d \times D \qquad \textit{Equation 1.2.9}$$

The displacement (D) estimated using simplified analysis and assumed nominal damping (ξ_{eff}) between 2% and 4% are used to calculate the characteristic strength (Q_d) of LDR bearing. The shear modulus (G) is assumed to be a constant in most numerical models however, its value varies with strain and axial loads. The experimental value of G incorporates the effects of axial load, thus can be used for horizontal stiffness of LDR bearings, and post-elastic stiffness of LR bearings. The effect of lateral displacement on vertical stiffness becomes significant only after lateral strain exceeds 100%. (Kumar et al., 2014)

The polyether urethane rotational element in disk bearing provides advantages such as a low profile, reduced plan area, excellent durability, and a wide working temperature range ($94\ to\ 250°F$). The rotation in the unconfined disk is accommodated by the differential deflection of the elastomeric element. The series of experimental studies and tests on the material properties of polyether urethane show that the material does not undergo plastic deformation until a pressure of 20 times the AASHTO maximum allowable pressure of 5000 psi. The usage of this element provides a huge factor of safety in vertical load transmission through a shear restriction mechanism. (Watson, 2014)

1.3.Scope of Work

The plan and profile report published by the MDOT for the MS7 Little Tallahatchie River Bridge is referred, to obtain the geometric and material detailing. Chapter II outlines the procedures and provisions being used for the pier design, modeling, and analyses from AASHTO Guide Specifications for LRFD Seismic Bridge Design, AASHTO LRFD Bridge Design Specifications, and other relevant design guides. The spatial coordinates of the Little Tallahatchie River Bridge, the Risk Category II, and the Site Class D are the input for the tool to obtain the seismic design parameters. The hand calculations are performed to get the dynamic characteristics of the 2DOF system in Chapter III. The linear elastic analysis is performed according to AASHTO provisions for the 2DOF system. The bilinear bearing isolation parameters are evaluated for the seismic isolation system by hand calculations. Chapter IV presents the results of pushover analyses and the time-history analyses to evaluate the time histories of the deck displacement and the pier cap displacement in transverse direction using

SAP2000(CSI, 2009). These analyses have only been performed to assess the effectiveness of seismic isolation for the force-based displacement capabilities.

CHAPTER II

AASHTO LRFD RECOMMENDED DESIGN AND MODELING PROCEDURE

2.1. Geometry, Classification, and Function of a Pier

The superstructure of a bridge is supported by the abutments at the extremities, and by the piers at intermediate points. The main function of a pier is to sustain and transfer the superstructure loads including the dead loads, live loads, and lateral loads to the foundation. As the expansion of the highway system continues, the piers are not merely constructed over a river or such natural barriers but also in a land over grade-separated highways or underpasses to allow the free flow of traffic. The geometry of design has to thus incorporate the aesthetic aspect on top of the strength and the economic parameters. The most used material in the construction of piers is reinforced concrete(Tonias & Zhao, 1995). However, timber has also been used in the construction of piers in the older bridges. The steel piers and the prestressed concrete piers are also sometimes used in special bridges.

The structural distinction of a pier from a simple column is based on the resistance against lateral forces; a column resists lateral force by flexure action but a pier uses a shear mechanism. The pier can be classified on a different basis: the connection to the superstructure or its cross-sectional shape or framing configuration. The superstructure rests on the bridge seat which is supported by the column(s) or the wall which in turn are connected to the pier foundation (footings or piles or a combination of both). The selection of piers for any bridge depends on functional, structural, and geometric requirements.

A steel-girder superstructure is usually supported with a cantilevered pier while the CIP concrete superstructures are supported by monolithic bents. The location of intermediate piers dictates the framing configuration: solid wall piers are usually used in the water crossings whereas hammerhead or column bent piers are used for overpasses or land viaducts especially in modern highways to save space and aesthetically pleasing shapes(Chen & Duan, 2003).

Some of the frequently used types of piers based on the typical cross-sectional shapes are shown in Figure *7*(Chen & Duan, 2014):

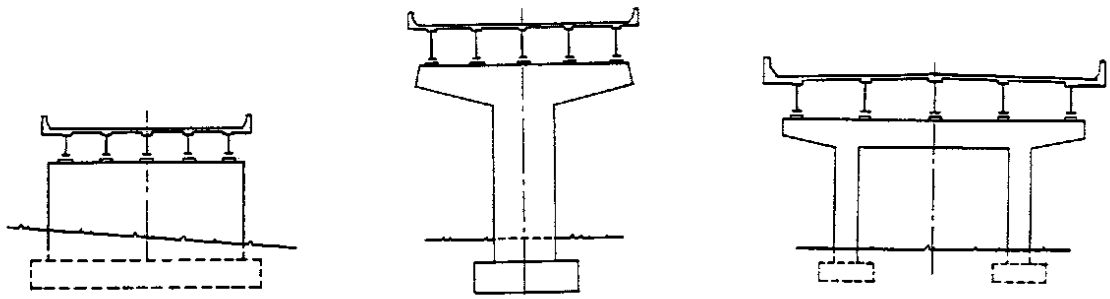

(a) Solid Wall　(c) Hammerhead pier　(b) Column bent pier

Figure 7: Typical pier types for steel bridges

The provisions for the selection and structural design of piers are laid out in Sections 5, 6, 7, and 8 of the AASHTO LRFD Bridge Design Specification.

2.2. Loading and Design Criteria

The design loads and load combinations for a pier are specified in the AASHTO LRFD Bridge Design Specification Section 3. The minimum requirements for loads, limit states, load factors, and load combinations for the design of new bridges as well as the analysis of existing bridges are covered in this section. The Load and Resistance Factor Design (LRFD) approach accounts for the variability in the loads on structure (Q) and the resistance (R) offered by the structure.

The LRFD design philosophy is consistent with other design specifications such as ACI and AASHTO while ensuring safety in different limit states and bridge types. The different limit states (LS) for the design consideration are Service Limit State, Strength Limit State, and Extreme Event Limit State.

The Service II LS is related only to the steel structures to control yielding and slip of slip-critical connection due to vehicular live load. The Strength I LS is related to providing enough strength or resistance to the basic load combination during normal vehicular use of the bridge without wind load. The earthquake loads (EQ) are evaluated using the Extreme Event I LS. The possibility of a major flood and an earthquake at the same time is negligible. Therefore, the elimination of water load is acceptable. The live-load factor (γ_{EQ}) is determined on a project-specific basis. The possibility of partial live-load i.e. $\gamma_{EQ} < 1.0$ is suggested, and $\gamma_{EQ} = 0$ is also acceptable(Chen & Duan, 2014).

2.2.1. Seismic Load and Seismic Design Procedures

The AASHTO Guide Specifications for LRFD Seismic Bridge Design is applicable to the design and construction of conventional bridges to resist the effects of horizontal motions [A3.10.1]. The AASHTO provisions require all the bridges to be checked against seismic loads; depending on the location of the bridge site, the seismic load may govern the design of the lateral load resistance system. The seismic design procedure involves the six sequential steps:

1. Preliminary Design: The seismic design procedure depends on the type of bridge, the number of spans, the height of the piers, a typical roadway cross-section, horizontal alignment, type of foundations, and subsurface conditions. The load transfer mechanism such as the connection of the deck to the girders, girders to the columns, presence of number and type of bearings, and columns to the foundations also influence the seismic response of the structure.

2. Seismic Design Parameters: The key seismic design parameters such as the peak ground acceleration (PGA) as a percent of gravity, short-period spectral acceleration (S_s), and the one-second spectral acceleration (S_1) are determined using USGS contour maps and software tools that use several building codes and specifications.

3. Site Coefficients: The site coefficients such as F_{pga}, F_a, and F_v that incorporate the geotechnical characteristics of the site such as the soil type are determined to adjust the spectral accelerations.

4. Operational Category: The operational category of the bridge is assigned based on the routes it serves and the essence of its serviceability during or after a seismic event. The operational category of a bridge might change if the bridge undergoes any deformation due to seismic activity.

5. Seismic Performance Zone: The seismic zones are the geographical regions defined on the US maps based on the value of the seismic design value. The greater value of acceleration or the design value corresponds to the greater risks in the region which demands the greater seismic performance requirements.

6. Response Modification Factors: These factors (R) are used in the elastic analysis of the bridge system to reduce the seismic force allowing to incorporate the energy dissipation through inelastic deformation (hinging) in the substructure.

These design steps provide the basis for determining the design forces, the design displacement requirements, and the level of seismic analysis. Based on the seismic zone, the geometry, and importance factor; the multiple-span bridge requires a single-mode or a multimode spectral analysis. A time history analysis is required for the critical bridges.

The two load cases are defined in two perpendicular horizontal directions, the longitudinal and the transverse axes of the bridge, because of the directional uncertainty of earthquake motions.

2.3. Structural Analysis and Modeling

The structural analysis can broadly be classified as static analysis and dynamic analysis. The basic difference is the time-dependency of the loads being applied in the structure. A dynamic analysis of a bridge under an earthquake incorporates time-dependent characteristics such as peak ground acceleration (PGA), duration, and frequency content. The magnitude of the force that the bridge and its components are subjected to depends on the intensity of the ground motion which is represented by the PGA. The longer duration of a seismic motion imparts larger energy to the bridge. An artificially generated time history including the magnitude, frequency, and duration at the bridge site is usually considered for the analysis.

There are several methods for the dynamic analysis of bridges depending on the geometry, seismic zone, structural type and material, and importance of the bridge being analyzed. The model created for the dynamic analysis must include the relevant characteristics such as distribution mass, stiffness, and damping of structural components(AASHTO, 2011). The required number of natural frequencies and the reliability of the expected mode shapes are the basis for selecting the minimum degree of freedom (DOF). A condensation procedure is recommended to reduce the number of DOF. Generally, the number of DOF should be double the number of frequencies required. The mass distribution in a model can be lumped mass or consistent mass, which is a function of the system and response being evaluated; the lumped mass model is preferred for the translational degree of freedom. The seismic analysis model should consider the non-linear effects such as inelastic deformation and cracking which decrease the stiffness. The cracked section property with a moment of inertia equal to one-half that of the uncracked section can be used while modeling the reinforced concreted columns in seismic zones 2, 3, and 4. The energy dissipation can be represented by equivalent viscous damping that can be neglected in the calculation of natural frequencies and associated nodal displacements. The transient response can only be obtained considering the effects of damping; about 2% for the concrete structures.

2.3.1. Dynamic Analysis

<u>Single-Mode Spectral Method:</u> This method is based on the fundamental mode of vibration assuming that seismic load acts as an equivalent static horizontal force in either the longitudinal or transverse direction.

Single Degree of Freedom (SDOF) System: The corresponding deformed shape of the single-degree-of-freedom (SDOF) model gives the natural period. This method is suitable for structures having evenly distributed mass and stiffness. The damping in the SDOF dynamic model is represented with a massless viscous damper. A simple mass-spring system is used as a reference to develop an SDOF dynamic model for the bridge. The mass of the superstructure is the concentrated mass, the stiffness of the column allowed to move in one direction is the spring, and the internal energy absorption in the concrete frame acts as viscous damping in the SDOF model of the bridge in *Figure 8*.

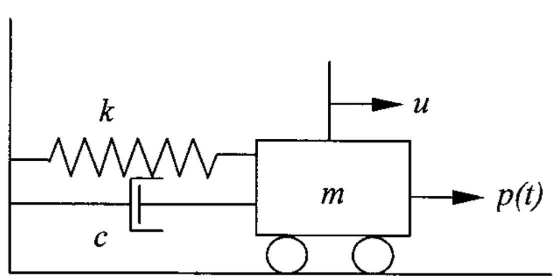

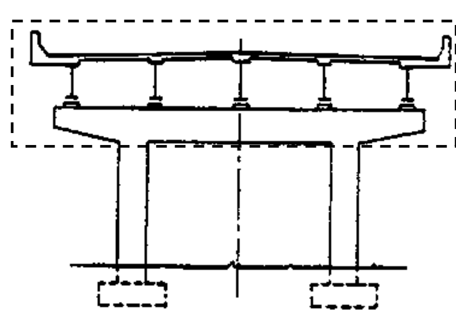

(a) Idealized damped SDOF mass-spring system

(b) Multiple-span bridge supported by two-columns as SDOF structure

Figure 8: Idealization of bridge structure as SDOF model

The response of each SDOF system depends on the mass (m), stiffness (k), damping (c), and external force (p(t)) or displacement (u).

The damping (c) is neglected to compute the natural frequency (f), and the equations of motion are applied in the inverted oscillator like the SDOF model of the bridge shown in *Figure 9*.

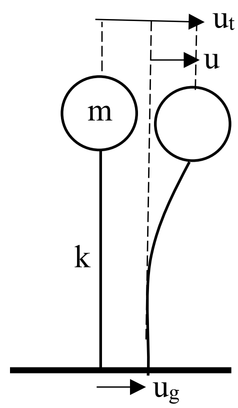

Figure 9: Earthquake-induced motion of an SDOF bridge model (without damping)

The total displacement of the mass relative to the ground (u_t) is the sum of the displacement at the ground level (u_g) and the displacement of the mass with respect to its centerline (u).

$$u_t = u + u_g \qquad \text{Equation 2.3.1}$$

The natural circular frequency of the undamped mass-spring system is:

$$\omega_n = \sqrt{\frac{k}{m}} \qquad \text{Equation 2.3.2}$$

Therefore, the natural cyclic frequency is:

$$f_n = \frac{\omega_n}{2\pi} = \frac{1}{2\pi}\sqrt{\frac{k}{m}} \qquad \textit{Equation 2.3.3}$$

And, the natural period of vibration is:

$$T_n = 2\pi\sqrt{\frac{m}{k}} \qquad \textit{Equation 2.3.4}$$

The response of the structures like the maximum displacement, moment, and shear can be determined based on the dynamic characteristics (T_n and ω_n) of the SDOF system(Naeim, 1989).

The graphical relationship between these response parameters and the dynamic characteristics of the system gives the response spectrum. Such a spectrum defined for an elastic structural system is called elastic response spectrum. The bridge structure is expected to experience inelastic behavior during the strong ground motion. Therefore, the inelastic response spectrum is pertinent. The inelastic behavior occurs during a major earthquake when the seismic energy experienced by the bridge is dissipated by viscous damping and yielding.

Multiple Degree of Freedom (MDOF) System: The SDOF model is not applicable for the analysis when the complexity arises from the multi-level frame structure, several support conditions, or the presence of bearings between superstructure and substructure. The MDOF system is defined for the response where the structure is discretized into several lumped masses and associated displacements. The equation of motion is similar to the SDOF system, but the mass (m), the stiffness (k), and the damping (c) are represented with matrices(Chopra, 2017).

$$[M]\{\ddot{u}\} + [C]\{\dot{u}\} + [K]\{u\} = -[M]\{B\}\ddot{u_g} \qquad \textit{Equation 2.3.5}$$

The vector {B} is a displacement transformation vector used to define the degree of freedom under the application of seismic load.

The first approach to understand the response of the MDOF system with N-DOF is to analyze the system under free vibration without damping such that [C] and $\ddot{u_g}$ are zero in *Equation 2.3.5.*

$$[M]\{\ddot{u}\} + [K]\{u\} = 0 \qquad \textit{Equation 2.3.6}$$

The rearrangement of the above equation and solving for the solutions gives the N natural frequencies of the dynamic system.

$$\left[[K] - \omega_n^2[M]\right]\{\phi_n\} = 0 \qquad \textit{Equation 2.3.7}$$

Where, $\{\phi_n\}$ *is deflected shape matrices or eigenvectors*

The eigenvectors represent only the deflected shape corresponding to the natural frequency, the matrix is normalized to get the actual deflection magnitude.

The modal analysis equation of the MDOF system under the earthquake expressed in terms of displacement as natural mode shapes and normalized matrices would be:

$$[M^*]\{\ddot{Y}\} + [C^*]\{\dot{Y}\} + [K^*]\{Y\} = -[\phi]^T[M][B]\ddot{u_g} \qquad \textit{Equation 2.3.8}$$

The term L_n is called the modal participation factor in the n^{th} mode. This equation when divided by M_n^* yields the generalized modal equation comparable to the SDOF system as:

$$\ddot{Y_n} + 2\xi_n\omega_n\dot{Y_n} + \omega_n^2 Y_n = \left(\frac{L_n}{M_n^*}\right)\ddot{u_g} \qquad \textit{Equation 2.3.9}$$

The solution to the above equation gives the value of Y_n that can be used to calculate the displacement in the n^{th} mode u_n as:

$$u_n(t) = \phi_n Y_n(t) \qquad \textit{Equation 2.3.10}$$

The total displacement can be determined by the superposition of all the modal displacements as:

$$u(t) = \sum \phi_n Y_n(t) \qquad \textit{Equation 2.3.11}$$

2.3.2. Nonlinear Analysis

A bridge shows non-linear behavior during seismic loading because of many factors such as material non-elasticity, geometric or second-order effects, non-linear soil-structure interaction (SSI), time-dependent effects like concrete creep and shrinkage, etc. The inelastic structural behavior of the bridge is assessed using the analysis of the non-linear bridge with appropriate modeling. The formulation of member stiffness matrices should account for the geometric non-linearities. The material non-linearity is accounted into the analysis based on the non-linear stress-strain relationship for the steel structure, and compression stress-strain relationship for concrete.

A non-linear section analysis is performed based on the assumptions that the plane sections do not deform under bending action i.e. plane section remains plane, stress-strain curves for concrete and steel are defined, and the bond between concrete and rebars is perfect in reinforced concrete(AASHTO, 2011). Also, the deformations under shear and torsion are negligible so neglected. The compatibility equations and the equilibrium equations are used for mathematical formulations.

The non-linear frame analysis is performed as elastic-plastic hinge formation. The elastic-plastic hinge analysis assumes the formation of “zero-length” plastic hinges about which the member reaches plastic moment capacity and rotates freely.

Static Push-Over Analysis

The displacement-based seismic design approach uses displacements as the limit states under the specified seismic loads rather than conventional forces in strength-based design. A static non-linear push-over analysis can be used to assess the performance of a new or existing bridge under displacement capacity. The collapse mechanism in an analytical frame model under incremental lateral loads is analyzed. A simplified fixed-fixed or fixed-pin column model ignoring the foundation flexibility of pile footing for pile cap is proposed for the two-dimensional pushover analysis(AASHTO, 2011). This model incorporates the effect of the seismic load path on the column axial load.

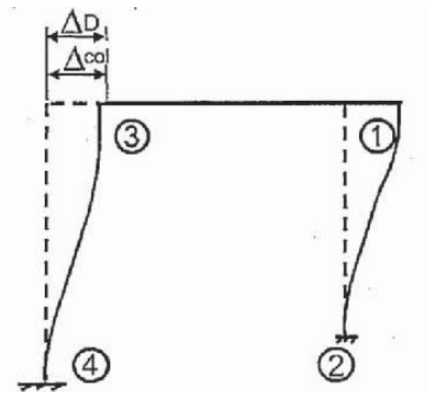

Figure 10: Plastic hinge sequence for rigid bent cap and rigid foundation

<u>Capacity Design Requirement</u>

The capacity design provisions ensure that the columns undergo plastic hinging/inelastic deformation to protect the secondary structure such as the cap beam or foundation(AASHTO, 2011). These provisions can be neglected if the seismic isolations (IS) system is used or the ductile diaphragm is used in the transverse direction of multi-column pier bent. The overstrength moment capacity of the reinforced concrete column resisting the seismic loads, and allowing the formation of plastic hinges is calculated using *Equation 2.3.12.*

$$M_{po} = \lambda_{mo} M_p$$

Where, M_p = plastic moment capacity of column (kip-in) *Equation 2.3.12*

λ_{mo} = overstrength factor taken as 1.2 or 1.4 [Article 8.5]

The analytical plastic hinge length of a reinforced concrete column is calculated using the following equation:

$$L_p(in) = 0.08L + 0.15 f_{ye} d_{bl} \geq 0.3 f_{ye} d_{bl} \qquad \textit{Equation 2.3.13}$$

Where,

L= length of the column from point of a maximum moment to the point of moment contra flexure (in)

f_{ye} = expected yield strength of longitudinal column reinforcing steel bars (ksi)

d_{bl} = nominal diameter of longitudinal column reinforcing bars (in)

The plastic hinge region in a reinforced concrete column is however taken as the maximum value of:

$$L_{pr} = MAX \begin{cases} 1.5\ times\ the\ gross\ CS\ dimension \\ region\ where\ moment\ demand > 75\% M_p \\ L_p \end{cases} \qquad \textit{Equation 2.3.14}$$

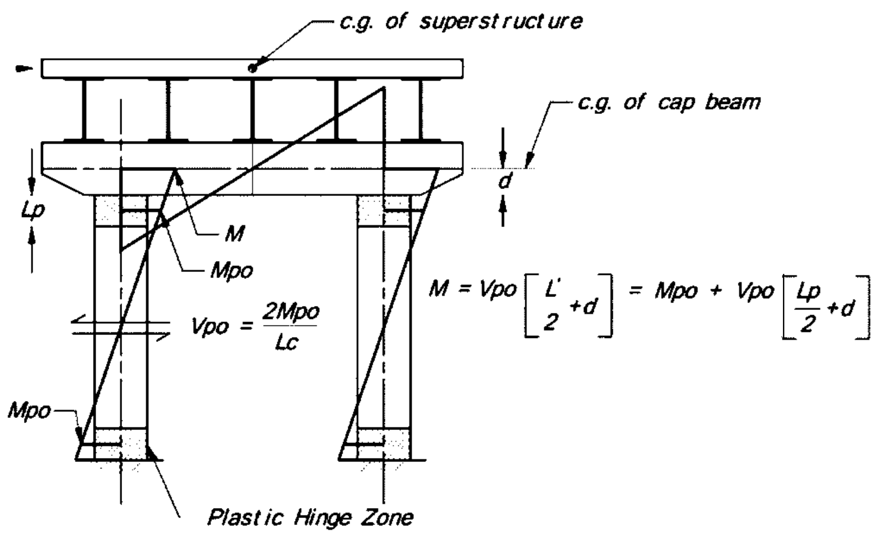

Figure 11: Transverse response of a dual column pier for Capacity Design

<u>Time History Analysis:</u>

The modal analysis is not applicable in the nonlinear range where the bridge structure shows non-classical damping properties. A numerical integration method called time-history analysis that captures the response by dividing the time-scale into a finite number of small steps is used. The equation of motion at an i^th interval of time that satisfies the response using time history analysis is:

$$[M]\{\ddot{u}_i\} + [C]\{\dot{u}_i\} + [K]\{u_i\} = -[M]\{B\}\ddot{u}_{gi} \qquad \textit{Equation 2.3.15}$$

2.4. Influence of Bridge Bearings

Bearings are the devices that allow the load transfer from the superstructure to the substructure and accommodate the relative movements: translations and rotations in both longitudinal and transverse directions. The selection of bearings depends based on load and displacement demand, site conditions, cost benefits, and geometric requirements. The main types of bridge bearings in the market are:

1. Sliding Bearings: This bearing has sliding metal plates sometimes sandwiching a layer of PTFE (poly-tetra-fluoro-ethylene) to accommodate the translational motions. It is commonly used in bridges where the rotational motions are negligible, more often as a component of other bearings.
2. Rocker and Pin Bearings: A rocker bearing is an expansion bearing facilitating the rotations as well as translations. However, the pin bearing is a fixed bearing that allows only rotations. These rocker and pin bearings are commonly used in steel bridges.
3. Elastomeric Bearings: These bearings have been extensively used recently as they can accommodate both translational and rotational movements, have no moving parts thus require low maintenance, and are economical (Konstantinidis et al., 2009). Among different types, the steel-reinforced elastomeric bearings are manufactured by vulcanizing elastomers to thin steel plates.

4. Disk Bearings: In a disk bearing the vertical loads are supported by a hard elastomeric disk made up of polyether urethane, and the horizontal movements are accommodated via the elastomer deformations.

   The elastomeric bearings and the disc bearings have been used under seismic loading conditions. The mechanical behavior, the numerical analysis procedure, and the modeling approaches have been extensively discussed in the literature review section. The requirements for the design and selection of bearings are included in Section 14 of LRFD Bridge Design Specifications. The elastomeric bearings can be modeled as elastic link elements in SAP2000 (Ghosh et al., 2011). The usage of bearings as seismic isolation devices to reduce the seismic forces to limit the inelastic deformations in bridge structures has become a common practice in seismic regions. The working principle of seismic isolation is the decoupling of the superstructure and substructure (pier) while allowing the load to transfer vertically. This is generally ensured with high vertical stiffness of the isolation bearings, and designed horizontal stiffness just enough to allow the horizontal displacement (limited by an expansion joint) that prevents the hammering of adjacent decks(Tubaldi et al., 2016).

   A representation of a bridge structure simplified to analyze during the seismic event as a 2DOF system is shown in Figure 12.

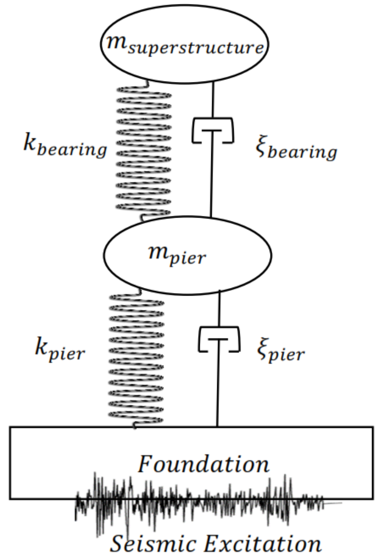

Figure 12: 2DOF system in transverse direction

2.5. Case Study: Little Tallahatchie River Bridge

The Little Tallahatchie River Bridge has been newly constructed to replace MS SR7 Bridge located across the Tallahatchie River in Lafayette County. The total length of the bridge is 2212.29 ft (0.419 miles). The bridge has 11 spans; supported by the abutments at the end and 10 intermediate two-column bent piers. The deck has been supported by the five 760 ft (approx. 240-300-240 ft) long continuous welded plate girder run from bent 2 to bent 5 and bent 5 to bent 8. The rest of the spans are supported by the seven 72" deep prestressed concrete bulb tee girders each having a span length of approximately 130 ft. The clear roadway spacing is 44' with an extension of 1'5" on each side to support the barriers. The barriers have a base thickness of 1'5", a height of 2' 8 5/16", and top width of 10" approximately. The typical depth of the deck is approximately 9" which varies along the length of the bridge. The intermediate bents are two-column supporting a pier cap, and foundation supported by the extended drilled shafts (piles with permanent casing). The transition between columns (piers) and the drilled shafts (piles) is supported by typical shear keys (2'6"x2'6"x4"). The dimensions of a typical pier cap are 5' −

$6''x6' - 9''x46' - 0''$. The columns are circular in cross-section with a diameter of 6'. The detailed dimensions, plans, and distribution, and material properties of all the components and elements of the bridges are shown in the calculation sheet and bridge plan layout attached in the appendices. The geometry has been simplified according to the applicable design guides to estimate the dead load contribution from each frame or element. These calculations and assumptions have been shown in the appendix.

The dead load is calculated using the geometric details and the material properties of each element. The whole 780 ft long span, extending from Pier 5 to Pier 8, has been used to calculate the linear weight distribution of the superstructure.

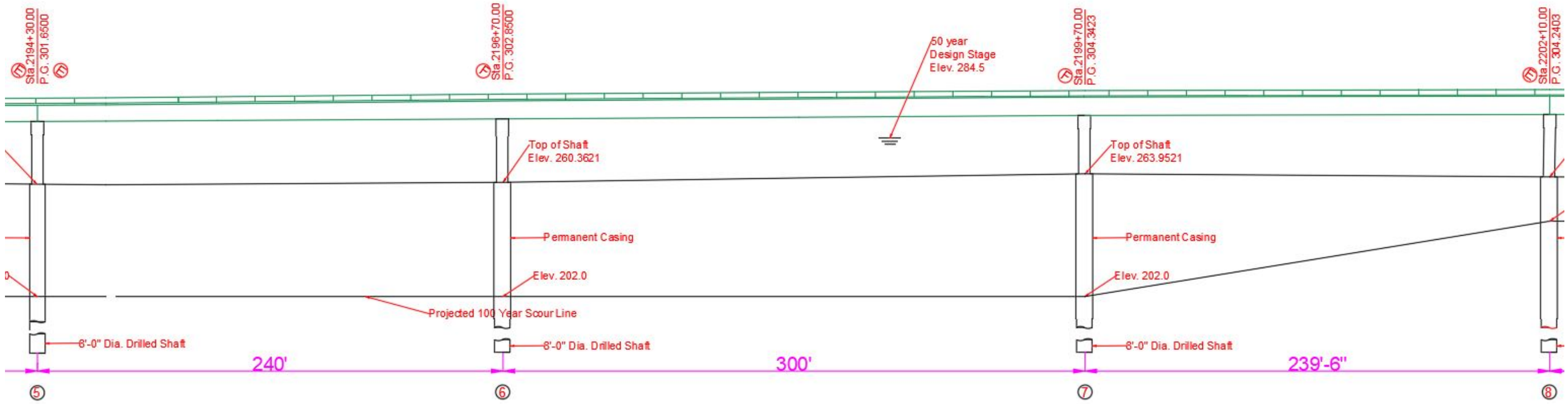

Figure 13: 780 ft long continuous welded plate girder span in a long view

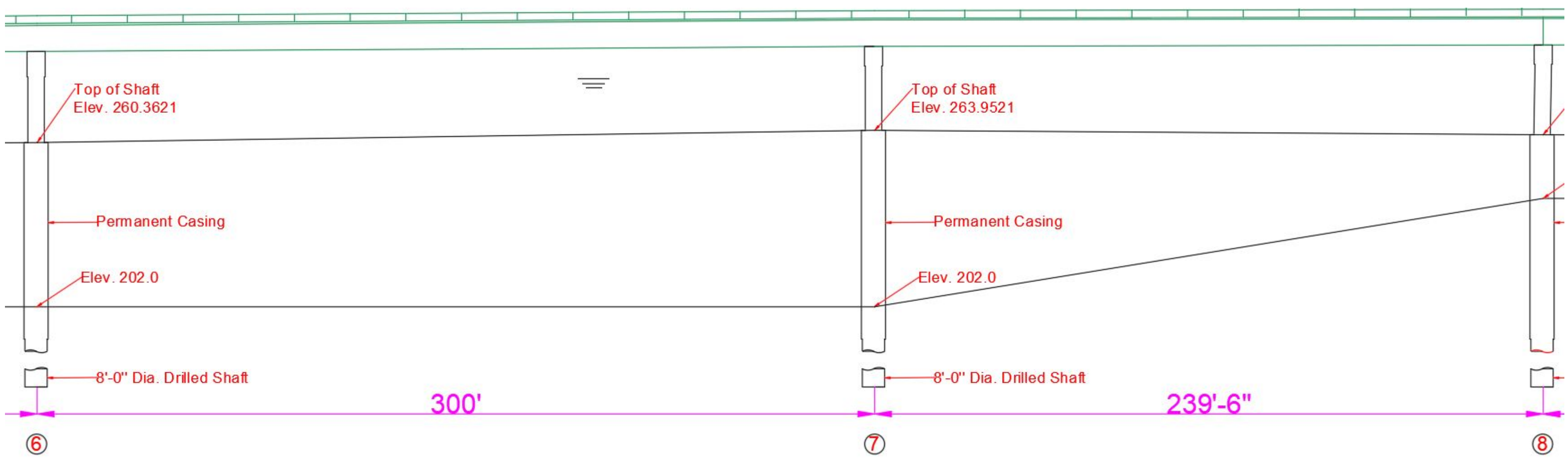

Owner

Figure 14: Elevation view of the span supported by Pier 7

Pier 7 is selected that supports half of the weight from 300 ft span (between Pier 6 and 7) and that from 240 ft span (between Pier 6 and 7). Pier 7 supports the weight from 270 ft long span on either side as shown in the schematic plan view in *Figure 15*.

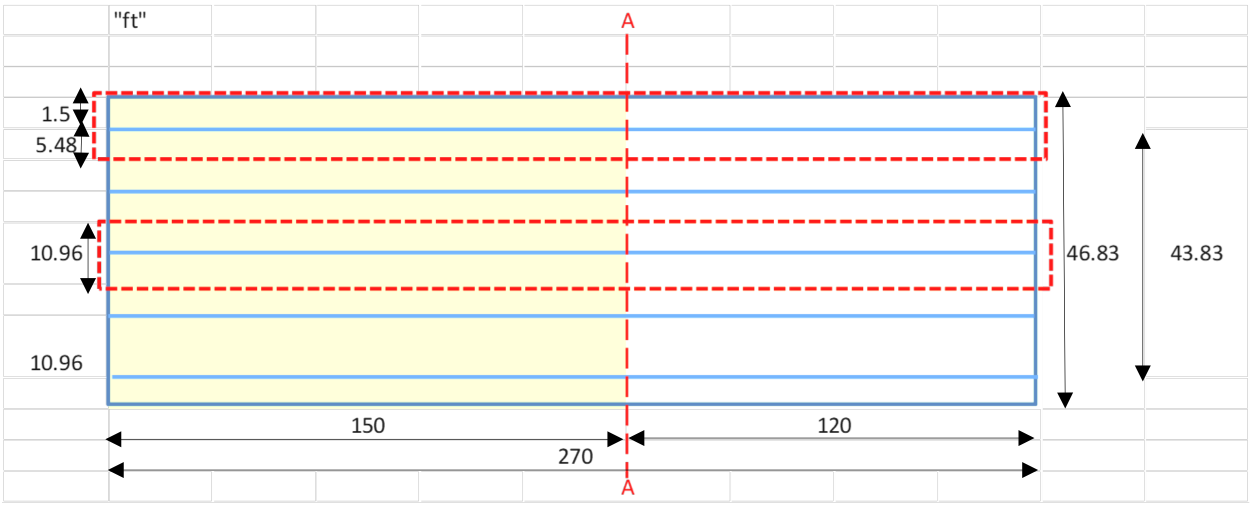

Figure 15: Plan View of the deck supported by Pier 7

The load is then linearly distributed in the transverse direction (A-A) as shown in *Figure 16*. The total load from the superstructure including the girders is 50.24 klf. The linear dead load distribution in the pier cap is 8.64 klf and that on each column is 4.40 klf.

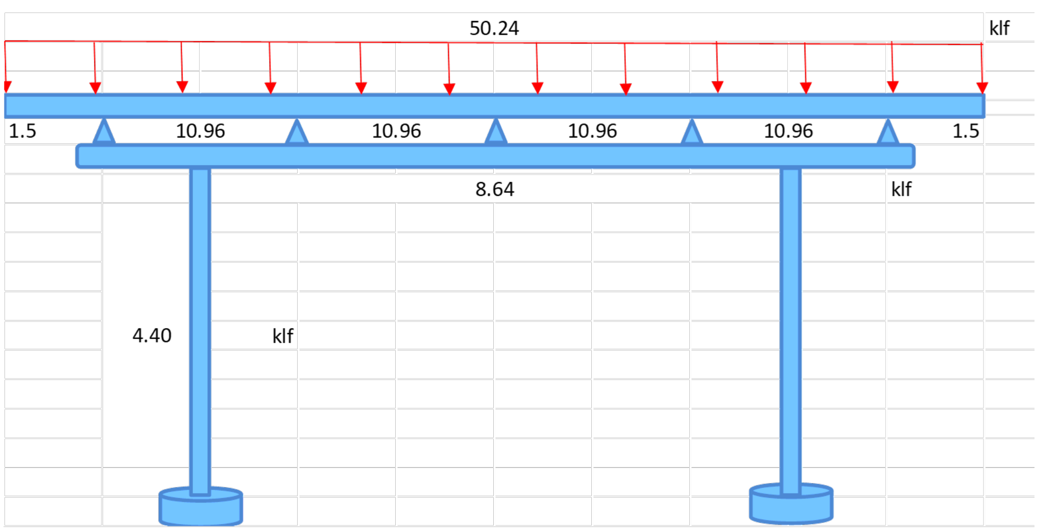

Figure 16: Schematic Weight distribution in transverse section (A-A) at Pier 7

The geometric configuration and the load distribution is used to calculate the center of masses for the superstructure (m_2) and the substructure (m_1) at height h_2 and h_1 from the base of the columns. The effective stiffness of the pier is k_1 and that of the bearings is k_2. The damping in the pier and the bearings are ξ_1 and ξ_2 respectively. A 2DOF system as a mass-spring is developed using these parameters.

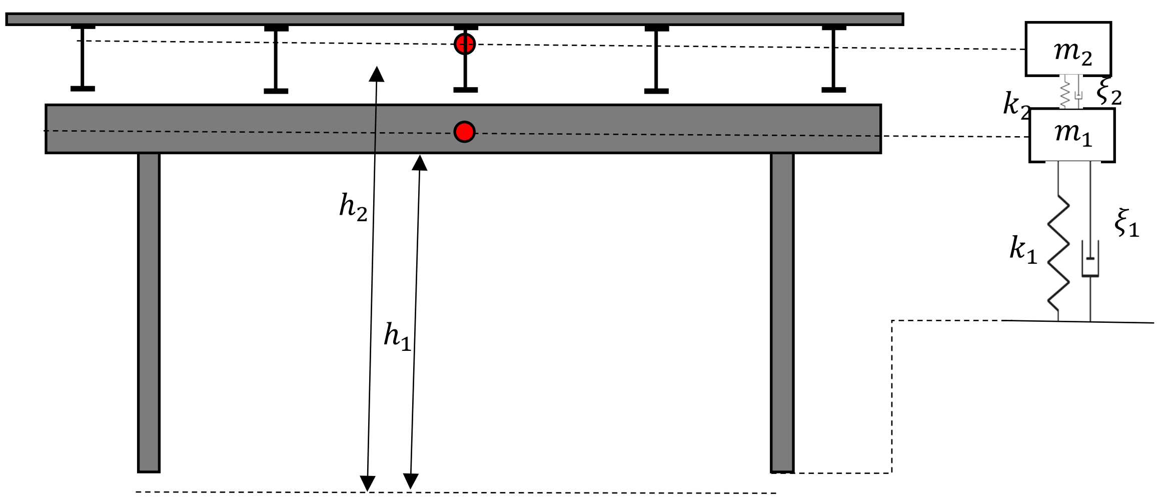

Figure 17: Idealization of the bridge as 2DOF system

The dead load and the 2DOF configuration are analyzed to get the dynamic properties of the bridge. After the first analysis, the system will be analyzed under seismic excitation. The spatial coordinates of the Little Tallahatchie River Bridge, the Risk Category II, and the Site Class D are the input for the tool to obtain the seismic design parameters as shown in *Table 1*. The peak ground acceleration (PGA) value at the site is 0.246g. The time history obtained for the M7.7 earthquake is scaled using this value of PGA as an input in a USGS tool. The non-linear time-history analysis is performed based on this time-history function.

Table 1: Seismic Design Parameters for Little Tallahatchie River Bridge

Description of Parameter	**Parameter Symbol**	**Value**
MCE_R ground motion. (for 0.2 second period)	S_S	0.456
MCE_R ground motion. (for 1.0s period)	S_1	0.194
Site-modified spectral acceleration value	S_{MS}	0.664
Site-modified spectral acceleration value	S_{M1}	0.429
Numeric seismic design value at 0.2 second SA	S_{DS}	0.443
Numeric seismic design value at 1.0 second SA	S_{D1}	0.286
Seismic design category	SDC	D
Site amplification factor at 0.2 second	F_a	1.428
Site amplification factor at 1.0 second	F_v	2.213
MCE_G peak ground acceleration	PGA	0.246
Site amplification factor at PGA	F_{PGA}	1.354
Site modified peak ground acceleration	PGA_M	0.333

CHAPTER III

TWO DEGREE OF FREEDOM (2DOF) MODAL ANALYSIS OF TWO COLUMN PIER

3.1. Formulation and 2DOF Solution

The 2DOF model of the bridge is first analyzed without any forcing function to get the dynamic characteristics. The mass matrix is formed based on the total mass of the superstructure (m_2) and the substructure (m_1) lumped at the center of masses. The mass of the superstructure based on the weight of all the components such as cross frames, lateral bracings, girders, deck, topping, barrier, and the major reinforcement steel is 6.089 $kip - s^2/in.$ Similarly, the weight of the reinforcement steel and the concrete used in the pier cap and the two columns is used to calculate the mass of the substructure, 1.518 $kip - s^2/in.$ The weight distributions in all of the key elements are accounted for to calculate the center of masses. The mass of the superstructure and that of the substructure are located at heights $h_1 = 20.74\,ft$ and $h_2 = 35.22\,ft$ from the base of the columns.

$$\begin{bmatrix} m_1 & 0 \\ 0 & m_2 \end{bmatrix} = \begin{bmatrix} 1.518 & 0 \\ 0 & 6.089 \end{bmatrix} \qquad \textit{Equation 3.1.1}$$

$$\begin{bmatrix} k_1 + k_2 & -k_2 \\ -k_2 & k_2 \end{bmatrix} \qquad \textit{Equation 3.1.2}$$

The stiffness matrix for the 2DOF system is a 2x2 matrix that includes the stiffness of two columns in parallel (k_1) and the stiffness of the bearing (k_2). The stiffness value in the matrix represents the effective stiffness accounted for the configuration and location of five bearings in parallel that link the superstructure to the substructure.

The geometric properties and the material properties have been used to calculate the stiffness of the bearings. These geometric properties have either been directly taken from the MDOT report and drawings, and the material properties have been retrieved from the database provided by the manufacturer of the bearings (R J Watson Inc.). The two types of bearings that are being investigated for their effectiveness in this study are laminated neoprene pad (LP1) and unidirectional fixed disc bearing (FB1). The bilinear properties of these bearings are listed in *Table 2*. The total heights of the rubber in each of LP1 and FB1 bearings are 4 in and 6.25 in respectively. The maximum horizontal displacement (u_{max}) that the bearing can undergo without deforming in the transverse direction is accounted for the seismic movement under extreme event limit state. The characteristic strength (Q_d) is based on the maximum transverse load under the service limit state. The post elastic stiffness (K_d) and the elastic stiffness (K_u) are in a ratio of 1:10 as commonly practiced (Feng & Zhang, 2020).

Table 2: Bearing Isolation Parameters

Type	F_y (kip)	u_y (in.)	F_{max} (kip)	u_{max} (in.)	K_u (kip/in.)	K_d (kip/in.)	Q_d (kip)
LP1	43.33	0.10	262.63	5.22	428.41	42.84	39
FB1	127.78	0.17	516.57	5.22	769.20	76.93	115

The dynamic properties of the undamped 2DOF system: the natural period (ω_n) and the period (T) using elastic stiffness, post-elastic stiffness, and the effective stiffness of each type of bearings are calculated. The 2DOF system has two characteristics phenomena; two natural frequencies, and two-mode shapes. The concept of computational matrix theory for the 2DOF system i.e. the concepts of eigenvectors and eigenvalues are employed to determine the natural frequencies and the mode shapes respectively. The 2DOF system is solved by hand calculations and also verified by a simple MatLab routine.

The results shown in *Table 3* demonstrate that the first modes of vibration (both masses moving in the same direction) have larger periods in each case as expected. The period drastically increases when the system shifts from elastic stiffness to the post-elastic stiffness bands especially in the first mode of vibration. The period is very low in the second mode (antagonistic direction of motion) as compared to the first mode in each case and does not significantly change moving from elastic stiffness to the post-elastic stiffness phase. The results also show that effective stiffness (K_{eff}) yields the frequencies and the periods numerically comparable to the post-elastic stiffness. Therefore, this parameter is not applicable to analyze the structure under seismic or other dynamic loadings where the bearing is expected to deform and lose stiffness at the loading stage beyond yielding force (F_y).

Table 3: Natural frequencies and period for different mode shapes of 2DOF system

Type		$\boldsymbol{K_u}$		$\boldsymbol{K_d}$		$\boldsymbol{K_{eff}}$	
		ω_n (rad/s)	T (s)	ω_n (rad/s)	T (s)	ω_n (rad/s)	T (s)
LP1	Mode 1	7.88	0.7972	2.63	2.3841	2.85	2.2024
	Mode 2	49.49	0.1262	47.08	0.1334	47.14	0.1333
FB1	Mode 1	10.08	0.6232	3.51	1.7882	3.97	1.5818
	Mode 2	52.15	0.1205	47.32	0.1382	47.47	0.1323

The maximum acceleration in the transverse direction from the time history is $64.41\ in/s^2$. This maximum ground acceleration when multiplied by the product of mass gives the response to the earthquake loading (Duhamel integral). The displacements of each mass in the 2DOF system can be conveniently calculated using the natural frequencies and the effective earthquake forces. The horizontal forces, which are the effective inertial forces as a result of two different modal contributions, being acted at the center of masses of the superstructure and the pier (cap and columns) are 392.2 kips and 97.77 kips respectively. The deflections when two different kinds of bearings have been used are shown in *Table 4*.

Table 4: Maximum deflection at peak pseudo-acceleration

	LP1		FB1	
	u_{1u} (in)	u_{2d} (in)	u_{1u} (in)	u_{2d} (in)
m_1	0.029	0.029	0.029	0.029
m_2	1.03	9.27	0.63	5.22

The isolation of the superstructure and the substructure due to the introduction of the isolation bearing (both LP1 and FB1) is evident from the displacement values of the center of masses. The use of both bearings limits the deflection of the pier to 0.029 *in* in horizontal direction. The displacement of the superstructure is dependent on the elastic and post-elastic stiffness values of each bearing. In the elastic stiffness range of LP1 and FB1 bearings, the maximum horizontal displacements of the superstructure are 1.03 in and 0.63 in respectively. After exceeding the elastic stiffness limit, these displacements significantly increase to 9.27 *in* and 5.22 *in*. The higher value of post elastic stiffness in FB1 limits the horizontal displacement within the acceptable range. Even if the decoupling of superstructure and substructure under seismic isolation is desirable to allow the deformation of the superstructure over sub-structural elements, it is expected to limit the horizontal displacement to avoid the pounding of the large super structural decks in the longitudinal direction or falling off in the transverse direction.

3.2. Equivalent SDOF solution neglecting bearings

The system is then analyzed as a single degree of freedom (SDOF) system with total mass lumped at the centroid of the pier cap without accounting for the stiffness provided by any of the bearings. This system without bearings can be treated as a fixed system (FS) which is similar to an inverted oscillator under simple harmonic motion. The stiffness of the two columns is high, and there is no energy dissipation mechanism available without the presence of bearings. The maximum displacement of this fixed system (FS) is calculated to 0.15 *in* the horizontal direction which is large as compared to the 0.029 in the displacement of the pier in an isolated system (IS).

Table 5: Maximum deflection without any functional bearings (SDOF)

M $(kip - s^2/in)$	P (kip)	K (kip/in)	u (in)	ω_n (rad/s)
7.61	489.97	3322.98	0.15	20.90

3.3. Linear Elastic Analysis: Comparison based on Demand-to-Capacity (D/C) ratios

This force-based approach also requires the evaluation of the strength capabilities such as shear and moment capabilities in the critical elements of the structure. The preliminary analysis is a linear elastic analysis of the two-column bent pier. The AASHTO LRFD Section 5.7 provisions, the resistance factors, and the axial-flexural capacity interaction diagrams are the guides used in computing the nominal flexural strength in the bending axis. Similarly, the nominal shear capacity of each column in the pier is calculated using the provisions from AASHTO LRFD design specification Section 5.8.3.3. The required or demand shear and flexural strength are calculated based on the forces acting at the maximum displacement of the structure and thus produced secondary effects.

The nominal capacities (subscripted n) computed using AASHTO guides, and the required capacities (subscripted r) obtained by linear elastic analysis are presented in *Table 6*. The D/C ratios of less than 1.0 ensure the safety of the structure without substantial damages.

Table 6: Demand-to-Capacity (D/C) ratios of the fixed system (FS) and isolated system (IS)

	V_n (kip)	V_r (kip)	M_n $(kip-ft)$	M_r $(kip-ft)$	D/C $(Shear)$	D/C $(flexure)$
FS	599.79	489.97	8846.97	5267.18	0.82	0.60
LP1	599.79	97.77	8846.97	3845.24	0.16	0.43
FB1	599.79	97.77	8846.97	3051.19	0.16	0.34

The recently constructed bridge has been analyzed, therefore the D/C ratios are less than 1.0 in both shear and flexural strength capacities as expected. The results confirm that the bearings are more effective in reducing the D/C capacities in both shear and flexure. In the transverse direction, the use of both LP1 and FB1 isolators lowers the D/C ratio to 0.16 as compared to the fixed system with a D/C ratio of 0.82. Also, the flexural D/C values are lowered to 0.43 and 0.34 by the LP1 and the FB1 isolators from 0.60 in the fixed system. These results from the linear elastic analysis demonstrating the reduction in the D/C ratios with the usage of bearings as isolation devices confirm the simplified procedure to evaluate seismic vulnerabilities

CHAPTER IV

FIXED BASE FRAME ANALYSIS OF TWO-COLUMN PIER

4.1.Static Pushover Analysis

The non-linear pushover analysis is performed to estimate the sequence and the pattern of plastic hinge formation, and evaluate the hinge status. The pushover analysis in SAP2000 involves the sequential steps: definition of lateral loads, the definition of hinge properties, and assignment of hinges, analysis, checking pushover curve, and target displacement, and checking hinge status for global and local deformation. The AASHTO LRFD seismic bridge design specification Section 4 and Section 5 are used to develop the model for pushover analysis. The cap beam is defined as a rigid beam element that does not allow the formation of any hinges. The translational displacements of four joints 17 and 18 at the base columns, and joints 40 and 47 at the top of the columns in the horizontal direction (U1) are monitored to allow a maximum magnitude of 5.22 *in*. The lateral non-linear load case (PUSHx) is defined and then assigned at Joint 40 and Joint 47 with a magnitude of 0.5 kips at each joint. The hinges are defined as 'auto hinge type' ASCE 41-13 Table 10-8 (concrete columns) with P-M2-M3 degree of freedom. The flexure/shear failure condition is selected.

The hinges are assigned at an offset location of 30 *in* from the joints. The auto hinges assigned at Joint 17, Joint 18, Joint 40, and Joint 47 are 15H1, 16H1, 15H2, and 16H2 respectively as shown in *Figure 18*: 2D pier model for pushover analysis: (a) Joint ID and (b) Hinge assignments. The model is then allowed to run the Gravity and PUSHx load cases. The hinge formation sequence and pattern were checked until the 'collapse prevention (CP)' hinge status was displayed. The linear response under the lateral force is observed at top of columns in both the hinges 15H2 and 16H2 up to Step 7, and also at the bottom of the columns in the hinges 15H1 and 16H1 up to Step 8. The non-linear 'CP' hinges are formed at Step 9 at the top of the columns.

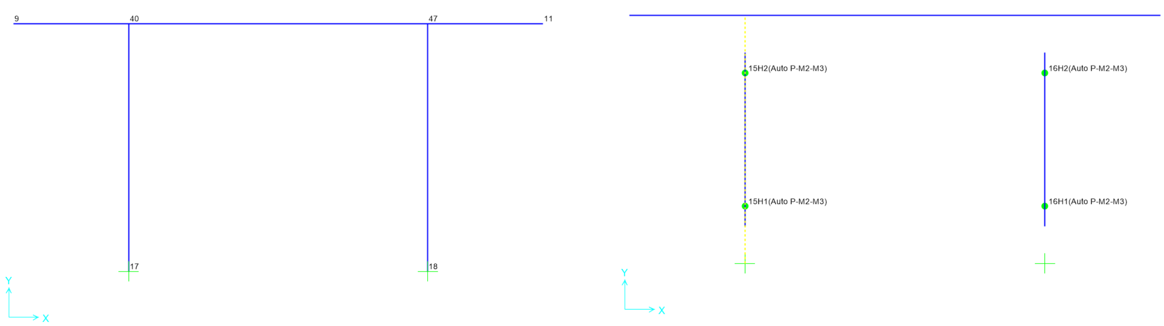

(a) Joint ID *(b) Column Plastic Hinge Location*

Figure 18: 2D pier model for pushover analysis: (a) Joint ID and (b) Hinge assignments

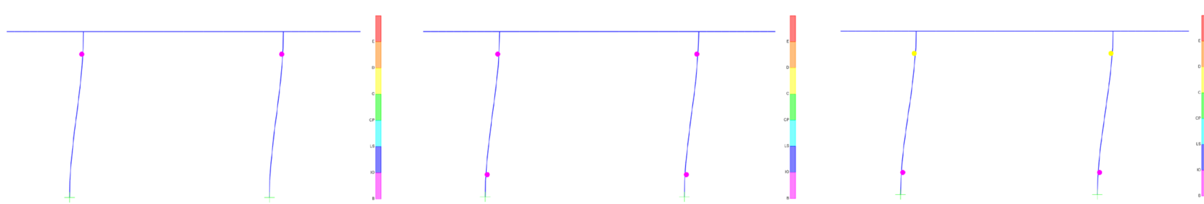

(a) Step 7: Initiation of Inelastic Response at top of columns *(b) Step 8: In Initiation of Inelastic Response bottom of columns* *(c) Step 9: Initiation of Non-linear 'Collapse Prevention (CP)' hinge at the top*

Figure 19: Hinges formation at different steps of pushover analysis

The response is linear until the hinge starts the form at the top of the pier at (step 7) and the bottom of the pier (step 8). The response follows the non-linear path until the fully plastic hinges are formed at step 55. The results and plots for all the four hinges in the linear response are displayed in *Figure 20*. The moments (M2) in both Hinges 15H1and 16H1 are 8855.54 kip-ft at Steps 7 and 8. The moments (M2) at Step 7 in the Hinges 15H2 and 16H2 are -8657.65 kip-ft.

The maximum moment at the location of 15H2 (30 in from Joint 17) is 8651.36 kip-ft, which is established to be the maximum moment capacity of the column from the pushover analysis.

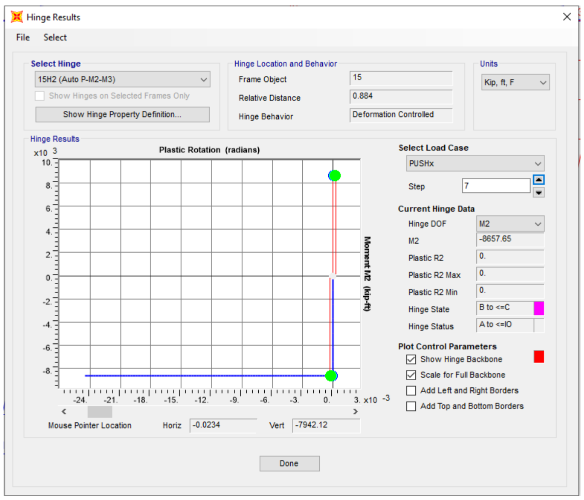

(a) 15H2

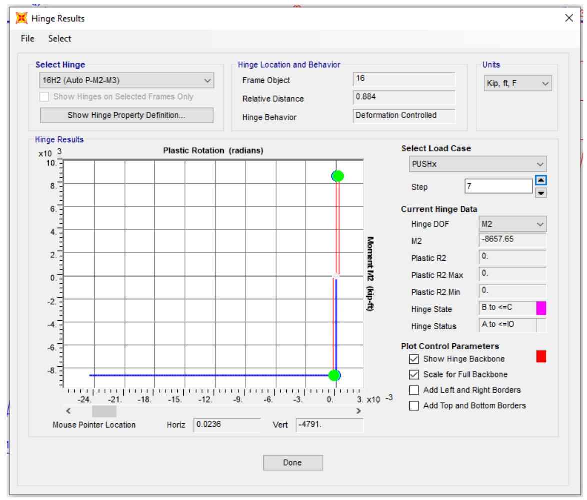

(b) 16H2

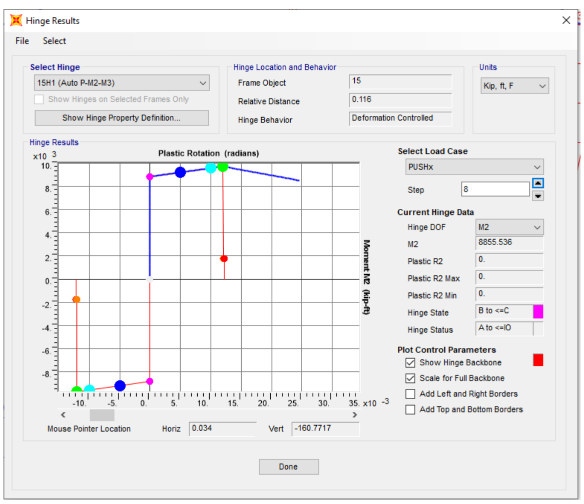

(c) 15H1

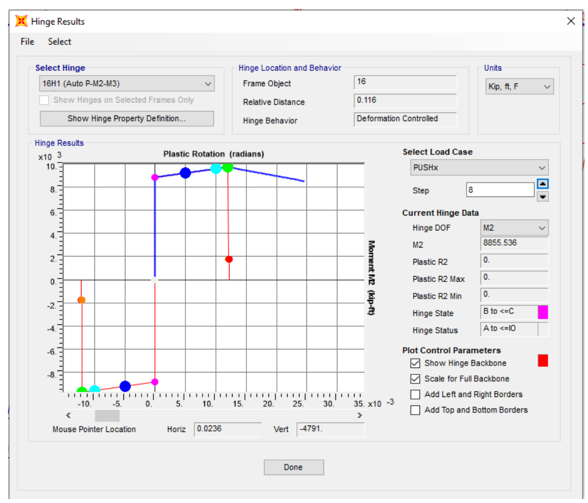

(d) 16H1

Figure 20: Hinges data and results at Step 7 of pushover analysis

The pushover curve is evaluated at Step 7 to get the maximum base shear (V_{bmax}) and maximum horizontal displacement in the linear zone (u_{max}) as shown in *Table 7*: Maximum base shear, moment, and deflection .

Table 7: Maximum base shear, moment, and deflection at different hinge stage

First Yield			Fully- plastic		
V_{bmax} (kip)	M_{max} $(kip-ft)$	u_y (in)	V_{bmax} (kip)	M_p $(kip-ft)$	u_p (in)
2497.73	8651.36	0.365	2681.95	9725.04	2.82

The pushover curve showing the base shear at different displacements is shown in *Figure 21*.

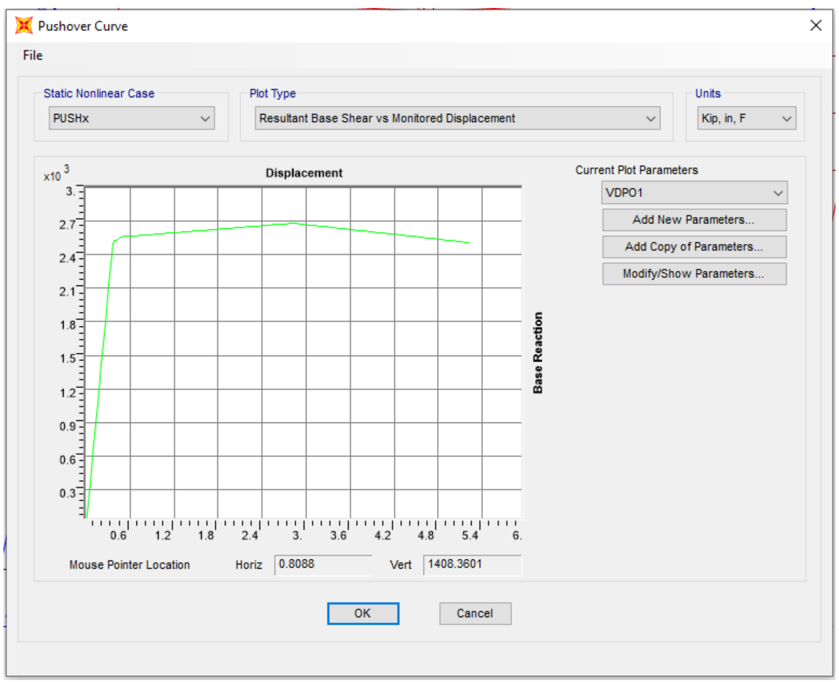

Figure 21: Pushover curve for displacement monitored analysis

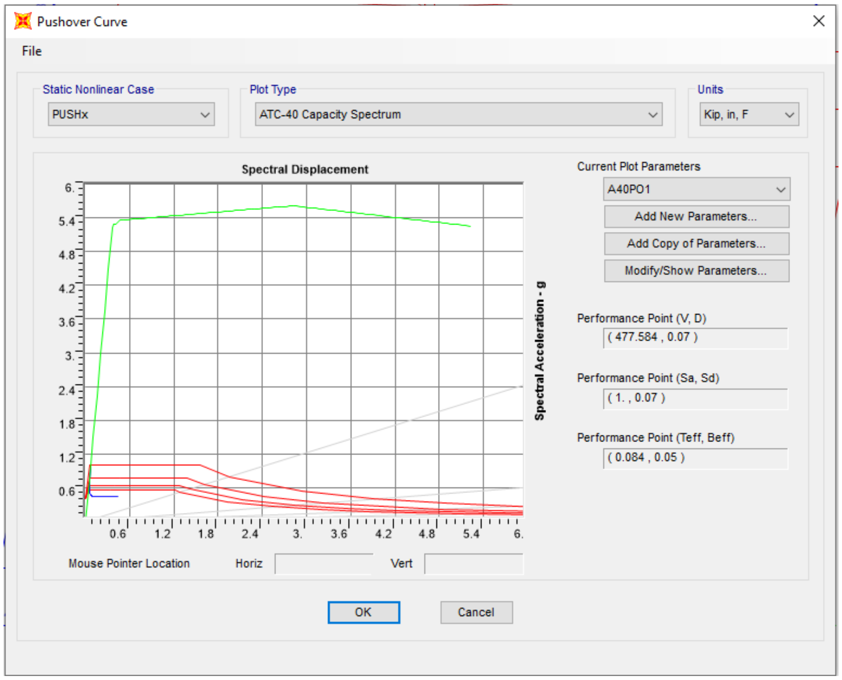

Figure 22: Base shear and capacity spectrum plot

Figure 22 shows the comparison of the capacity curve (green) with the demand spectrum (red).

The blue line represents the single demand spectrum with variable damping. The comparison shows that the capacity curve is significantly greater than the demand spectrum based on the response spectra. The performance point is the intersection point of the demand and the capacity curve. The pushover analysis is used to predict the potential weak areas of the structure estimating the strength capacity up to the post-elastic or ultimate limit and tracking the progressive damages through hinge formation. The formation of hinges under displacement-controlled pushover analysis estimates the high flexural or shear displacements that are expected to crack or yield at high intensity. The assessment of the hinge formation at the performance point shows that there is no local deformation. Therefore, the flexural or shear displacement value of the top of the column at the initial stage of hinge formation is compared against the displacements in further dynamic analyses.

4.2. Non-linear Time History Analysis

The dynamic analysis is performed to evaluate the time histories of the deck displacement and the pier cap displacement in the transverse direction. These relative displacements have been analyzed under different linking conditions between the superstructure and the substructure.

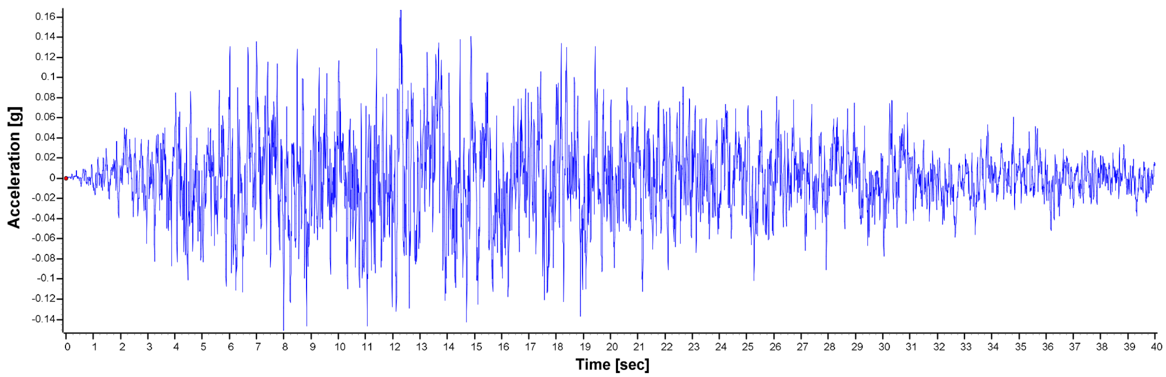

Figure 23: Ground acceleration time history scaled to MCE spectrum

The time history function for the Maximum Considered Earthquake (MCE) dominated by the motions in the transverse direction ($1.0EQ_x + 0.3EQ_y$) under the site-specific conditions is shown in *Figure 23*. All the seismic design parameters are calculated using the ASCE 7-16 Seismic Hazard tool, and the corresponding site-specific response spectrum for damping of 5% is shown in *Figure 24*.

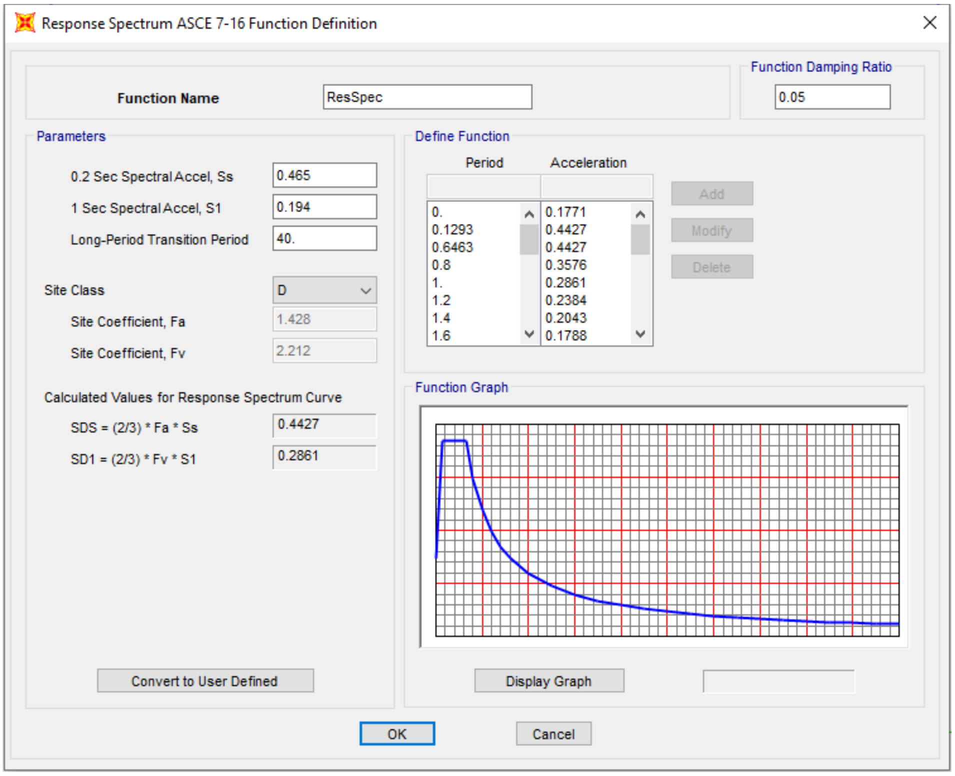

Figure 24: Site-specific response spectrum curve

The three different load cases are defined for the 2D model of the SAP2000 model: modal case, dead load case, and time history load case. As the superstructure is linked to the substructure using joint link elements, the dead load being applied should be defined as the non-linear time-history load. A ramp function with a ramp time of 5 seconds and an amplitude of 1 unit is defined. The slow ramp function is set as a time-history function to apply the dead load as dynamic load with high modal damping of 99% to limit the dynamic excitation of the system. The modal load case is modified to generate a maximum of 20 modes starting with the acceleration in x-direction as load vector. The dead load pattern and the built-in deformation modes for the joint links are also added in this load case. The fast non-linear analysis (FNA) load case is set up to start after the dead load case. The scaled MCE time history record in the transverse direction is the load applied in this load case. The time step data are defined to get the response for 40 seconds with the time steps size 0.001 second. The modal damping constant in this case is chosen as 5%.

The first analysis is run as a fixed system (FS) with a rigid link between the superstructure and the substructure at the position of the bearings. The relative displacements and the accelerations of both the deck and the pier cap overlap as shown in the plot functions in *Figure 25*.

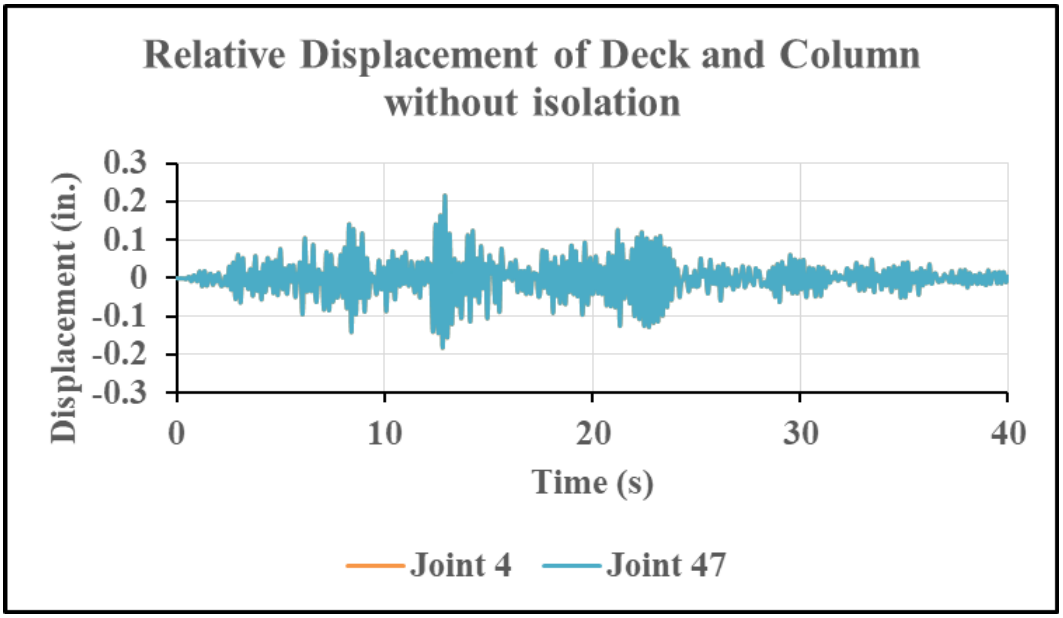

Figure 25: Displacement and pseudo-acceleration (PSA) plots in FS

The maximum displacements of the pier cap and the deck in the horizontal direction are 0.216 in and 0.217 in respectively. The displacement at the top of the column is equal to that of the pier cap as these are modeled as rigid elements. The maximum value of displacement from FNA does not exceed the displacement limit of 0.365 at the beginning of the hinge formation as observed in pushover analysis.

The response curve for the pseudo spectral accelerations at various levels of damping is shown in *Figure 26*. The graph shows that increasing the damping decreases the PSA at Joint 40 which is at the top of the column.

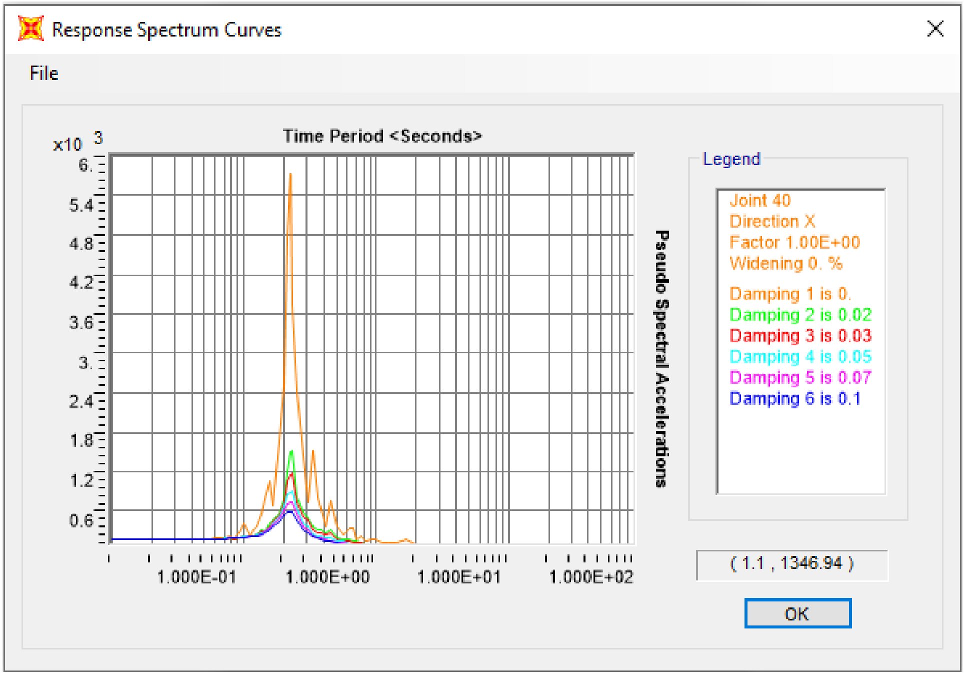

Figure 26: Response spectrum curve for the displacement of Joint 40 in FS

4.3. Influence of bearings in the isolation system

The bearing properties for two types of bearings are defined in the Link/Support Property command in SAP2000. The bearings are drawn as one joint link element as the multilinear plastic-type. The bearings are assumed to have a kinematic hysteresis curve obtained by plotting multilinear force-deformation values. The hysteresis sketch and the multilinear force-deformation parameters for the LP1 bearings are shown in *Figure 27*. Similarly, the parameters are defined for the FB1 in the separate model.

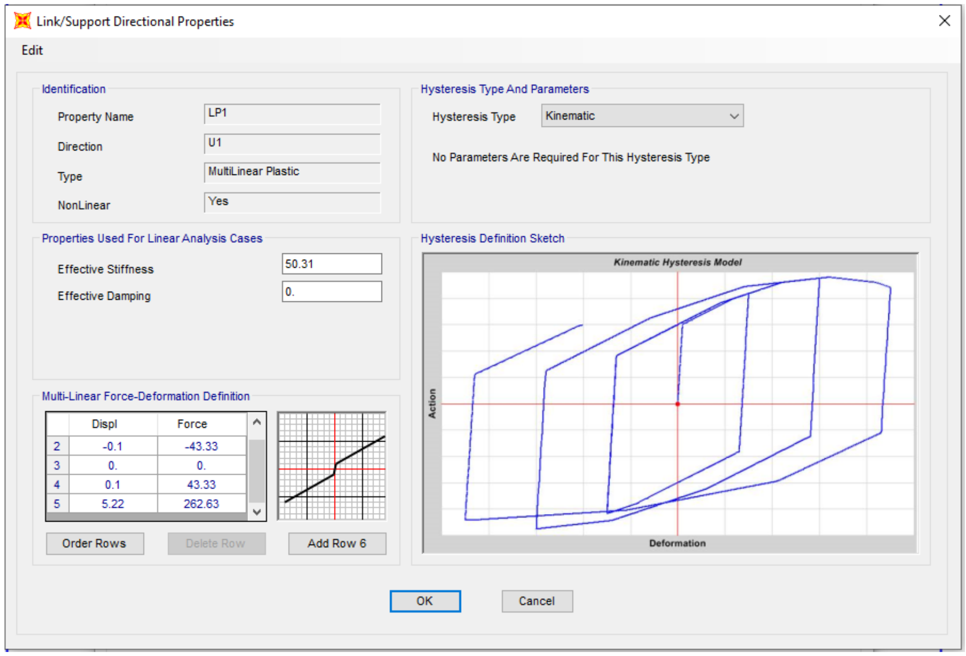

Figure 27: Definition of multi-linear plastic link: LP1

All three load cases are run after assigning the joint link as LP1 and FB1 successively at the location of bearings in the pier-cap beam element. The deformed shapes under the time-history load case are displayed at multiple time steps; the table for the relative displacements of the Joints is taken as output to obtain the maximum values of displacements at Joint 4 (in the superstructure) and Joint 47 (top of the right column). The displacement plots of relative joint displacement vs. time-period of loadings in both cases with LP1 and FB1 demonstrate that the superstructure is isolated from the substructure as shown in *Figure 28* and *Figure 29* respectively.

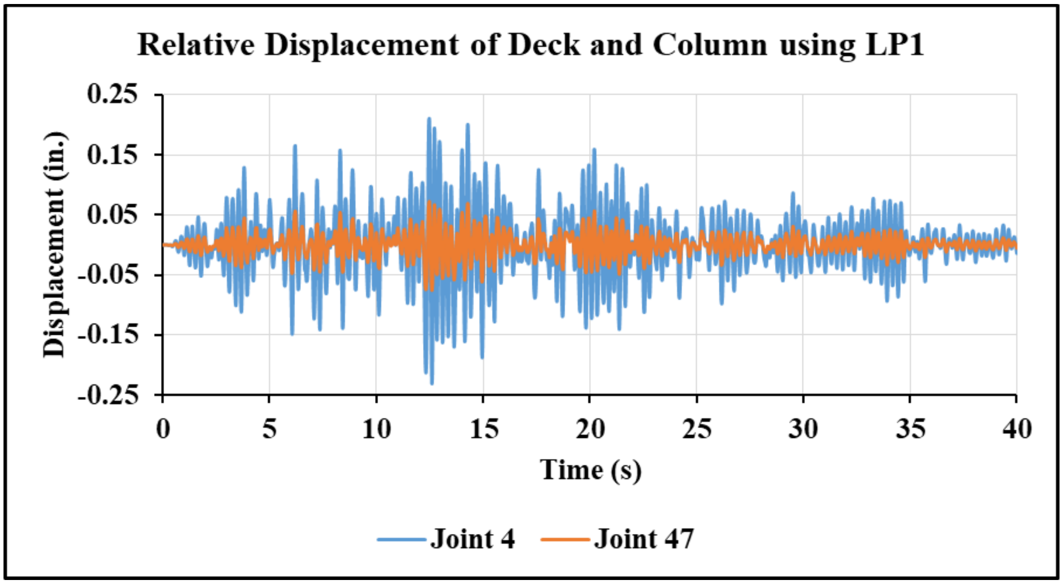

Figure 28: Relative displacement plots for Joint 4 and Joint 47 in LP1

The joint displacement in the deck (Joint 4) is greater than the joint displacement at top of the right column (Joint 47) as expected in isolated systems (IS).

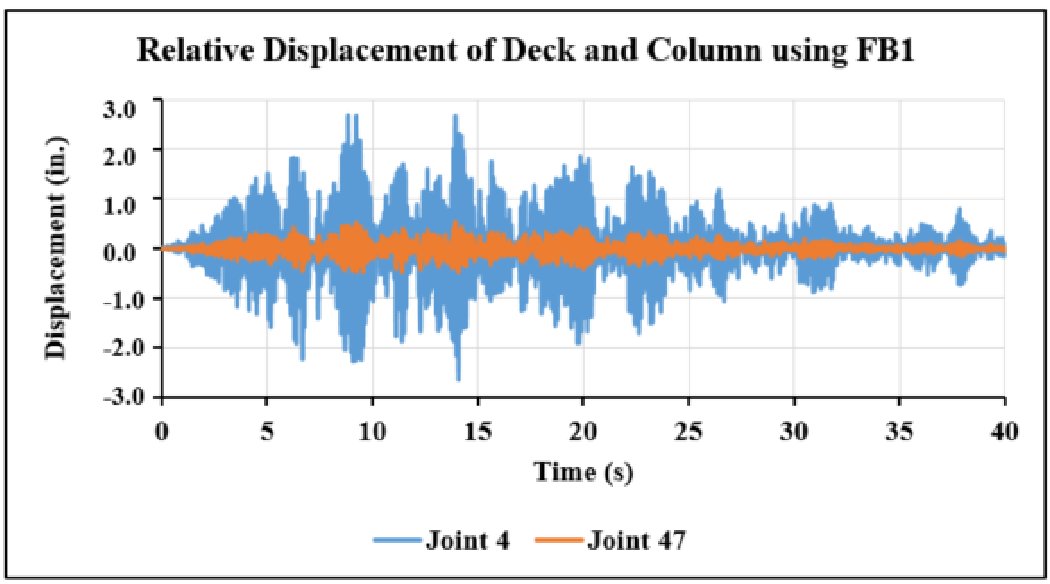

Figure 29: Relative displacement plots for Joint 4 and Joint 47 in FB1

The relative joint displacements in each scenario of link assignments are tabulated in *Table 8*. The relative displacements decrease at Joint 47 (top of the column) and increase at Joint 4 (deck) as compared to the FS case with the application of both LP1 and FB1 in the system. The relative joint displacement decreases to 0.011 *in* in FB1 system as compared to 0.075 *in* Joint 47. And, the relative joint displacements in the deck (Joint 4) increases from 0.213 *in* LP1case to 2.701 in in FB1 case. These values of relative displacements confirm that the FB1 allows the displacements of the superstructure more than that of the LP1 system, and this horizontal displacement is still in the range of maximum allowable displacement in the bridge system. The lower value of horizontal displacement at the top of the column ensures the risks of damages in the sub-structural system. The ductility demand ($\mu_D < 6.0$) for a two-column pier has been calculated for each case according to the AASHTO provision. The ductility demand (μ_D) decreases by 23.89% while using LP1. Similarly, it decreases by 35.22% while using FB1.

Table 8: Relative displacement in a column under time history analysis

	u_{47} (in)	u_4 (in)	μ_D (pier)	T_1 (s)	ω_1 (rad/s)
FS	0.216	0.217	1.59	0.22	27.97
LP1	0.075	0.231	1.21	0.27	22.54
FB1	0.011	2.701	1.03	0.25	24.19

As all of the values of the joint displacements in the columns are smaller than the critical value obtained from pushover analysis and the joint displacements in the deck are smaller than the maximum allowable due to bridge system constraints, the time history analyses confirm the effectiveness of bearings as isolation devices in this bridge model. The time-history analyses have only been performed for the force-based displacement capabilities, and the strength capabilities have not been investigated.

CHAPTER 5

CONCLUSIONS AND RECOMMENDATIONS

5.1. Summary and Conclusions

The 2DOF model of the bridge is first analyzed without any forcing function to get the dynamic characteristics. The dynamic properties of the undamped 2DOF system: the natural period (ω_n) and the period (T) are calculated using elastic stiffness, post-elastic stiffness, and the effective stiffness of each type of bearings. The displacements of each mass in the 2DOF system can be conveniently calculated using the natural frequencies and the effective earthquake forces (Duhamel integral). The isolation of the superstructure and the substructure due to the introduction of the isolation bearing (both LP1 and FB1) is evident from the displacement values of the center of masses. The system is then analyzed as a single degree of freedom (SDOF) system with total mass lumped at the centroid of the pier cap without accounting for the stiffness provided by any of the bearings. The maximum displacement of this fixed system (FS) is calculated to 0.15 *in* the horizontal direction which is large as compared to the 0.029 in the displacement of the pier in an isolated system (IS).

The non-linear pushover analysis is performed to estimate the sequence and the pattern of plastic hinge formation, and evaluate the hinges status. The inelastic linear response under the lateral force is observed first at top of columns in both the hinges 15H2 and 16H2 at Step 7, and also at the bottom of the columns in the hinges 15H1 and 16H1 at next Step 8. The non-linear 'CP' hinges are formed at Step 9 at the top of the columns.

The pushover curve is evaluated at Step 7 to get the maximum base shear ($V_{bmax} = 2144.85\ kip$) and maximum horizontal displacement ($u_{max} = 0.313\ in$). The assessment of the hinge formation at the performance point shows that there is no local deformation. The dynamic analysis is performed to evaluate the time histories of the deck displacement and the pier cap displacement in the transverse direction. The fast non-linear analysis (FNA) load case is set up to start after the dead load case. The displacement plots of relative joint displacement vs. time-period of loadings in both cases with LP1 and FB1 demonstrate that the superstructure is isolated from the substructure. These values of relative displacements confirm that the FB1 (2.701 in) allows the displacements of superstructure more than that of the LP1 (0.231 in) system, and this horizontal displacement is still in the range of maximum allowable displacement (5.22 in) in the bridge system.

5.2. Recommendation for Future Work

The scope of this work is limited to the analysis of one pier out of three piers supporting the 780 ft long girders. These static and dynamic analyses provide quick results on the effectiveness of different types of bearings as isolation devices. However, the following recommendations are made for more accurate and reliable analyses to design or analyze the isolation system in newly planned bridges or the bridges that require retrofitting.

1. Instead of modeling the fixed-base of columns; use the soil-structure interaction (SSI) approach
2. Account for the eccentricity of the bearings based on their attachment in the pier cap, and analyze the deformations in the link elements representing the bearings
3. Incorporate the deck stiffness in the transverse direction
4. Evaluate the strength capabilities, not merely the displacement capabilities.

BIBLIOGRAPHY

AASHTO. (2010). AASHTO LRFD Bridge Design Specifications. In *Chemistry &* Fourth edition with 2008 interim revisions. Washington, D.C. : American Association of State Highway and Transportation Officials, [2008] ©2007. https://search.library.wisc.edu/catalog/9910071548102121

AASHTO. (2011). AASHTO guide specifications for LRFD seismic bridge design. In *Transportation* (Issue May). AASHTO. https://searchworks.stanford.edu/view/11842518%0Ahttps://bookstore.transportation.org/item_details.aspx?ID=1915

Black, W., Freyne, S., Cummins, J., Stacy, B., Strange, C., Crittle, M., & Chapin, G. (2021). *2020 Mississippi Infrastructure Report Card*. https://infrastructurereportcard.org/state-item/mississippi/

Chen, W.-F., & Duan, L. (2003). *Bridge engineering: substructure design*. CRC Press.

Chen, W.-F., & Duan, L. (2014). *Bridge engineering handbook: construction and maintenance*. CRC press.

Chopra, A. K. (2017). Dynamics of structures. theory and applications to. *Earthquake Engineering*.

CSI. (2009). *SAP2000: Integrated software for structural analysis and design* (21.0.2). Computers and Structures Inc. https://www.csiamerica.com/

Feng, D., & Zhang, F. (2020). Seismic Isolation Retrofitting of Typical Multi-Span Steel Girder Bridges in New York State. *Transportation Research Record*, *2674*(8), 785–798. https://doi.org/10.1177/0361198120924665

Ghosh, G., Singh, Y., & Thakkar, S. K. (2011). Seismic response of a continuous bridge with bearing protection devices. *Engineering Structures*, *33*(4), 1149–1156. https://doi.org/10.1016/j.engstruct.2010.12.033

Konstantinidis, D., Kelly, J. M., & Makris, N. (2009). Experimental investigation on the seismic response of bridge bearings. *International Conference on Advances in Experimental Structural Engineering*, *2009-Octob*(October).

Kumar, M., Whittaker, A. S., & Constantinou, M. C. (2014). An advanced numerical model of elastomeric seismic isolation bearings. *Earthquake Engineering and Structural Dynamics*, *43*(13), 1955–1974. https://doi.org/10.1002/eqe.2431

Lo Monte, F., Pozzuoli, C., Mola, E., & Mola, F. (2018). Seismic Vulnerability Assessment and Retrofitting Design of a Multispan Highway Bridge: Case Study. *Journal of Bridge Engineering*, *23*(2), 05017016. https://doi.org/10.1061/(asce)be.1943-5592.0001148

Manos, G. C., Mitoulis, S., Kourtidis, V., Sextos, A., & Tegos, I. (2007). Study of the behavior of Steel Laminated Rubber Bearings under prescribed loads. *10th World Conference on Seismic Isolation, Energy Dissipation and Active Vibrations Control of Structures*, *2*(December), 12.

Manos, George C., Mitoulis, S. A., & Sextos, A. G. (2012). A knowledge-based software for the preliminary design of seismically isolated bridges. *Bulletin of Earthquake Engineering*, *10*(3), 1029–1047. https://doi.org/10.1007/s10518-011-9320-0

Mullen, C. L. (2011). *SEISMIC VULNERABILITY OF CRITICAL BRIDGES*.

Naeim, F. (1989). *The seismic design handbook*. Springer Science & Business Media.

Naeim, F., & Kelly, J. M. (1999). Design of Seismic Isolated Structures: From Theory to Practice. In *John Wiley & Sons, Inc.* (Vol. 16, Issue 3). https://doi.org/10.1193/1.1586135

Qiang, Z., Yaozhuang, L., & Kolozvari, K. (2018). Numerical modeling of steel–concrete composite structures. *Structural Concrete*, *19*(6), 1727–1739. https://doi.org/10.1002/suco.201700094

Raffaele, D., Porco, F., Fiore, A., & Uva, G. (2014). Simplified vulnerability assessment of reinforced concrete circular piers in multi-span simply supported bridges. In *Structure and Infrastructure Engineering* (Vol. 10, Issue 8, pp. 950–962). Taylor & Francis. https://doi.org/10.1080/15732479.2013.772642

Ryan, K. L., Kelly, J. M., & Chopra, A. K. (2005). Nonlinear Model for Lead–Rubber Bearings Including Axial-Load Effects. *Journal of Engineering Mechanics*, *131*(12), 1270–1278. https://doi.org/10.1061/(asce)0733-9399(2005)131:12(1270)

Sanchez, J., Masroor, A., Mosqueda, G., & Ryan, K. (2013). Static and Dynamic Stability of Elastomeric Bearings for Seismic Protection of Structures. *Journal of Structural Engineering*, *139*(7), 1149–1159. https://doi.org/10.1061/(asce)st.1943-541x.0000660

Takahashi, Y. (2012). *Damage of Rubber Bearings and Dambers of Bridges in 2011 Great East Japan Earthquake*. 1333–1342.

Tonias, D. E., & Zhao, J. J. (1995). *Bridge engineering: design, rehabilitation, and maintenance of modern highway bridges*. McGraw-Hill.

Tubaldi, E., Mitoulis, S. A., Ahmadi, H., & Muhr, A. (2016). A parametric study on the axial behaviour of elastomeric isolators in multi-span bridges subjected to horizontal seismic excitations. *Bulletin of Earthquake Engineering*, *14*(4), 1285–1310. https://doi.org/10.1007/s10518-016-9876-9

Warn, G. P., Whittaker, A. S., & Constantinou, M. C. (2007). Vertical Stiffness of Elastomeric and Lead–Rubber Seismic Isolation Bearings. *Journal of Structural Engineering*, *133*(9), 1227–1236. https://doi.org/10.1061/(asce)0733-9445(2007)133:9(1227)

Watson, R. J. (2014). High Load Multirotational Disk Bearings for Civil Engineering Structures. *Istanbul Bridge Conference*.

Yamamoto, S., Kikuchi, M., Ueda, M., & Aiken, I. D. (2009). A mechanical model for elastomeric seismic isolation bearings including the influence of axial load. *Earthquake Engineering and Structural Dynamics*, *38*(2), 157–180. https://doi.org/10.1002/eqe.847

LIST OF APPENDICES

A1. MDOT Relevant Bridge Drawings

A1.1. Overall Bridge and Elevation

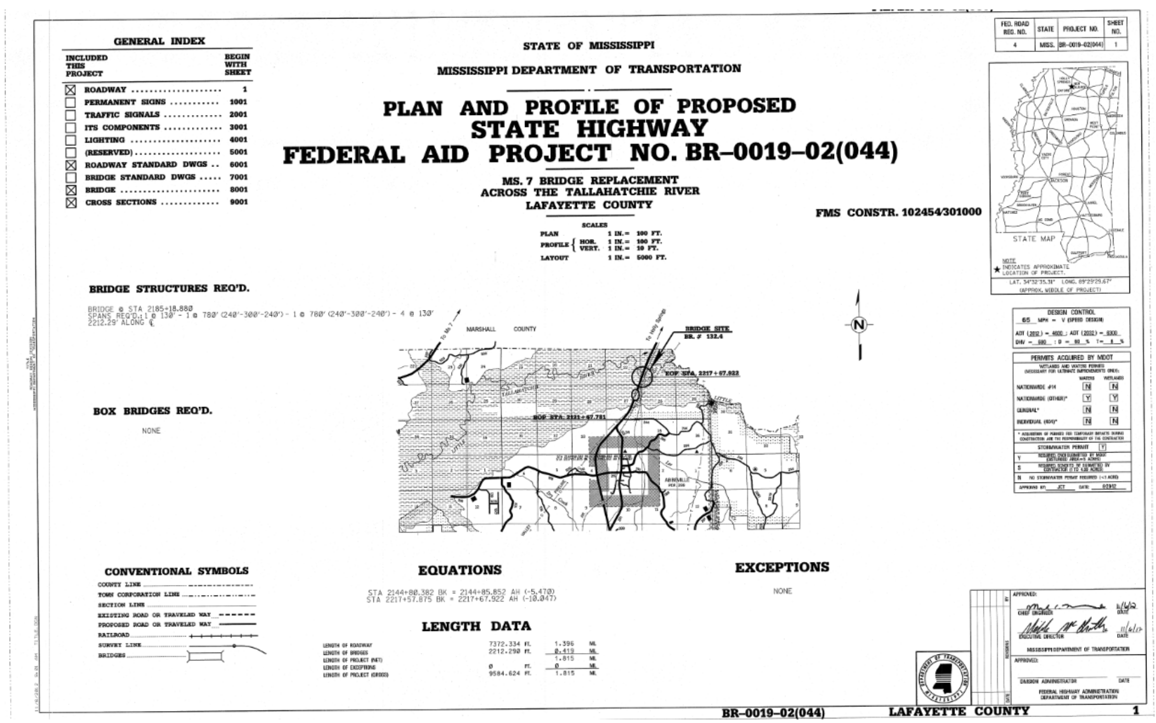

Image A 1: Location and Project Outline of Little Tallahatchie River Bridge

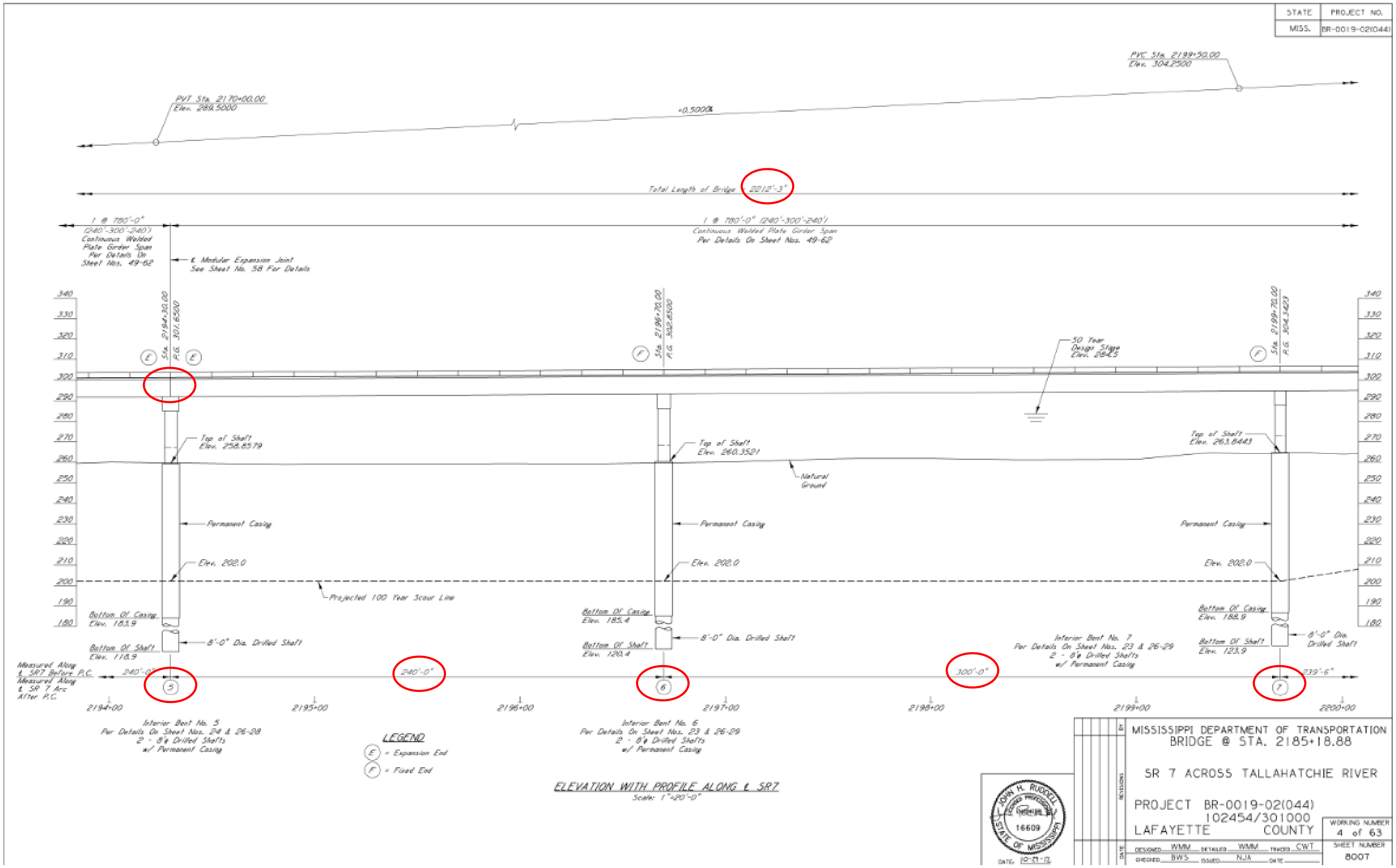

Image A 2: Beginning of 780 ft steel-girder supported over Piers 5, 6 and 7

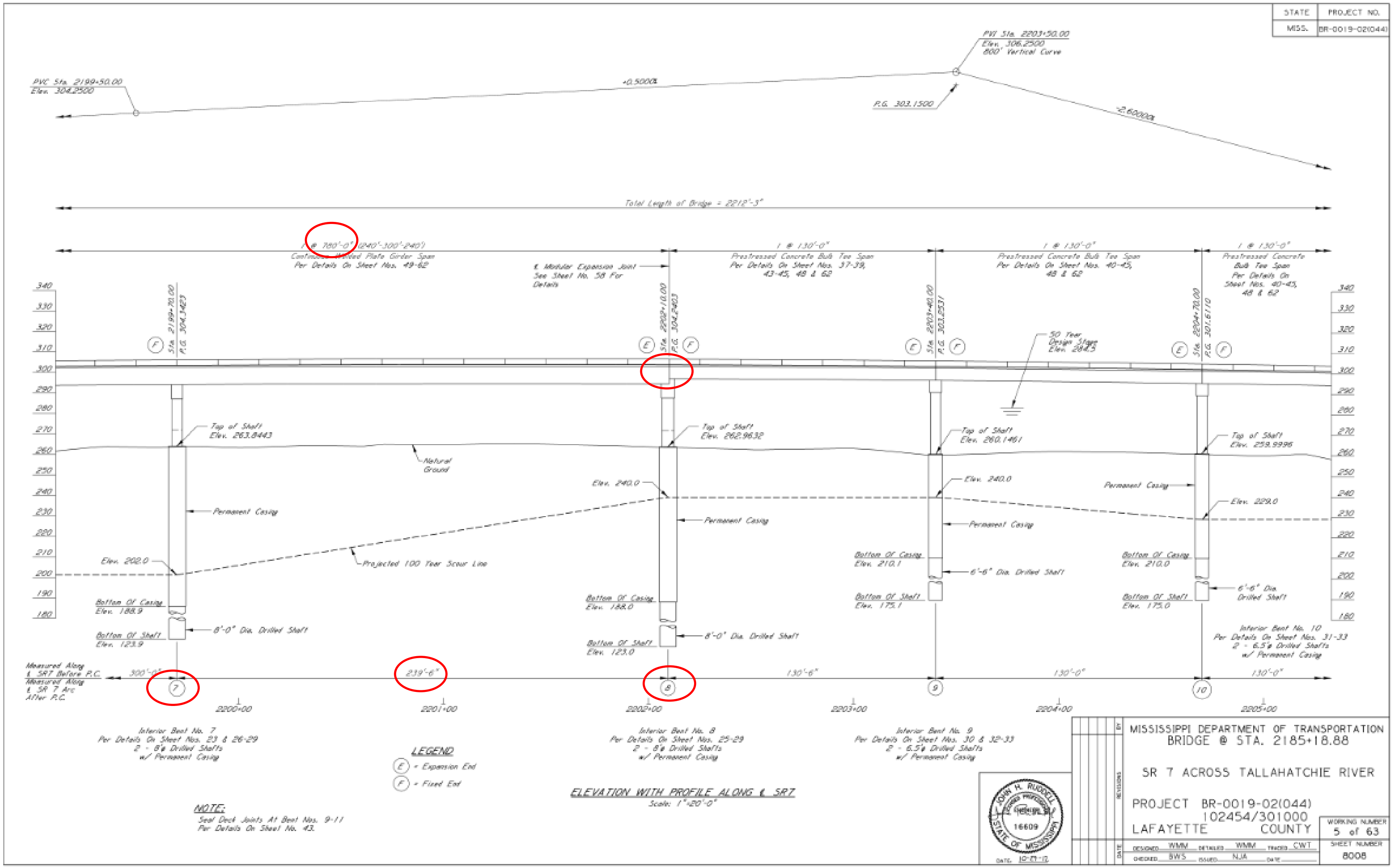

Image A 3: End of 780 ft steel-girder supported over Piers 7 and 8

A1.2. Pier Details

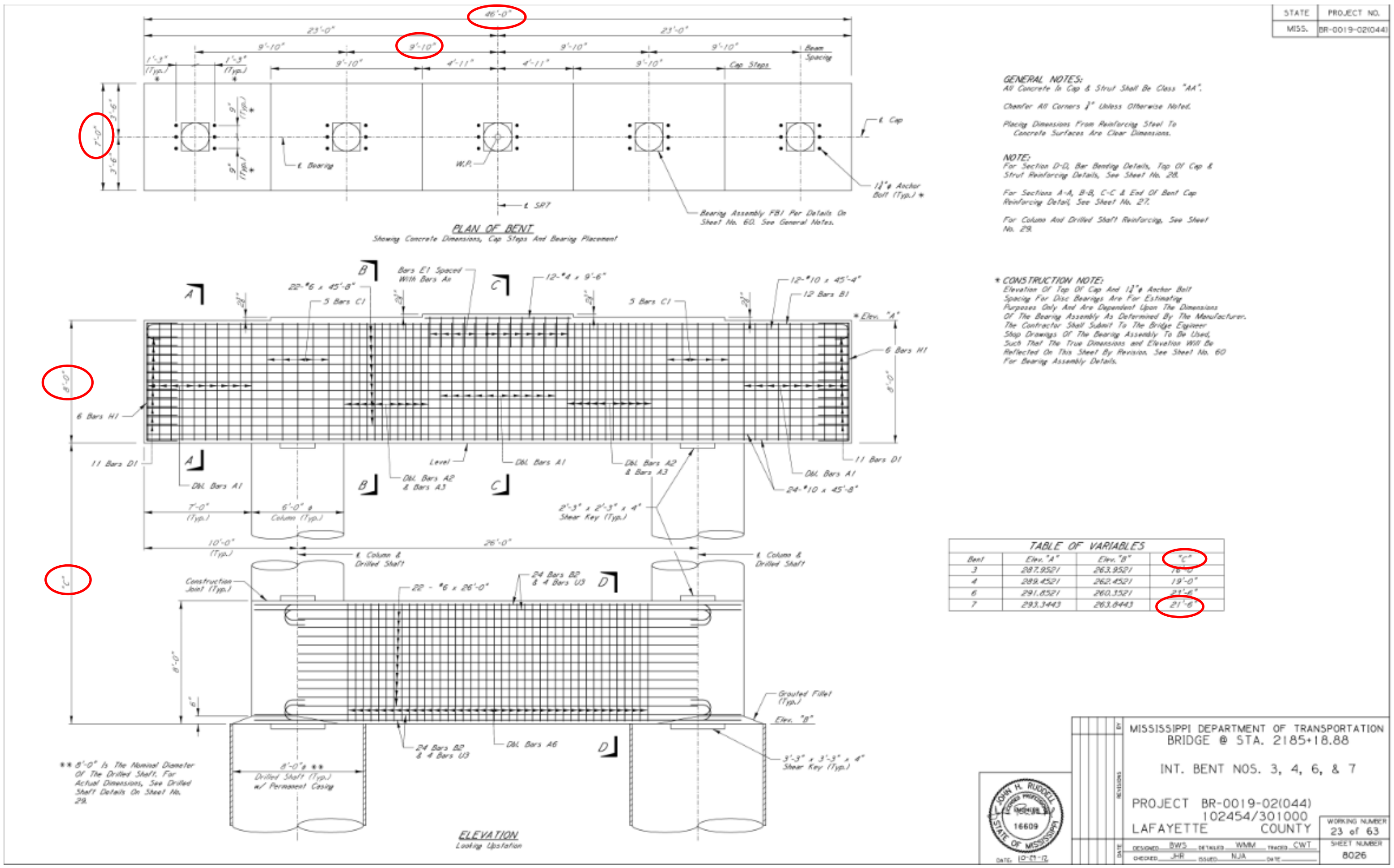

Image A 4: Dimensions and details of Bent No. 7

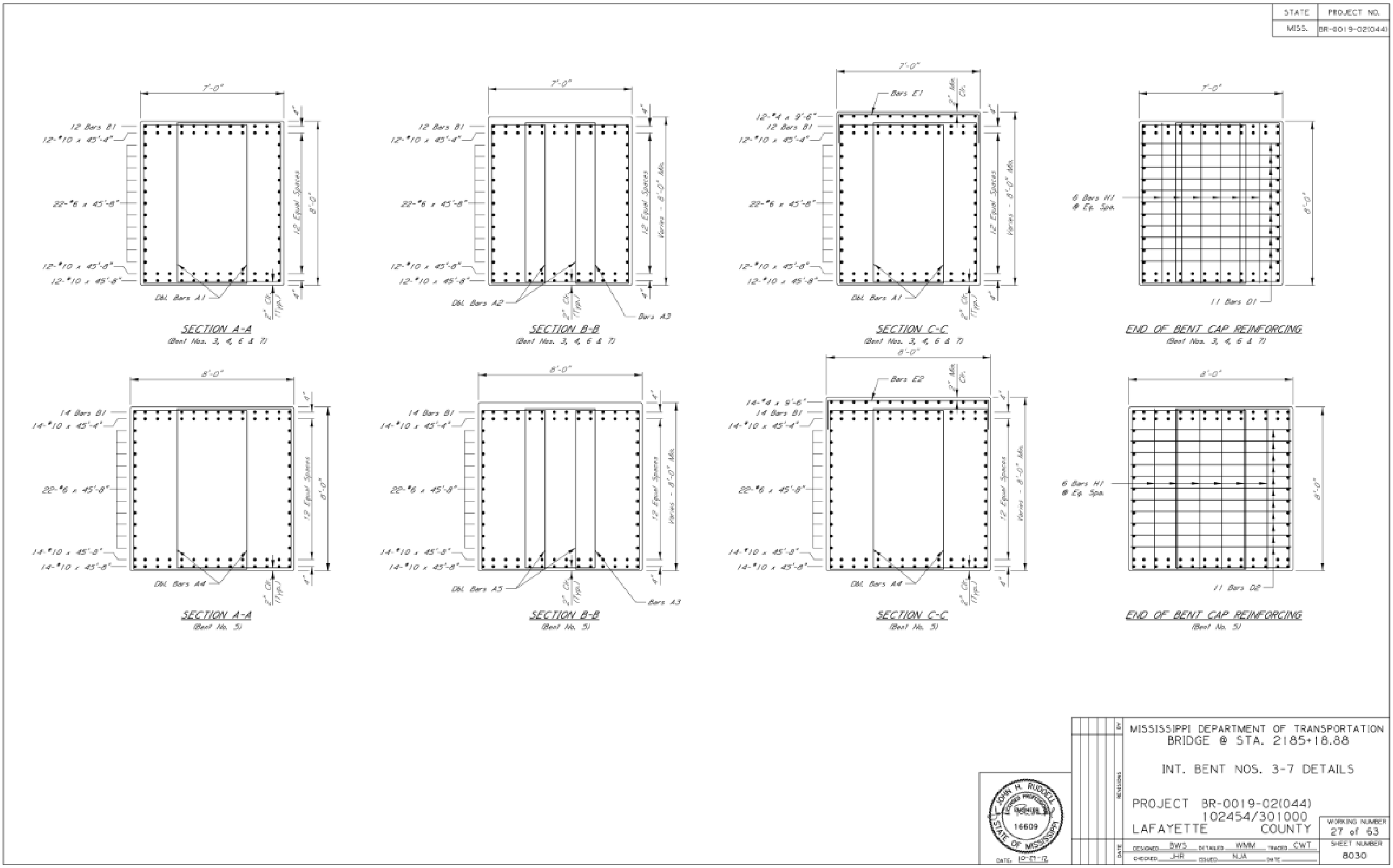

Image A 5: Cross-sectional details of Bent 7

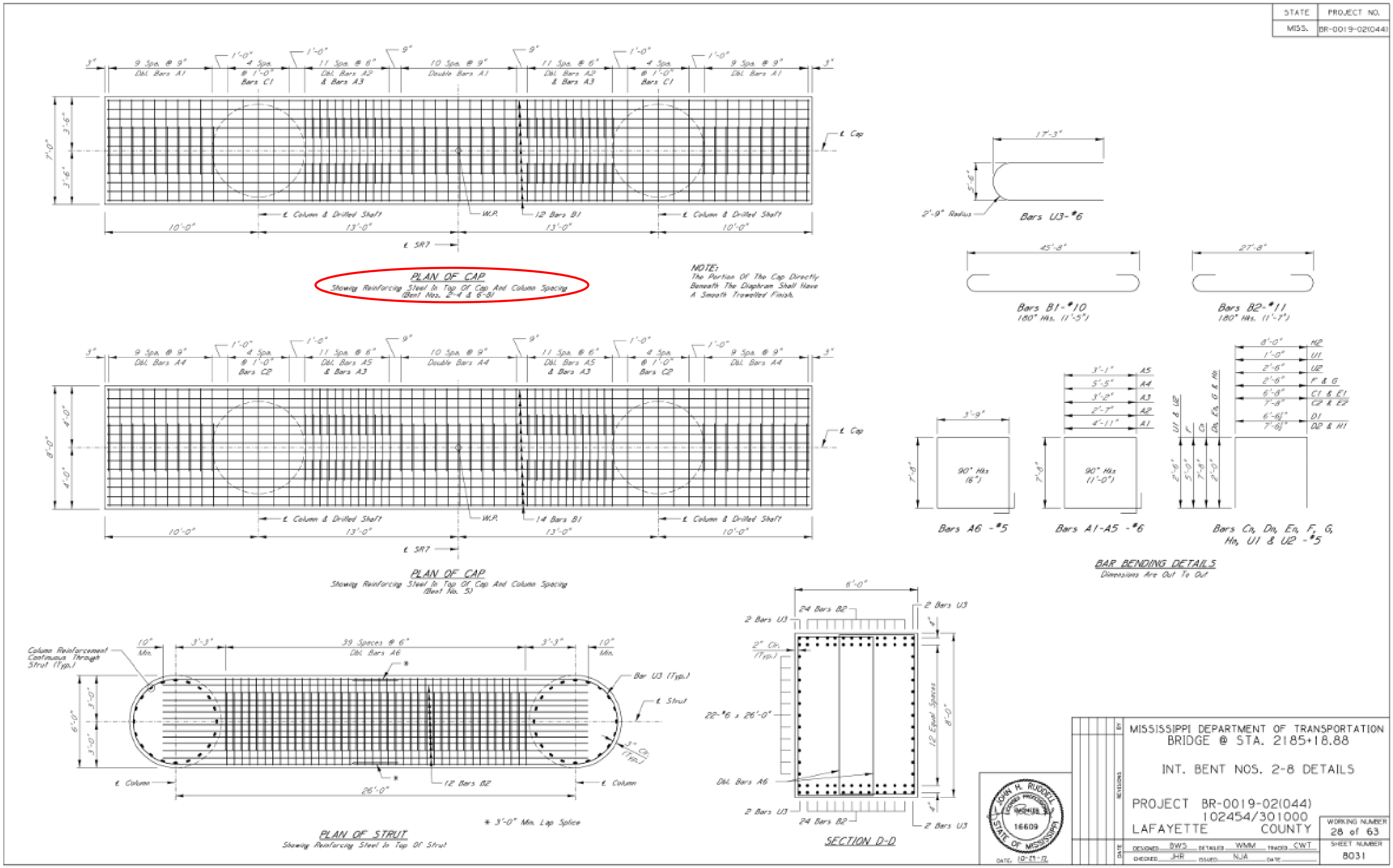

Image A 6: Plan view and reinforcement distribution in Bent 7

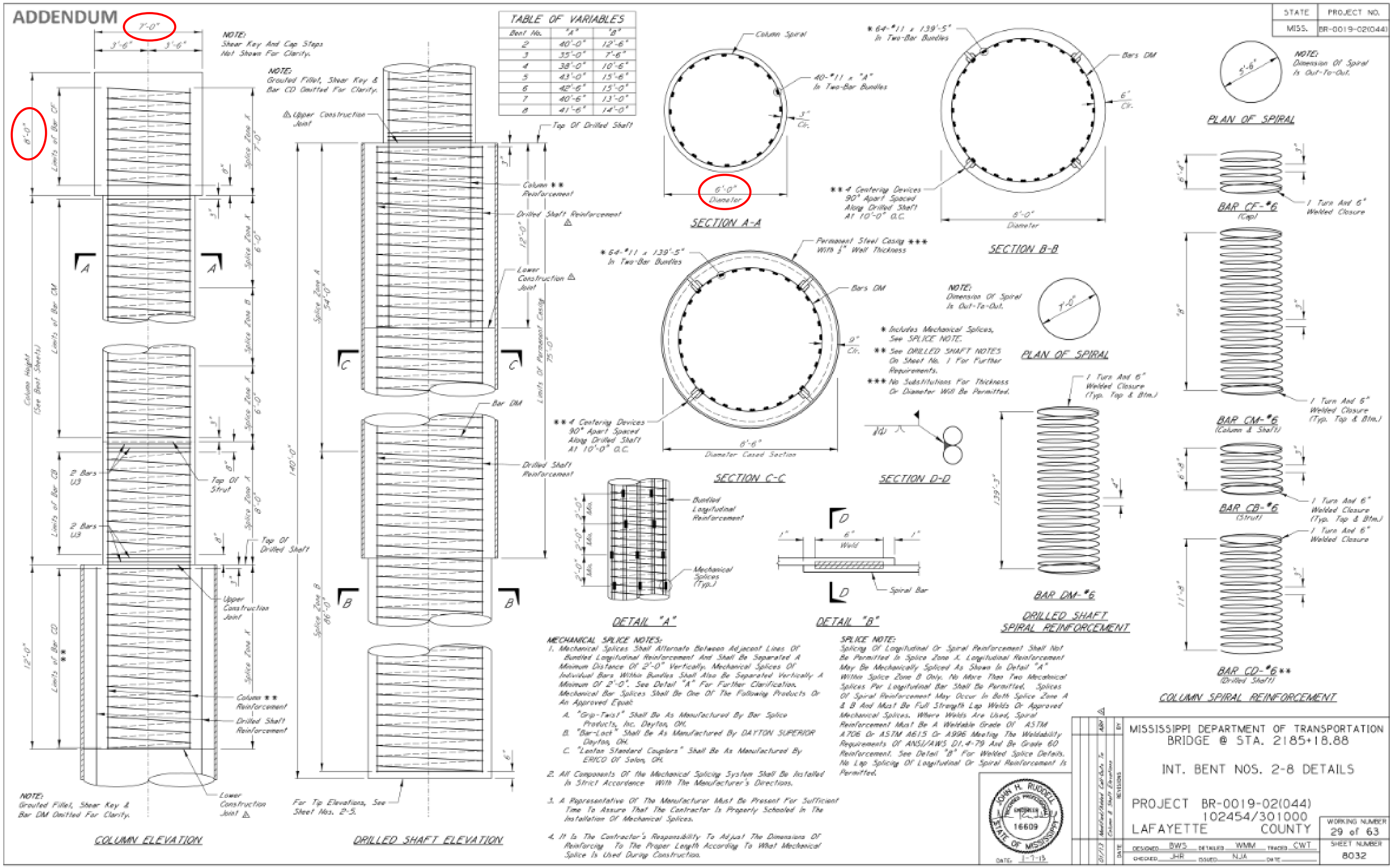

Image A 7: Dimensions and reinforcements in columns in Bent 7

A1.3. Span Details

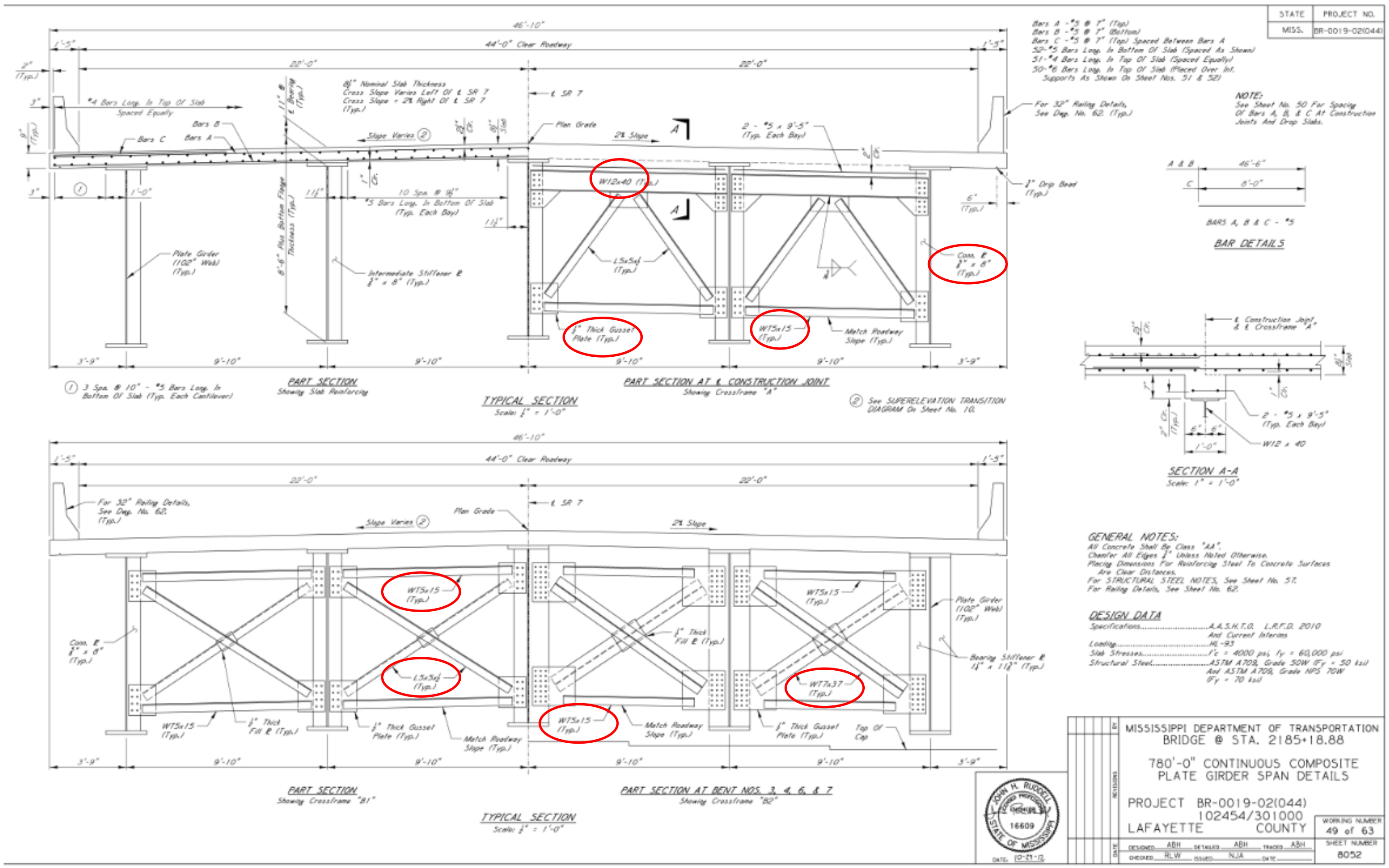

Image A 8: Typical sections of cross frames in the transverse direction of 780 ft girder

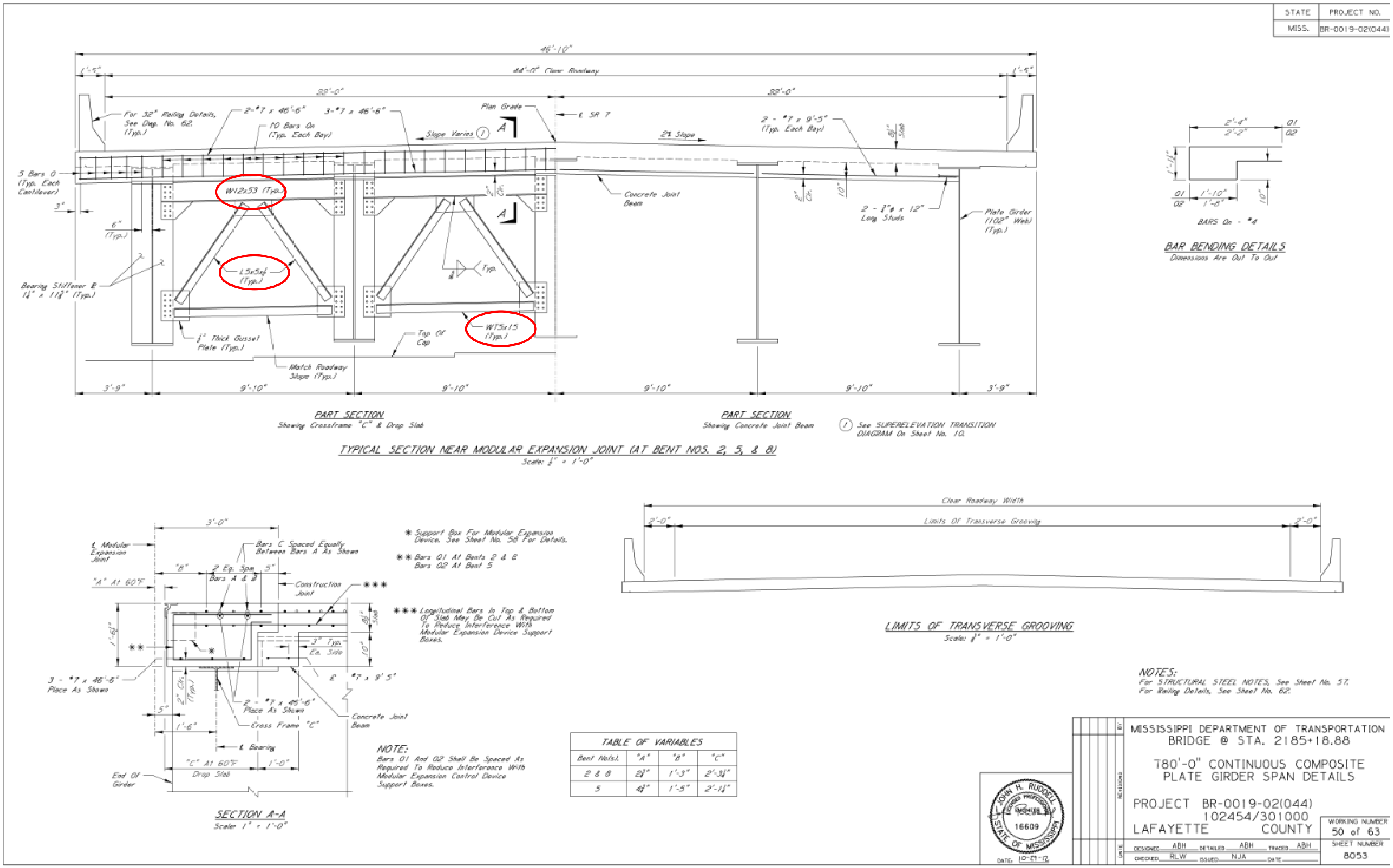

Image A 9: Typical sections of cross frames in the transverse direction of 780 ft girder

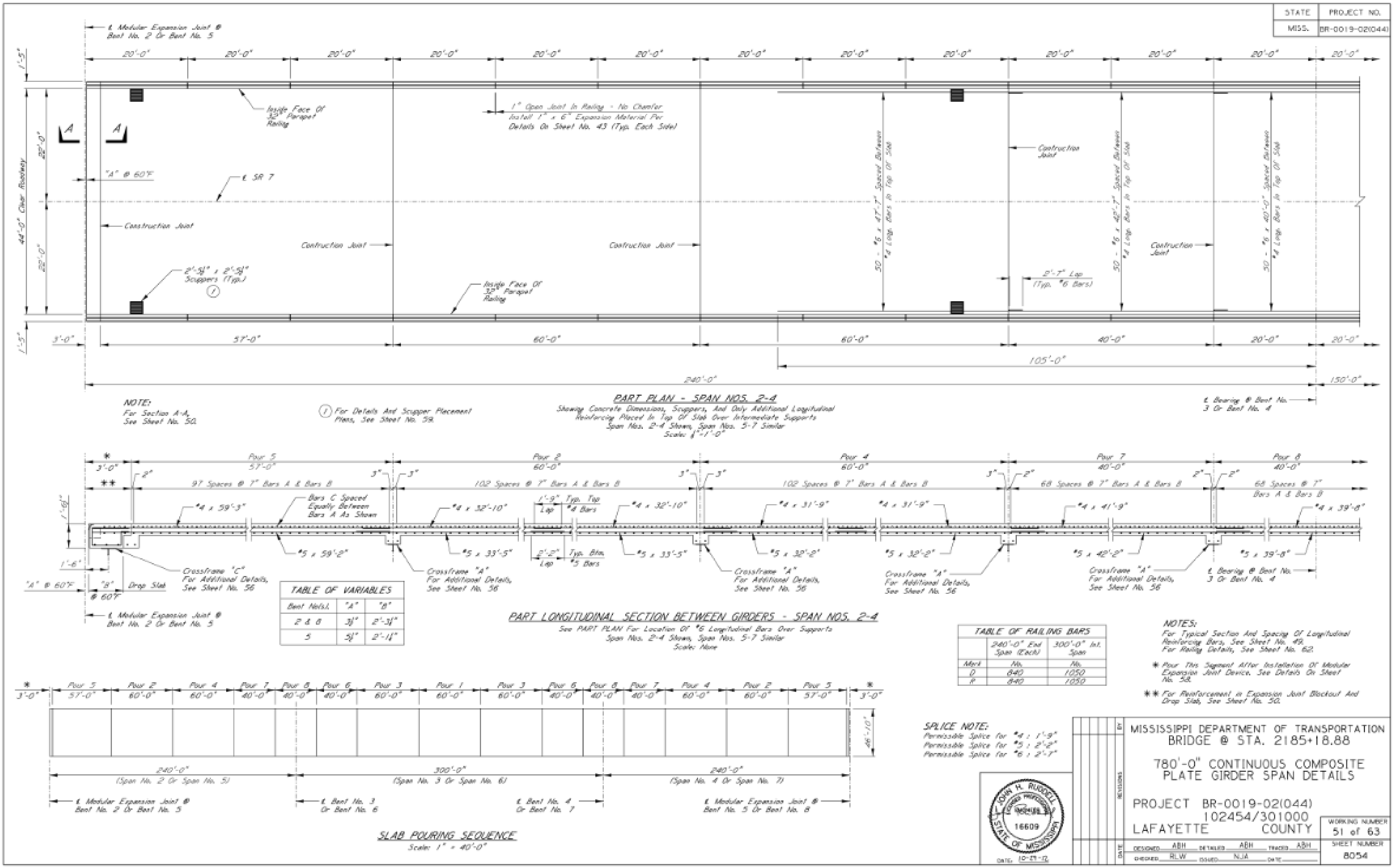

Image A 10: Beginning of span details

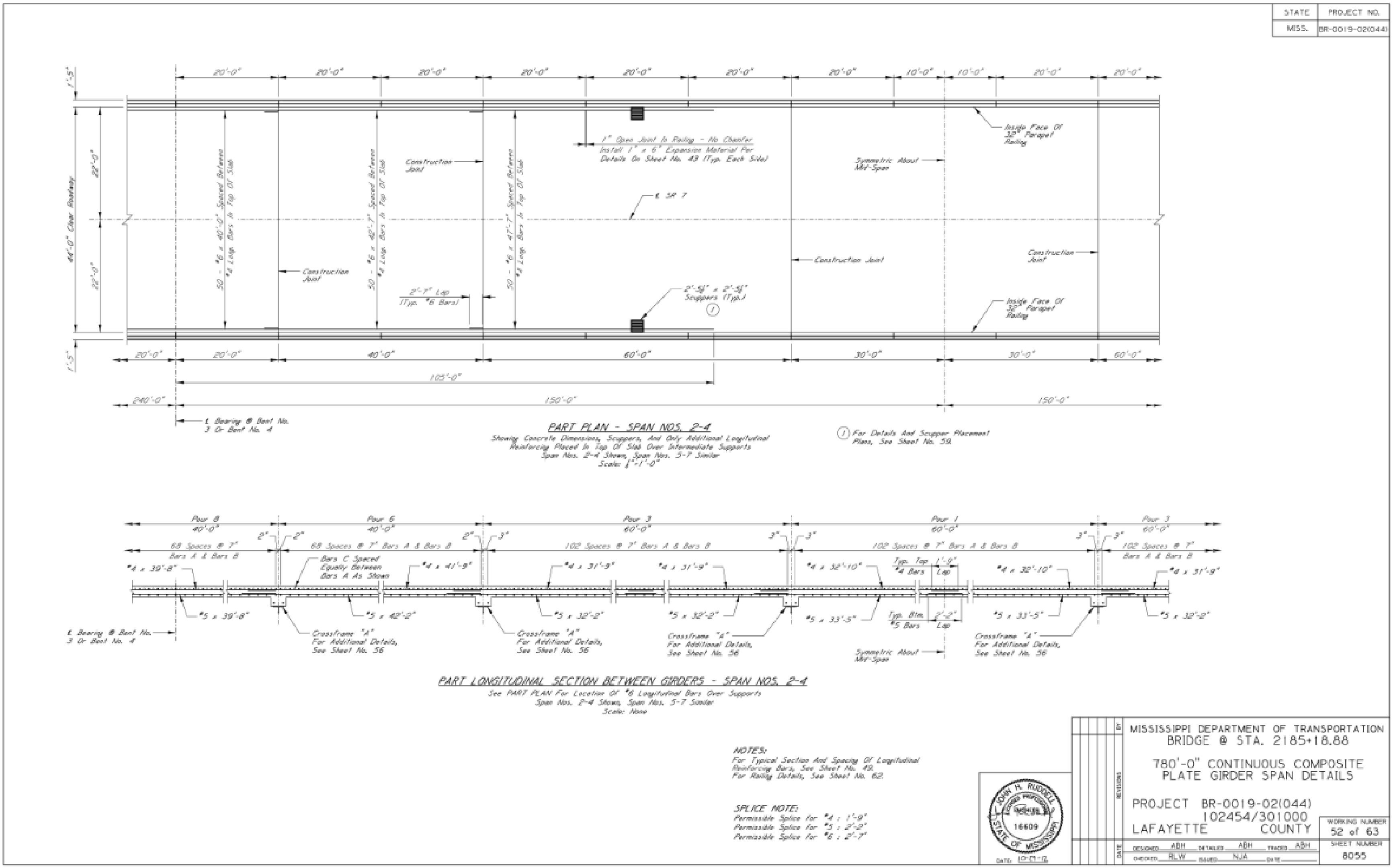

Image A 11: End of span details

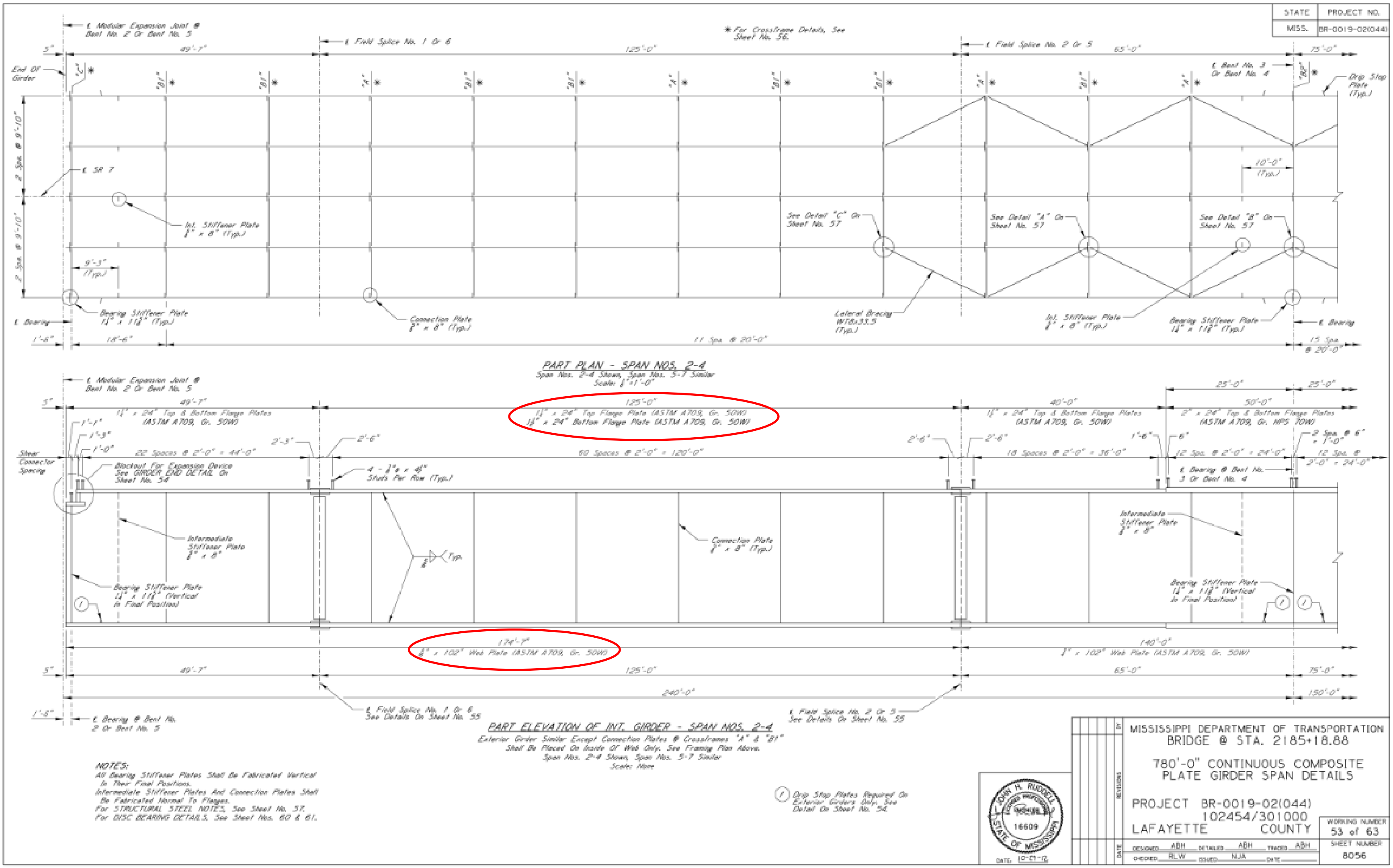

Image A 12: Bracing locations and dimension detailing in the span

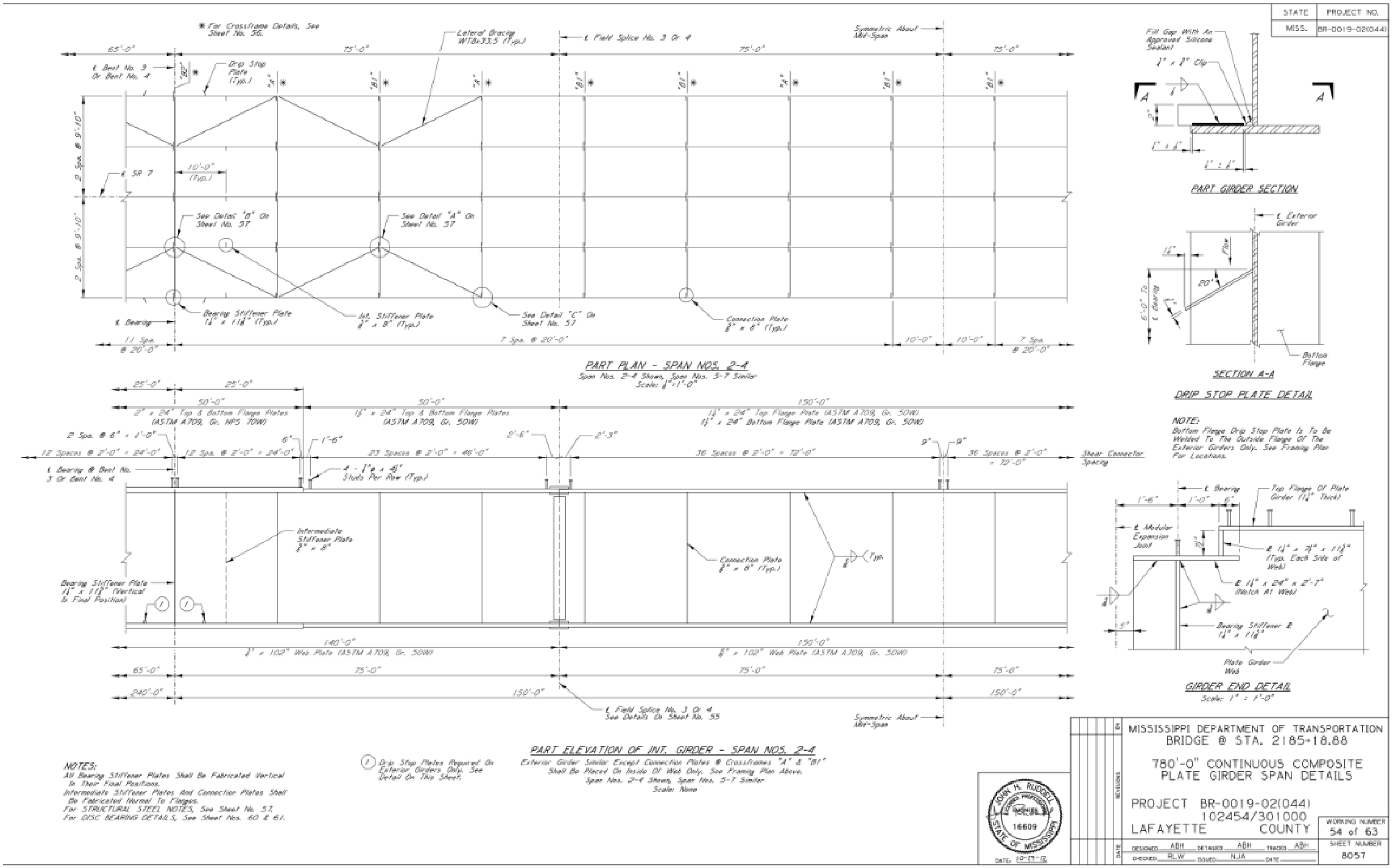

Image A 13: Bracing locations and dimension detailing in the span

A1.4. Bearing Details

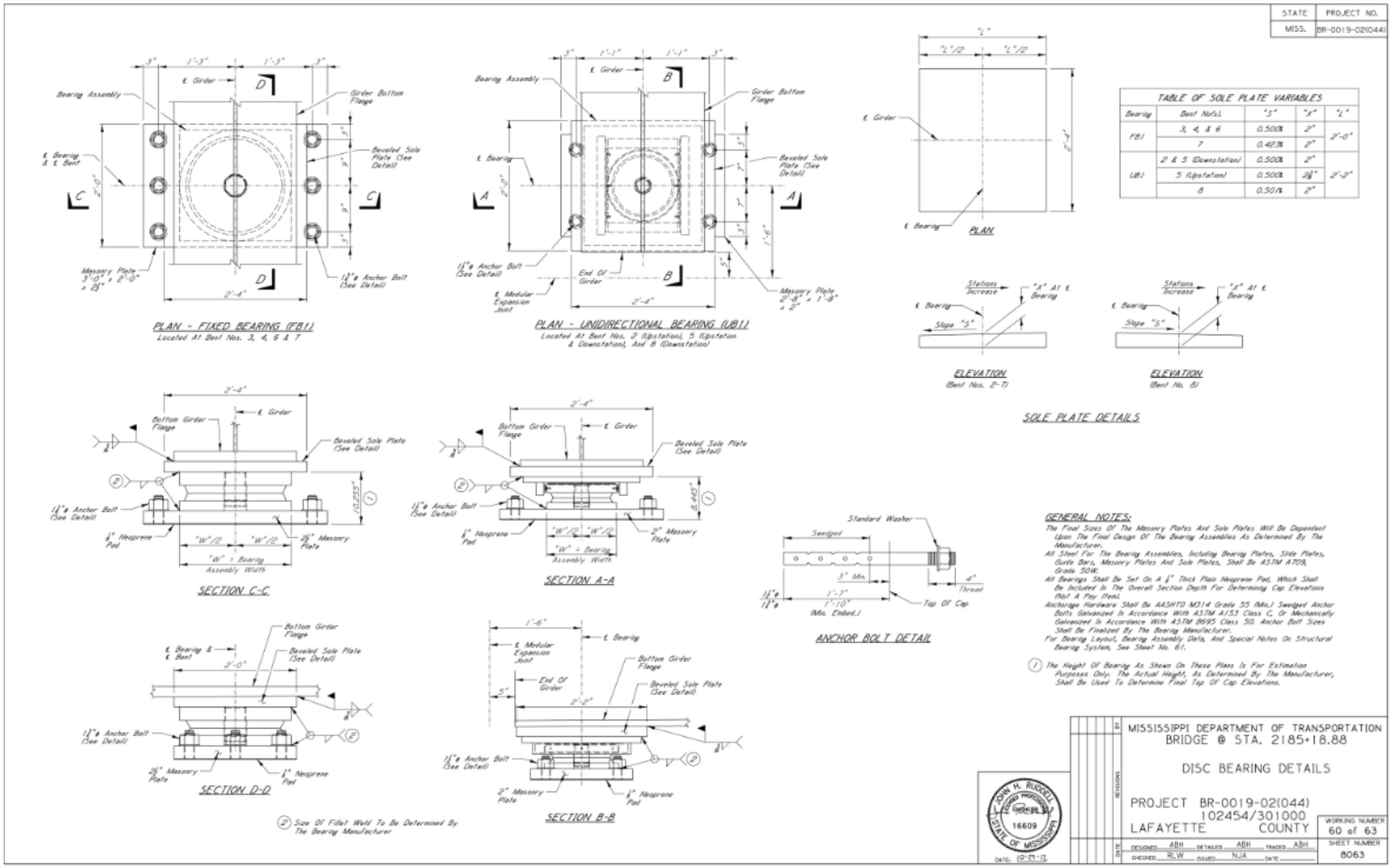

Image A 14: Disc bearings details

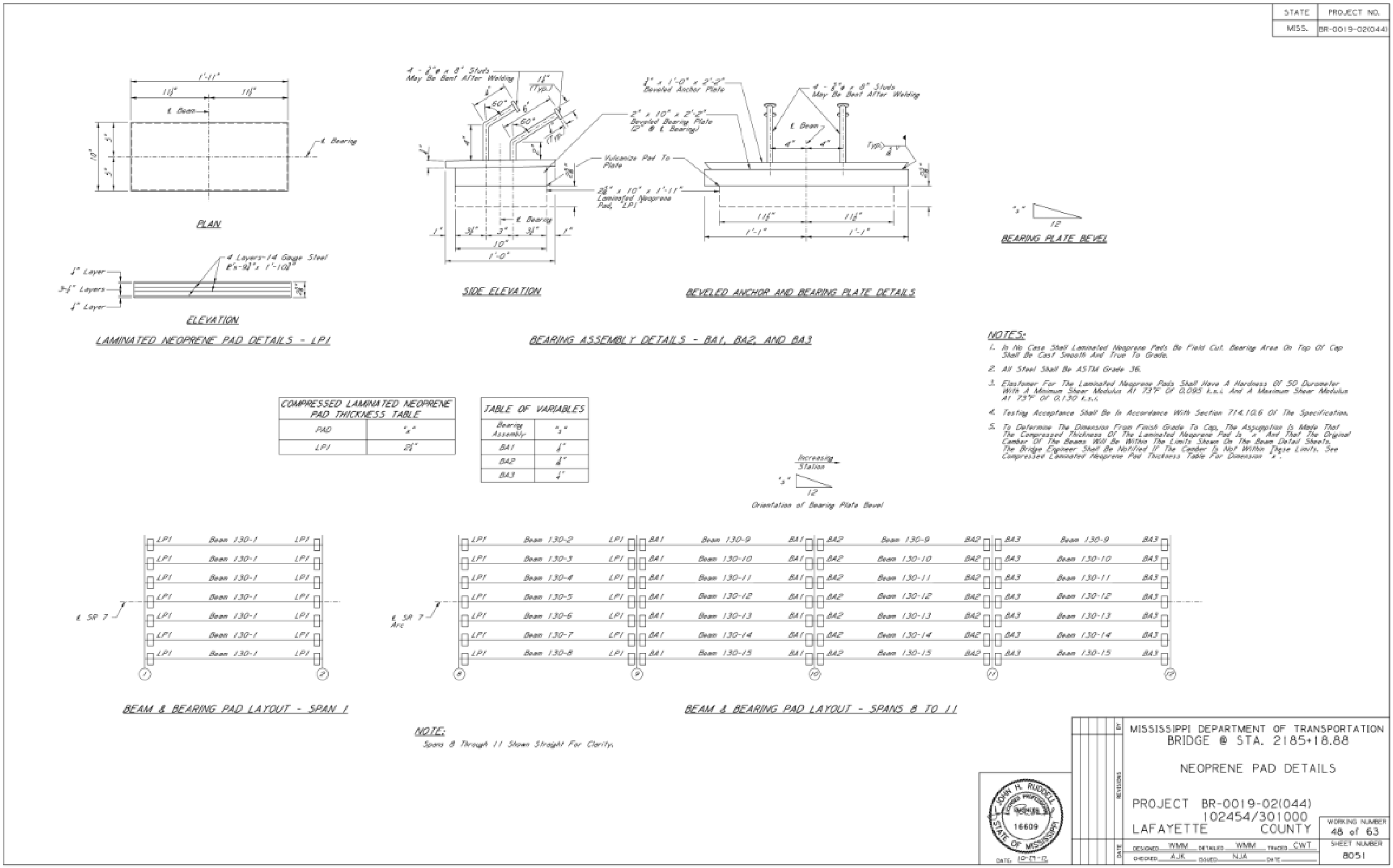

Image A 15: Neoprene pad details

1st O.REV.

SPECIAL NOTES ON STRUCTURAL BEARING SYSTEM

DESIGN:

Scope Of Work: This Work Shall Consist Of Furnishing Multi-Rotational, High Load Disc Bearings And Installing Disc Bearing Assemblies At The Locations Shown On The Plans In Accordance With These Specifications And The AASHTO LRFD Bridge Design And Construction Specifications. Bearing Assemblies Shall Include Disc Bearing Device, Sole And Masonry Plates, Neoprene Pads, And Anchor Bolts & Connection Hardware. Disc Bearings Shall Consist Of A Polyether Urethane Structural Element (Disc) Confined By Upper And Lower Steel Bearing Plates. The Bearing Shall Be Equipped With A Shear Resisting Mechanism, And/Or Positive Location Device To Prevent Lateral Movement Of The Disc. Bearings Shall Adequately Provide For The Thermal Expansion And Contraction, Rotation, Camber Changes, And Creep And Shrinkage Of Structural Members, Where Applicable. Disc Bearings Shall Be Supplied As Fixed Bearings And Guided Expansion (Unidirectional) Bearings As Designated In The Plans.

Qualified Suppliers: The Following Suppliers Have Displayed The Capability Of Supplying Disc Bearings With Characteristics That Conform To The General Requirements Of These Contract Specifications.

(1) R.J. Watson, Inc.
11035 Walden Ave.
Alden, NY 14004
Telephone: 716-901-7020
Fax: 716-901-7015

(2) The D.S. Brown Company
300 East Cherry Street
North Baltimore, OH 45872
Telephone: 419-257-3561
Fax: 419-257-2200

The Contractor Should Note That He/She Is Not Limited To Sourcing The Disc Bearings From The Above Suppliers As Long As The Alternate Supplier Meets The Qualification Requirements.

Qualification Requirements: Disc Bearings And The Bearing Supplier Shall Be Subject To The Following Qualification Requirements For Acceptance. Disc Bearings Shall Be Designed, Fabricated, Tested, And Installed In Accordance With AASHTO LRFD Bridge Design Specifications 5th Edition, Section 14, And AASHTO LRFD Bridge Construction Specifications 3rd Edition, Section 18. Disc Bearings Shall Be Designed To Resist All Loads Presented In The Table Under "BEARING ASSEMBLY DATA AND DESIGN REQUIREMENTS". The Supplier Shall Show Previous History In The Design And Fabrication Of Disc Bearings. Documentation Showing A Minimum Of Five Years Experience And Five Bridge Installations Within The Last Five Years Shall Be Provided To The Engineer. Sliding Bearings Shall Be Stiff In Shear (i.e. Negligible Shear Displacements Shall Occur Within The Vertical Load Support Element).

Shop Drawings: The Contractor Shall Submit Drawings To The Engineer For Approval, And Shall Have Received Said Approval Prior To The Construction Of The Beam Seats And Fabrication Of Disc Bearings. These Drawings Shall Include, But Not Be Limited To, The Following Information.

(1) Plan And Elevation Of Each Disc Bearing Size
(2) Complete Details And Sections Showing All Materials (With ASTM Or Other Designations) Incorporated In The Disc Bearings.
(3) Vertical And Horizontal Load Capacities.
(4) All Bearing Connection Details.
(5) Design Calculations Verifying Compliance With AASHTO LRFD Standards.

The Shop Drawings And Design Calculations Shall Be Sealed By A Mississippi Registered Professional Engineer Employed By The Bearing Supplier With At Least 5 Years Of Documented History Of Disc Bearing Design Experience.

CONSTRUCTION:

All Materials Shall Be New And Unused, With No Reclaimed Material Incorporated In The Finished Bearing.

The Physical Properties Of The Polyether Urethane Elements Shall Conform To AASHTO LRFD Bridge Construction Specifications, Table 18.3.2.8-1.

All Steel Plates Except Stainless Steel Components Of The Bearing Shall Conform To The Requirements Of The Type Of Steel Designated On The Contract Plans.

Stainless Steel Shall Conform To The Requirements Of ASTM A240 Type 304. Higher Grades Of Stainless Are Permissible. Stainless Steel In Contact With PTFE Shall Be Polished To A No. 8 Bright Mirror Finish. The Minimum Thickness Of Stainless Steel Sheet Shall Be 16 Gage.

Polytetrafluoroethylene (PTFE) Sheet Shall Be Manufactured From Pure Virgin (Not Reprocessed) PTFE Resin. PTFE Sheet Shall Meet The Applicable Material Requirements Of AASHTO LRFD Bridge Construction Specifications, Section 18.8.2.

Elastomeric Rotational Element Shall Be Molded As A Single Piece. Separate Layers Are Not Allowed.

Fabrication Details: The Contractor Shall Provide The Engineer With Written Notification 60 Days Prior To The Start Of Bearing Fabrication. This Notification Shall Include All Of The Information Required For Qualification And Shop Drawings. The Bearing Fabricator Shall Be Certified By The American Institute Of Steel Construction (AISC) For Simple Steel Bridges Category. All Steel Surfaces Exposed To The Atmosphere, Except Stainless Steel Surfaces, Shall Be Cleaned In Accordance With Section 14 Of The Standard Specifications And Special Provision No. 907-810, Structural Steel. Stainless Steel Sheet Shall Be Attached To Its Steel Substrate With A Continuous Seal Weld. All Welding Shall Conform To, And All Welders Shall Be Qualified In Accordance With, The Requirements Of The American Welding Society (AWS). Except As Noted, All Bearing Fabrication Tolerances Shall Be In Accordance With AASHTO LRFD Bridge Construction Specifications, Table 18.1.4.2-1. Every Bearing Shall Have An Individual Bearing Serial Number Indelibly Marked With Ink. After Assembly, Including Sole Plates And Masonry Plates As Applicable, Bearing Components Shall Be Held Together With Steel Strapping Or Other Means To Prevent Disassembly Until The Time Of Installation.

Production Bearing Sampling And Testing: Production Bearing Sampling And Testing Shall Be Performed In Accordance With AASHTO LRFD Bridge Construction Specifications, Section 18.3.4. The Long-Term Deterioration Test Per AASHTO LRFD Bridge Construction Specifications, Section 18.1.5.2.7 Shall Be Satisfied By Pre-Qualification Unless Otherwise Specified In The Contract Plans. Each Bearing Shall Be Visually Examined Both During And After Testing. Any Resultant Defects, Such As Bond Failure, Physical Destruction Or Cold Flow Of PTFE To The Point Of Debonding, Shall Be Cause For Rejection. Defects Such As Permanently Extruded Or Severely Deformed Elastomer Or Cracked Steel Shall Also Be Cause For Rejection. Minor Deformations In The Elastomer Are Allowed.

INSTALLATION:

Bearings Delivered To The Bridge Site Shall Be Stored Under Cover On A Platform Above The Ground Surface. Bearings Shall Be Protected At All Times From Damage. When Placed, Bearings Shall Be Dry, Clean, And Free From Dirt, Oil, Grease, Or Other Foreign Substances.

Bearing Devices Shall Not Be Disassembled Unless Otherwise Permitted By The Engineer Or Manufacturer.

Bearings Shall Be Installed In Accordance With The Alignment Plan And Installation Scheme As Shown In The Contract Plans. Upon Final Installation Of The Bearings, The Engineer Shall Inspect The Bearing Components To Assure That They Are Level And Parallel To Within 0.0311 Inch Per One Foot. Any Deviations In Excess Of The Allowed Tolerances Shall Be Corrected.

Bearings Assemblies Shall Be Handled By Their Bottom Surfaces Only, Unless Specially Designed Lifting Brackets Are Used. Do Not Lift Bearings By Their Tops, Sides And/Or Shipping Bands. Lifting Brackets Shall Be Approved By The Bearing Supplier Prior To Use.

Caution Shall Be Taken To Ensure That The Steel Temperature Directly Adjacent To The Polyether Urethane Rotational Element Does Not Exceed 225°F. The Polyether Urethane Disc Must Not Be Exposed To Direct Flame Or Sparks.

CERTIFICATE OF COMPLIANCE:

In Addition To Records Of Test Results, The Contractor's Disc Bearing Supplier Shall Submit Certificates Of Compliance For The Disc Bearings Indicating The Materials, Fabrication, Testing, And Installation Are As Specified Herein.

PAYMENT:

All Bearings, Including Sole Plates, Masonry Plates, Neoprene Pads, And Anchor Bolts & Anchorage Hardware, Shall Be Paid For Under Pay Item "Disc Bearing Device", Each.

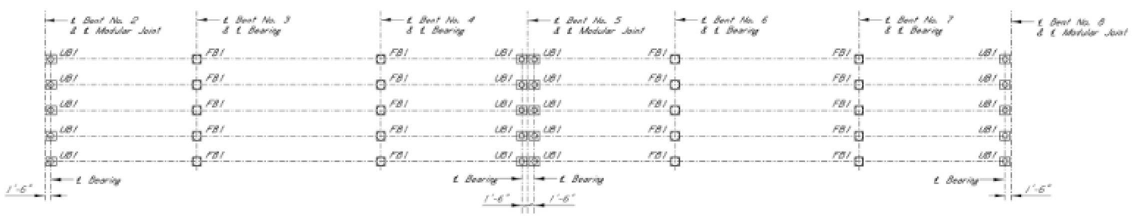

BEARING LAYOUT

Governed By The Maximum Design Coefficient Of Friction = 0.150 Multiplied By The Design Vertical Load From The Applicable Load Combination. (4)

STATE	PROJECT NO.
MISS.	BR-0019-02(044)

BEARING ASSEMBLY DATA AND DESIGN REQUIREMENTS

			Unidirectional Bearing (UB1)	Fixed Bearing (FB1)
Quantity			20	20
Location			Bent Nos. 2 (U.S.), 5, & 8 (D.S.)	Bent Nos. 3, 4, 6 & 7
SERVICE Limit State (Max)	Vertical Load	Dead	146 k	512 k
		Live (w/o IM)	117 k	255 k
		Total	263 k	767 k
	Uplift Load		N/A	N/A
	Horizontal Load	Max. Longitudinal	39 k (4)	156 k
		Concurrent Trans.	8 k	6 k
		Max. Transverse	39 k (1)	115 k (1)
		Concurrent Long.	0 k	0 k
STRENGTH Limit State (Max Factored)	Vertical Load	Dead	182 k	640 k
		Live (w/o IM)	205 k	447 k
		Total	387 k	1087 k
	Uplift Load		N/A	N/A
	Horizontal Load	Max. Longitudinal	58 k (4)	115 k (1)
		Concurrent Trans.	0 k	0 k
		Max. Transverse	39 k (1)	115 k (1)
		Concurrent Long.	0 k	0 k
	Rotation (+/-)	Due To Live Load (w/o Impact)	0.0054 rad (3)	0.0040 rad (3)
		Due To Fab. & Const. Tolerances	0.0050 rad	0.0050 rad
		Total	0.0104 rad	0.0090 rad
	Movement (+/-)	Longitudinal	2.85 in. (2)	0.00 in.
		Transverse	0.00 in.	0.00 in.
EXTREME EVENT Limit State (Max Factored)	Vertical Load	Dead	182 k	640 k
		Live (w/o IM)	0 k	0 k
		Total	182 k	640 k
	Uplift Load		N/A	N/A
	Horizontal Load	Max. Longitudinal	39 k (1)	224 k
		Concurrent Trans.	0 k	93 k
		Max. Transverse	147 k	364 k
		Concurrent Long.	27 k (4)	41 k
	Movement (+/-)	Longitudinal	5.22 in.	0.00 in.
		Transverse	0.00 in.	0.00 in.

(1) Governed By AASHTO LRFD 14.7.8.4 - Shear Resisting Mechanism Shall Be Capable Of Resisting A Horizontal Force In Any Direction Equal To A Minimum Of 15% Of The Design Vertical Load At The Service Limit State.

(2) Value Represents 65% Of The Total Design Thermal Movement Range And Includes An LRFD Load Factor Of 1.2.

(3) Beveled Sole Plate Is Used To Account For The Proposed Grade. Rotation Due To Dead Load Is Negligible.

MISSISSIPPI DEPARTMENT OF TRANSPORTATION
BRIDGE @ STA. 2185+18.88

DISC BEARING DETAILS

PROJECT BR-0019-02(044)
102454/301000
LAFAYETTE COUNTY

JOHN H. RUDDELL
16609
STATE OF MISSISSIPPI
DATE: 12-2-11

WORKING NUMBER 61 of 63
SHEET NUMBER 8064

DESIGNED ABH DETAILED ABH TRACED ABH
CHECKED RLW ISSUED NJA DATE

Image A 16: Bearings locations, assembly, and design data

A1.5. Barrier and Railing Details

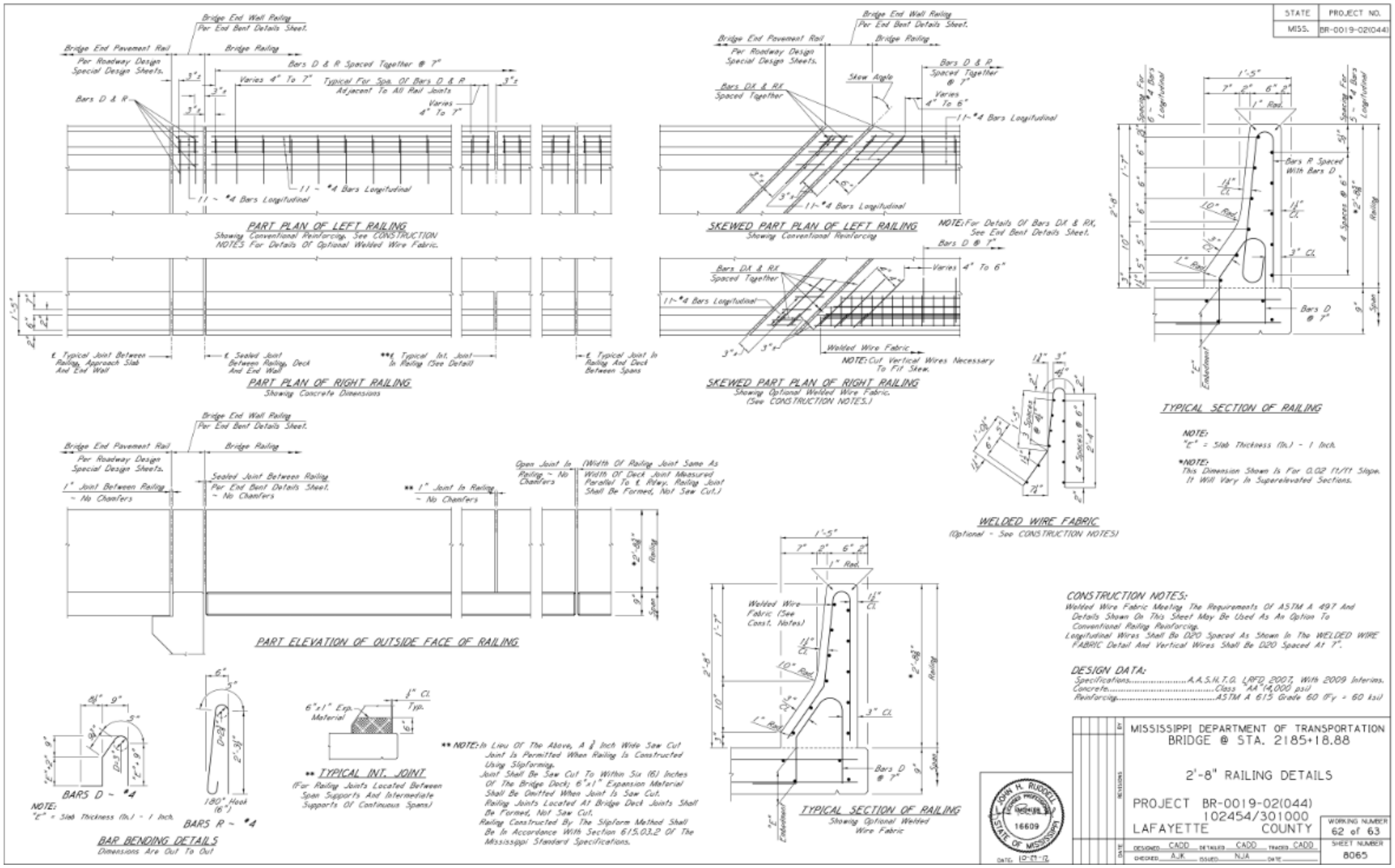

Image A 17: Barrier details

A2. Annotated Excel and MatLab Calculations

Crossframe "A"									
Number	Unit Wt								
6	490								
	pcf								
Elements	Numbers	Dimensions							
		Length	Width	Thickness	Area	Volume	Linear Wt	Wt/ele	Total Wt
		in	in	in	in^2	in^3	lb/ft	lb	lb
Gusset Plates I	5.00	18.00	16.00	0.50	288.00	144		40.83	204.1667
Gusset Plates II	4.00	22.00	7.00	0.50	154.00	77		21.83	87.33796
Gusset Plates III	4.00	10.00	10.00	0.50	100.00	50		14.18	56.71296
W12x40	2.00	106.00					40	353.33	706.6667
L5x5x1/2	4.00	88.00		0.50			16.2	118.80	475.2
WT5x15	2.00	115.00					15	143.75	287.5
P5/8x8	4.00	102.00		0.63			8	68.00	272
									2089.584
Holes not deducted/bolts not added									
Total Weight=	12.54	kip							

Crossframe "B1"									
Number	Unit Wt								
18	490								
	pcf								
Elements	Numbers	Dimensions							
		Length	Width	Thickness	Area	Volume	Linear Wt	Wt/ele	Total Wt
		in	in	in	in^2	in^3	lb/ft	lb	lb
Gusset Plates I	8.00	18.00	16.00	0.50	288.00	144		40.83	326.67
Gusset Plates II	2.00	10.00	7.00	0.50	70.00	35		9.92	19.85
L5x5x1/2	4.00	88.00		0.50			16.2	118.80	475.20
WT5x15	4.00	99.00					15	123.75	495.00
P5/8x8	4.00	102.00		0.63			8	68.00	272.00
									1588.72
Holes not deducted/bolts not added									
Total Weight=	28.60	kip							

Crossframe "B2"									
Number	Unit Wt								
14	490								
	pcf								
Elements	Numbers	Dimensions							
		Length	Width	Thickness	Area	Volume	Linear Wt	Wt/ele	Total Wt
		in	in	in	in^2	in^3	lb/ft	lb	lb
Gusset Plates I	8.00	23.00	25.00	0.50	575.00	287.5		81.52	652.20
Gusset Plates II	4.00	8.00	10.00	0.50	80.00	40		11.34	45.37
WT7x37	4.00	106.25					37	327.62	1310.47
WT5x15	4.00	87.00					15	108.75	435.00
P1-1/4x11-5/8	5.00	102.00		1.25			11.625	98.81	494.06
									2937.10
Holes not deducted/bolts not added									
Total Weight=	41.12	kip							

Crossframe "C"									
Number	Unit Wt								
1	490								
	pcf								
Elements	Numbers			Dimensions				Weight	
		Length	Width	Thickness	Area	Volume	Linear Wt	Wt/ele	Total Wt
		in	in	in	in^2	in^3	lb/ft	lb	lb
Gusset Plates I	5.00	18.00	16.00	0.50	288.00	144		40.83	204.1667
Gusset Plates II	4.00	22.00	7.00	0.50	154.00	77		21.83	87.33796
Gusset Plates III	4.00	10.00	10.00	0.50	100.00	50		14.18	56.71296
W12x53	2.00	106.00					53	468.17	936.3333
L5x5x1/2	4.00	83.50		0.50			16.2	112.73	450.9
WT5x15	2.00	115.00					15	143.75	287.5
P1-1/4x11-5/8	4.00	102.00		1.25			11.625	98.81	395.25
									2418.201
Holes not deducted/bolts not added									
Total Weight=	2.42	kip							

Image A 18: Weight calculations from cross-frames

Lateral Bracings					
Element	Numbers	Unit Wt	Length	Total Wt	
WT8x33.5	44	33.5	22.3	32850.51	32.85
		lb/ft	ft	lb	kip

"Girders"													
Length	Web		Bottom Flange		Top Flange		CS Area		Volume	Unit wt	Total Wt		
	width	depth	width	depth	width	depth							
ft	in	in	in	in	in	in	in^2	ft^2	ft^3	pcf	lb	kip	plf
780	0.6875	102	24	1.5	24	1.25	136.125	0.945313	737.3438	490	361298.4	361.30	463.20
Weight of	5	girders is	1806.5	kips.									
			903.25	tonnes.									

"Barriers"									
Number	Length	CS Area		Volume	Unit wt	Wt/barrier	Wt/side	Total wt	Linear wt
37	20	281.33	1.954	39.07	150	5861.1	216.86	433.72	293.1
	ft	in^2	ft^2	ft^3	pcf	lb	kip	kip	plf
Longitudinal Reinforcement									
#bar	d_b	As	In CS	Volume/side	Unit Wt	Wt/barrier		Wt/side	
11	0.5	0.19635	2.16	19179.42	490	147.0	7.35	5.44	
	in	in^2	in^2	in^3	pcf	lb	plf	kip	
Bar R (#4 @ 7")									
Length CS	Spacing	#/barrier	Vol/barrier	Vol/side	Wt/barrier		Wt/side		
68.46	7	35	470.48	10.07	133.41	6.67	4.94		
in	in		in^2	ft^3	lb	plf	kip		
Bar D included in slab wt									
Total weight of Barriers (both sides)									
454.47	614.2	plf							
kip	454.47	kip							

Image A 19: Weight calculations from lateral bracings, girders, and barriers

Deck																
	Slab thickness	Width	Length	Volume	Unit wt	Weight										
	0.708	46.83	780.000	25875.42	150	3881313	**3881.313**	4.98								
	ft	ft	ft	ft^3	pcf	lb	kip	klf								
	Reinforcement		Unit wt	490	pcf											
									Total Length	Area		Volume	Wt		Total Wt	
					240 ft				ft	in^2	ft^2	ft^3	lb	kip		
Top	#4 bars	5747.25	3349.00	3349.00	3238.50	3238.50	2839.00	2697.33	24458.58	0.1963	0.001364	33.35022	16341.61	16.34		
	#6					47.58	42.58	40.00	6508.33	0.4418	0.003068	19.96732	9783.985	9.78		
	n#6					50.00	50.00	50.00								
Bottom	#5 bars	59.17	33.42	33.42	32.17	32.17	42.17	38.67	271.17	0.3068	0.002131	0.577728	283.0869	0.28		
									31238.08		0.006562	53.89526	26408.68	**26.41**	52.82	
					150 ft											
Top	#4 bars	2697.33	2839.00	3238.50	3238.50	3349.00			15362.33	0.1963	0.001364	20.94713	10264.09	10.26		
	#6	40.00	42.58	47.58					6508.33	0.4418	0.003068	19.96732	9783.985	9.78		
	n#6	50.00	50.00	50.00												
Bottom	#5 bars	39.67	42.17	32.17	32.17	33.42			179.58	0.3068	0.002131	0.382607	187.4777	0.19		
									22050.25			41.29706	20235.56	**20.24**	40.47	
															93.29	kips

Columns											
Concrete											
Length	Diameter	Area	Volume	Unit Wt	Total Wt						
ft	ft	ft	ft^3	pcf	lb	kip	klf				
21.5	6	28.27	607.90	150	91184.73	**91.18**	**4.24**				
Reinforcement		Unit Weight	490	pcf							
Longitudinal Bar											
Designation	Number	Length	Total Leng	d_b	Area		Volume	Wt			
		ft	ft	in	in^2	ft^2	ft^3	lb	kip		
#11	40	29.5	1180.00	1.375	1.484893	0.010312	12.16788	5962.3	**6.0**		
Spiral											
	H	p	n	C	Length	d_b (#6)	Area		Volume	Wt	
	ft	in		ft	ft	in	in^2	ft^2	ft^3	lb	kip
Bar CF	8	3	32	18.85	610.78	0.75	0.441786	0.003068	1.8738	918.18	0.92
Bar CM	13	3	52	18.85	992.51	0.75	0.441786	0.003068	3.0450	1492.05	1.49
Bar CB	8.5	3	34	18.85	648.95	0.75	0.441786	0.003068	1.9910	975.57	0.98
									Total	3385.80	**3.39**

Image A 20: Weight calculations from deck and columns

Pier Cap									
Concrete									
Length	Width	Depth	Volume	Unit Wt	Total Wt				
ft	ft	ft	ft^3	pcf	lb	kip	klf		
46	7	8	2576	150	386400	386.4	8.4		
Reinforcement		Unit Wt							
		490	pcf						
Designation	Number	Length	Total Length	d_b	Area		Volume	Wt	
		ft	ft	in	in^2	ft^2	ft^3	lb	kip
#4	12	9.5	114.00	0.5	0.19635	0.001364	0.155443	76.2	0.076167
#10	12	45.333	544.00	1.25	1.227185	0.008522	4.636031	2271.7	2.271655
#6	22	45.667	1004.67	0.75	0.441786	0.003068	3.082279	1510.3	1.510317
#10	12	45.667	548.00	1.25	1.227185	0.008522	4.670119	2288.4	2.288358
#10	12	45.667	548.00	0.75	0.441786	0.003068	1.681243	823.8	0.823809
A1(#6)	10	25.167	251.67	0.75	0.441786	0.003068	0.772104	378.3	0.378331
C1(#5)	5	28.667	143.33	0.625	0.306796	0.002131	0.305376	149.6	0.149634
A2(#6)	12	20.500	246.00	0.75	0.441786	0.003068	0.754719	369.8	0.369812
A3(#6)	12	21.667	260.00	0.75	0.441786	0.003068	0.79767	390.9	0.390858
A1(#6)	11	25.167	276.83	0.75	0.441786	0.003068	0.849314	416.2	0.416164
A2(#6)	12	20.500	246.00	0.75	0.441786	0.003068	0.754719	369.8	0.369812
A3(#6)	12	21.667	260.00	0.75	0.441786	0.003068	0.79767	390.9	0.390858
C1(#5)	5	28.667	143.33	0.625	0.306796	0.002131	0.305376	149.6	0.149634
A1(#6)	10	25.167	251.67	0.75	0.441786	0.003068	0.772104	378.3	0.378331
E1(#5)	12	17.333	208.00	0.625	0.306796	0.002131	0.44315	217.1	0.217144
H1(#5)	12	19.083	229.00	0.625	0.306796	0.002131	0.487891	239.1	0.239067
D1(#5)	22	17.083	375.83	0.625	0.306796	0.002131	0.800724	392.4	0.392355
								10812.3	10.81231
							plf	235.05	
							klf	0.24	

Image A 21: Weight calculations from pier cap

Weight Distribution		
	780	270

1 Exterior Girder	kip	kip	klf (A-A)
Slab	3881.31	200.21	4.28
Slab Steel "240"	26.41	1.97	0.04
Slab Steel "150"	20.24	1.51	0.03
Barrier Concrete/side	216.86	75.07	1.60
Barrier Steel/side	10.37	3.59	0.08
Girder	361.30	125.06	2.67
Crossframe A	12.54	4.34	0.09
Crossframe B1	28.60	9.90	0.21
Crossframe B2	41.12	14.23	0.30
Crossframe C	2.42	0.84	0.02
Lateral Bracings	32.85	11.37	0.24
	Total	**448.09**	**9.57**

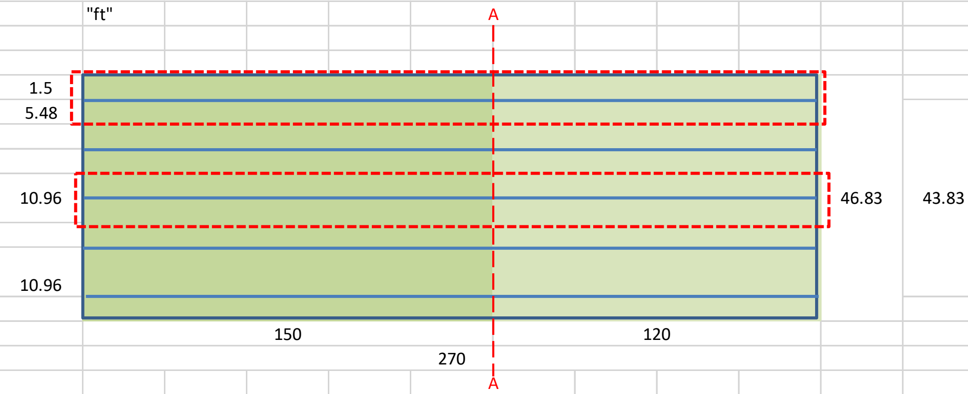

1 Interior Girder	kip	klf (A-A)
Slab	314.37	6.71
Slab Steel "240"	3.09	0.07
Slab Steel "150"	2.37	0.05
Girder	125.06	2.67
Crossframe A	4.34	0.09
Crossframe B1	9.90	0.21
Crossframe B2	14.23	0.30
Crossframe C	0.84	0.02
Lateral Bracings	11.37	0.24
Total	**485.57**	**10.37**

Image A 22: Weight distribution in 270 ft long span supported by pier 7

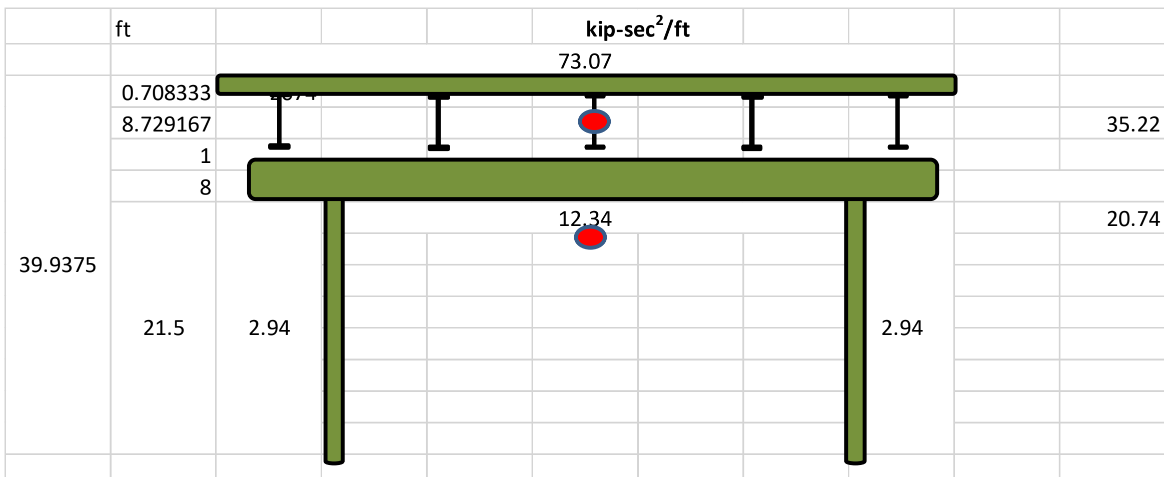

Image A 23: Mass distribution in the transverse direction

				t_r						
G	L	W	1st	2nd	3rd	total		Δ_{max}	Q_d1	Q_d2
ksi	in	in	in	in	in	in		5.22	39	115
0.175	23	10	0.25	3.5	0.25	4		in	kip	kip
K_H=	10.0625	k/in								
K_eff=	50.3125	k/in	(parallel)							
F_max	**K_d**	**K_u**	Δ_y	**F_y**						
262.63	42.84	428.41	0.10	43.33						
kip	kip/in	kip/in	in	kip						
FB										
G	D	t_r	A							
ksi	in	in	in^2							
0.175	30	6.25	706.8583							
K_H=	19.79	k/in								
K_eff=	98.96	k/in								
F_max	**K_d**	**K_u**	Δ_y	**F_y**						
516.57	76.93	769.30	0.17	127.78						
kip	kip/in	kip/in	in	kip						

Image A 24: Calculations for bearings stiffness

ft	ft	in^4	in^4	ksi	k/in	k/in

Image A 25: Calculations for column stiffness

beta	theta	b_v	d_v	f'c	A_v	s	fy
2	45	72	66	4000	0.44	3	60
		in	in	psi	in^2	in	ksi
V_c	V_s						
18.99	580.8						
kip	kip						
V_n	V_n	M_n					
599.79	4752	8846.966					
kip	kip						

Image A 26: Shear and moment calculations based on AASHTO C5.8.2.9

MatLab Code for solving 2DOF mass-spring system:

```
clc;
clear all;
%Enter M and K
M1=18.22/12; %Unit: k-s^2/in
M2=73.07/12;
K1=3322.98; %Unit: k/in
K2=98.96;
%Mass and Stiffness matrices
M=[M1 0;
   0 M2];
K=[K1+K2 -K2;
   -K2 K2];
fprintf('The Mass Matrix is\n')
disp(M)
fprintf('The Stiffness Matrix is\n')
disp(K)
%Eigenvalue and eigenvector calculations
[v,d]=eig(K,M);
w=sqrt(d);
%natural frequency and time period
fprintf('The natural frequencies are (rad/s)\n')
w1=w(1,1);
w2=w(2,2);
disp([w1;w2])
fprintf('The natural time period are (s)\n')
T1=(2*pi)/w(1,1);
T2=(2*pi)/w(2,2);
disp([T1;T2])
 %normalization of mode shape vectors
for i=1:2
   v(:,i)=v(:,i)/v(2,i);
end
 %Modal shape Matrix
fprintf('The normalized modal matrix is \n')
disp(v);
 %Mode shapes plots
H=[0;248.88;422.64];
for i=1:2
   subplot(1,2,i)
   plot([0;v(:,i)],H);
   ylabel('Location of center of masses (in)','FontSize',12);
   title(['Mode Shape',num2str(i)],'FontSize',18)
end
```

A3. Seismic Design Data and Tools

3/23/2021 U.S. Seismic Design Maps

Little Tallahatchie River Bridge

Latitude, Longitude: 34.54319835, -89.49178712

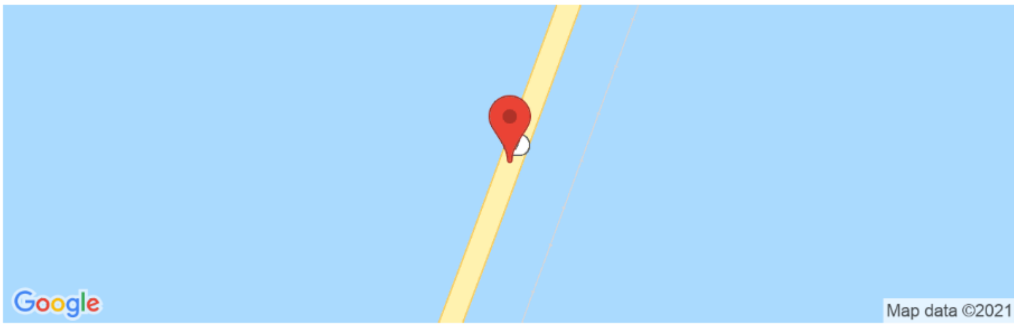

Date	3/23/2021, 10:32:26 AM
Design Code Reference Document	ASCE7-16
Risk Category	II
Site Class	D - Default (See Section 11.4.3)

Type	Value	Description
S_S	0.465	MCE_R ground motion. (for 0.2 second period)
S_1	0.194	MCE_R ground motion. (for 1.0s period)
S_{MS}	0.664	Site-modified spectral acceleration value
S_{M1}	0.429	Site-modified spectral acceleration value
S_{DS}	0.443	Numeric seismic design value at 0.2 second SA
S_{D1}	0.286	Numeric seismic design value at 1.0 second SA

Type	Value	Description
SDC	D	Seismic design category
F_a	1.428	Site amplification factor at 0.2 second
F_v	2.213	Site amplification factor at 1.0 second
PGA	0.246	MCE_G peak ground acceleration
F_{PGA}	1.354	Site amplification factor at PGA
PGA_M	0.333	Site modified peak ground acceleration
T_L	12	Long-period transition period in seconds
SsRT	0.465	Probabilistic risk-targeted ground motion. (0.2 second)
SsUH	0.536	Factored uniform-hazard (2% probability of exceedance in 50 years) spectral acceleration
SsD	1.5	Factored deterministic acceleration value. (0.2 second)
S1RT	0.194	Probabilistic risk-targeted ground motion. (1.0 second)
S1UH	0.224	Factored uniform-hazard (2% probability of exceedance in 50 years) spectral acceleration.
S1D	0.6	Factored deterministic acceleration value. (1.0 second)
PGAd	0.5	Factored deterministic acceleration value. (Peak Ground Acceleration)
C_{RS}	0.869	Mapped value of the risk coefficient at short periods
C_{R1}	0.864	Mapped value of the risk coefficient at a period of 1 s

https://seismicmaps.org 1/2

Image A27: Seismic design parameters obtained from ASCE 7-16 Hazard tool

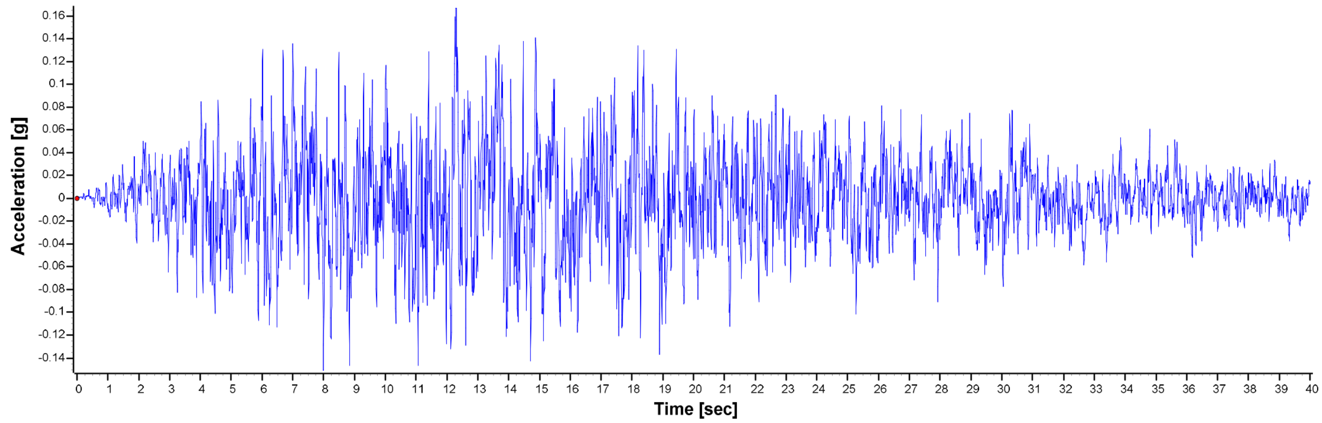

Image A 28: Time history in transverse direction scaled for the location of MS7 Bridge (PGA 0.246g)

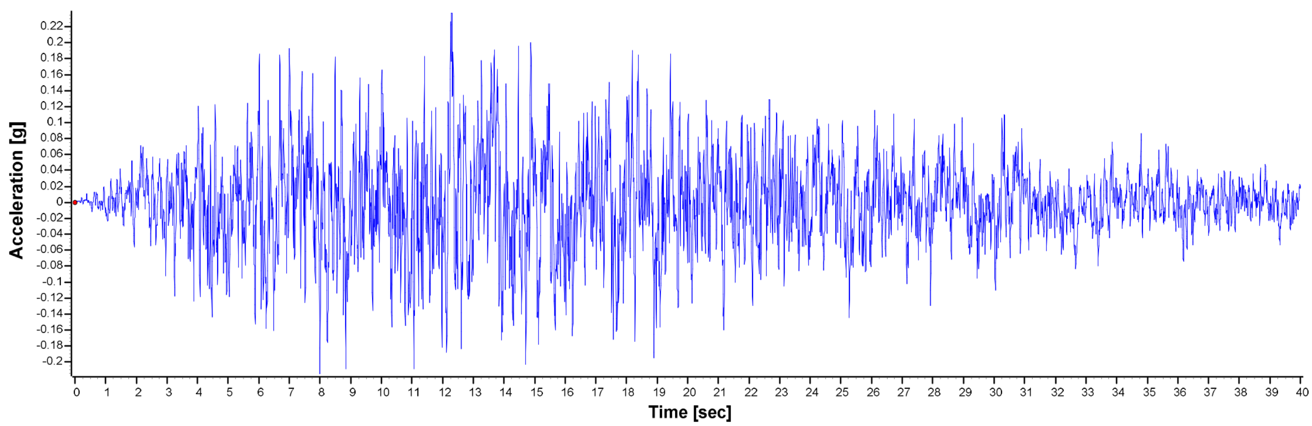

Image A 29: Time history at the location of Goodman Rd Bridge (PGA 0.35g)

A4. AASHTO Provisions

Table 9: Soil Profiles for seismic analysis (AASHTO Table 3.10.3.1-1)

Type	Description
A	Hard rock (F_{pga}, F_a, *and* F_v are less than one, 0.8 is typical)
B	Rock (the base case upon which the spectral acceleration require no site adjustment; F_{pga}, F_a, *and* F_v are equal to one)
C	Dense soil and rock (F_{pga}, F_a, *and* F_v are greater than one)
D	Stiff soil
E	10 ft or more of soft clay
F	Very loose soil (peat, highly plastic, etc.) These require a detailed site investigation.

Table 10: Operational Classification of bridges (AASHTO A3.10.5, C3.10.5)

Operational Category	Description
Critical bridges	Must remain open to all traffic after the design earthquake (1000-year return period event) and open to emergency vehicles after a large earthquake (2500-year return period event).
Essential bridges	Must be open to emergency vehicles after the design earthquake.
Other bridges	May be closed for repair after a large earthquake.

Table 11: Seismic Performance Zone based upon AASHTO Table 3.10.6-1

Acceleration Coefficient	Seismic Zone
$S_{D1} \leq 0.15$	1
$0.15 < S_{D1} \leq 0.30$	2
$0.30 < S_{D1} \leq 0.50$	3
$0.50 < S_{D1}$	4

Table 12: Response Modification Factors—Substructures (AASHTO Table 3.10.7.1-1)

	Operational Category		
Substructure	Other	Essential	Critical
Wall-type piers—larger dimension	2.0	1.5	1.5
Reinforced concrete pile bents			
(a) Vertical piles only	3.0	2.0	1.5
(b) One or more batter piles	2.0	1.5	1.5
Single columns	3.0	2.0	1.5
Steel or composite steel and concrete pile bents			
(a) Vertical piles only	5.0	3.5	1.5
(b) One or more batter piles	3.0	2.0	1.5
Multiple column bents	5.0	3.5	1.5

Table 13: Minimum Analysis Requirements for Seismic Effects (AASHTO Table 4.7.4.3.1)

		Multispan Bridges					
		Other Bridges		Essential Bridges		Critical Bridges	
Seismic Zone	Single-Span Bridges	Regular	Irregular	Regular	Irregular	Regular	Irregular
1	None[a]	None	None	None	None	None	None
2	None	SM/UL[b]	SM	SM/UL	MM	MM	MM
3	None	SM/UL	MM[c]	MM	MM	MM	TH
4	None	SM/UL	MM	MM	MM	TH[d]	TH

[a]None = no seismic analysis is required.
[b]SM/UL = single-mode or uniform-load elastic method.
[c]MM = multimode elastic method.
[d]TH = time–history method.

The Load and Resistance Factor Design (LRFD) approach accounts for the variability in the loads on structure (Q) and the resistance (R) offered by the structure. The statistically determined load factors (γ) and resistance factors (ϕ) are used in the inequality equation to ensure that the effect of the load is smaller than the total resistance.

$$\phi R_n \geq effect\ of\ \sum \gamma_i Q_i$$

$$Where, \phi \leq 1.0\ and\ \gamma \geq 1.0$$

All the design limit states are expected to satisfy the following load and resistance inequality,

$$\sum \eta_i \gamma_i Q_i \leq \phi R_n$$

$$Where, \eta_i\ is\ load\ modification\ factor$$

The load modifier factor (η_i) incorporates the ductility factor (η_D), redundancy factor (η_R), and operational importance factor (η_I). The ductility and redundancy factor are related to the strength of the bridge and the operational importance factor relates to the consequences after the damage to the bridge.

For γ_i maximum, $\quad \eta_i = \eta_D \eta_R \eta_I \geq 0.95$

For γ_i minimum, $\quad \eta_i = 1/\eta_D \eta_R \eta_I \leq 1.0$

The prescribed values of ϕ, η_I, η_R & η_D is 1.0 for all the non-strength limit-states.

Table 14: Load Combinations and Load Factors (AASHTO -Table 3.4.1-1)

Load Combination Limit State	*DC DD DW EH EV ES EL PS CR SH*	*LL IM CE BR PL LS*	*WA*	*WS*	*WL*	*FR*	*TU*	*TG*	*SE*	Use One of These at a Time *EQ*	*BL*	*IC*	*CT*	*CV*
Strength I (unless noted)	γ_p	1.75	1.00	—	—	1.00	0.50/1.20	γ_{TG}	γ_{SE}	—	—	—	—	—
Strength II	γ_p	1.35	1.00	—	—	1.00	0.50/1.20	γ_{TG}	γ_{SE}	—	—	—	—	—
Strength III	γ_p	—	1.00	1.40	—	1.00	0.50/1.20	γ_{TG}	γ_{SE}	—	—	—	—	—
Strength IV	γ_p	—	1.00	—	—	1.00	0.50/1.20	—	—	—	—	—	—	—
Strength V	γ_p	1.35	1.00	0.40	1.0	1.00	0.50/1.20	γ_{TG}	γ_{SE}	—	—	—	—	—
Extreme Event I	γ_p	γEQ	1.00	—	—	1.00	—	—	—	1.00	—	—	—	—
Extreme Event II	γ_p	0.50	1.00	—	—	1.00	—	—	—	—	1.00	1.00	1.00	1.00
Service I	1.00	1.00	1.00	0.30	1.0	1.00	1.00/1.20	γ_{TG}	γ_{SE}	—	—	—	—	—
Service II	1.00	1.30	1.00	—	—	1.00	1.00/1.20	—	—	—	—	—	—	—
Service III	1.00	0.80	1.00	—	—	1.00	1.00/1.20	γ_{TG}	γ_{SE}	—	—	—	—	—
Service IV	1.00	—	1.00	0.70	—	1.00	1.00/1.20	—	1.0	—	—	—	—	—
Fatigue I—*LL*, *IM* & *CE* only	—	1.50	—	—	—	—	—	—	—	—	—	—	—	—
Fatigue II—*LL*, *IM* & *CE* only	—	0.75	—	—	—	—	—	—	—	—	—	—	—	—

For circular members, such as reinforced concrete columns or prestressed concrete piles, d_v can be determined from Eq. C5.8.2.9-1 provided that M_n is calculated ignoring the effects of axial load and that the reinforcement areas, A_s and A_{ps}, are taken as the reinforcement in one-half of the section. Alternatively, d_v can be taken as $0.9d_e$, where:

$$d_e = \frac{D}{2} + \frac{D_r}{\pi} \qquad \text{(C5.8.2.9-2)}$$

where:

D = external diameter of the circular member (in.)
D_r = diameter of the circle passing through the centers of the longitudinal reinforcement (in.)

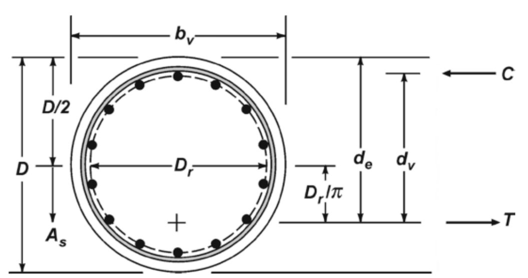

Figure C5.8.2.9-2—Illustration of Terms b_v, d_v, and d_e for Circular Sections

Circular members usually have the longitudinal reinforcement uniformly distributed around the perimeter of the section. When the member cracks, the highest shear stresses typically occur near the middepth of the section. This is also true when the section is not cracked. It is for this reason that the effective web width can be taken as the diameter of the section.

Image A 30: AASHTO provisions to determine effective dimensions of circular sections

A5. SAP2000: Models and Output

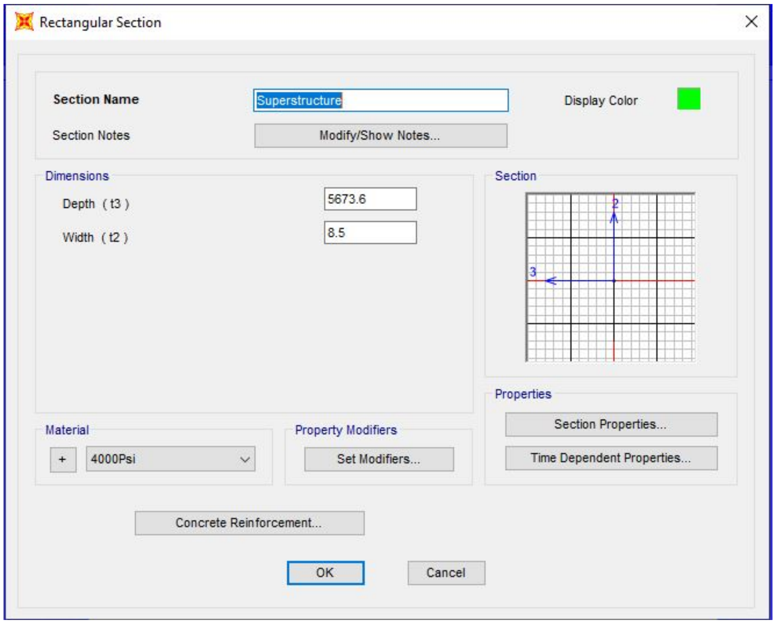

Image A 31: Rectangular section defined for the superstructure to represent total weight

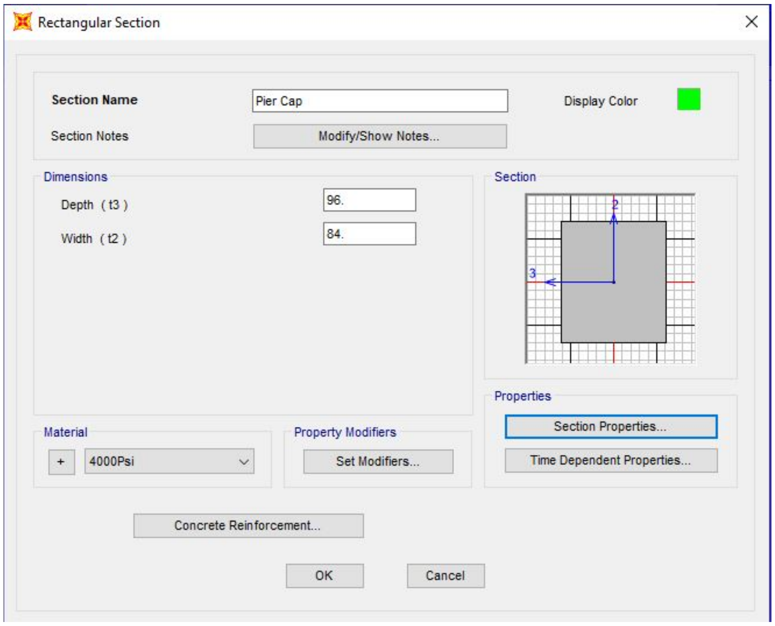

Image A 32: Cross-section defined for pier cap

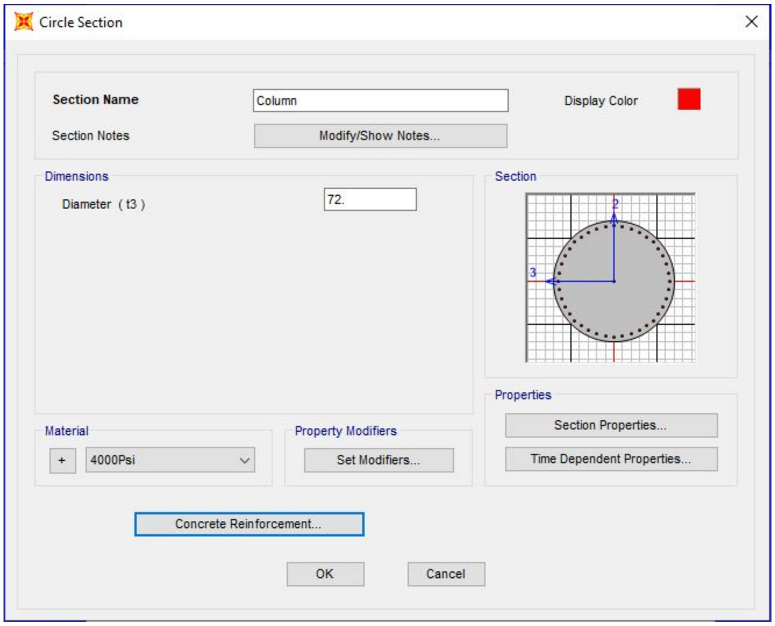

Image A 33: Circular cross-section including major defined for columns

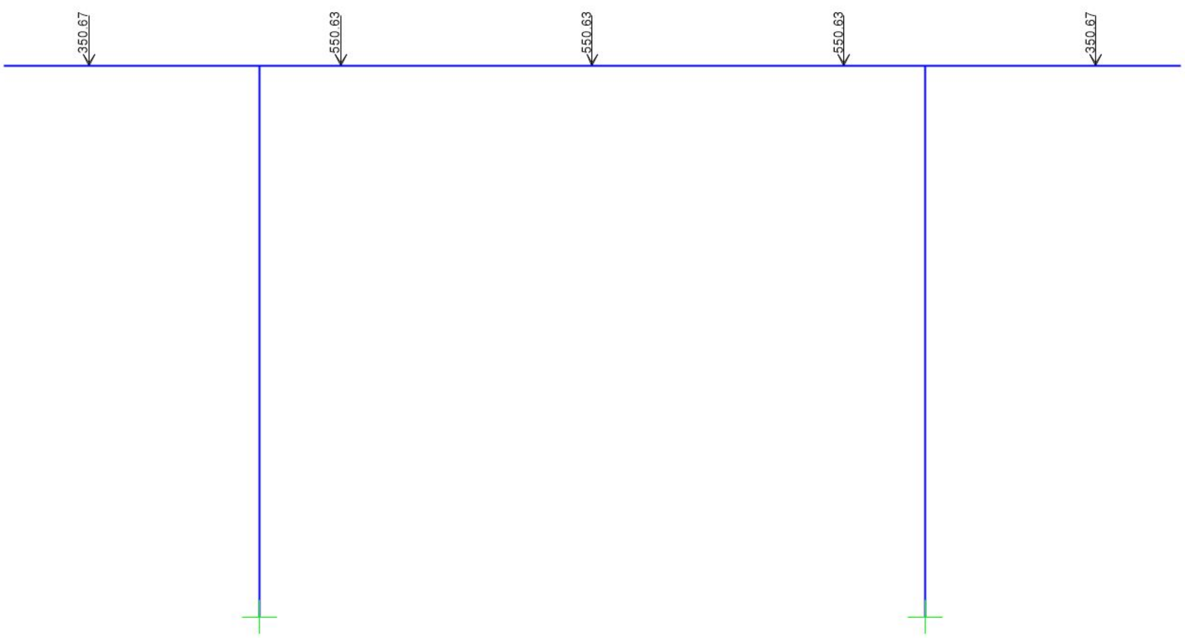

Image A 34: The load from superstructure applied at the location of bearings in the fixed two-column frame

Pushover Analysis

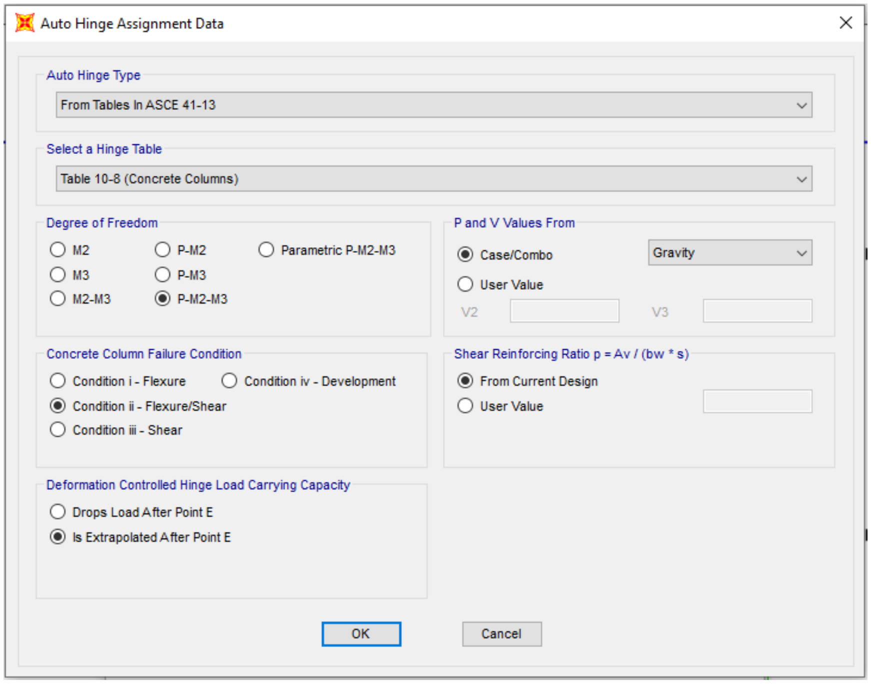

Image A 35: Hinges definition and assignment

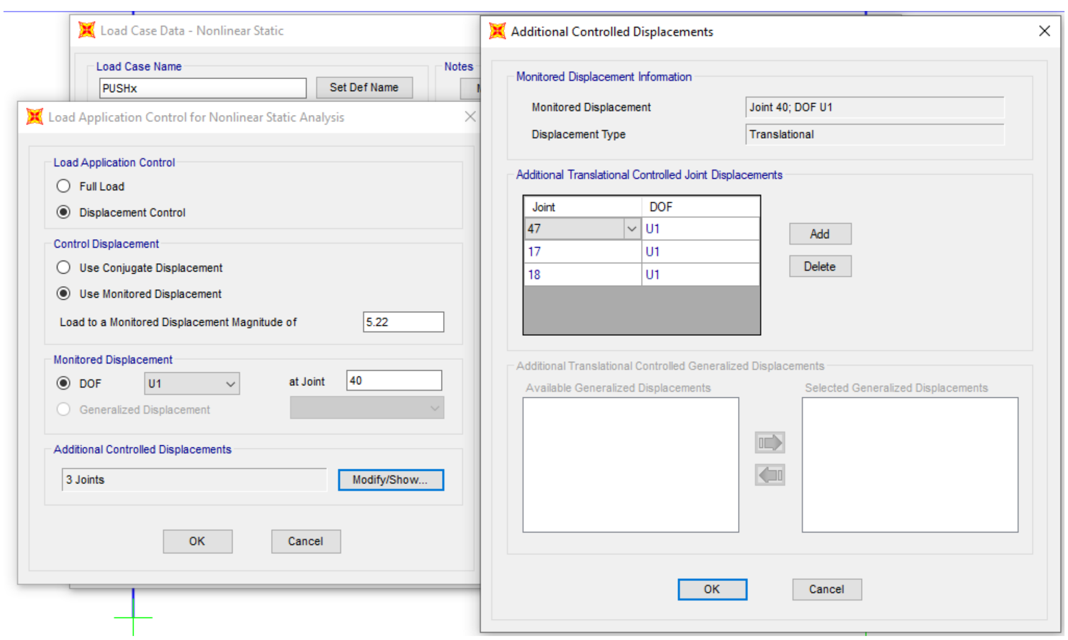

Image A 36: Displacement controlled load case set up for pushover analysis

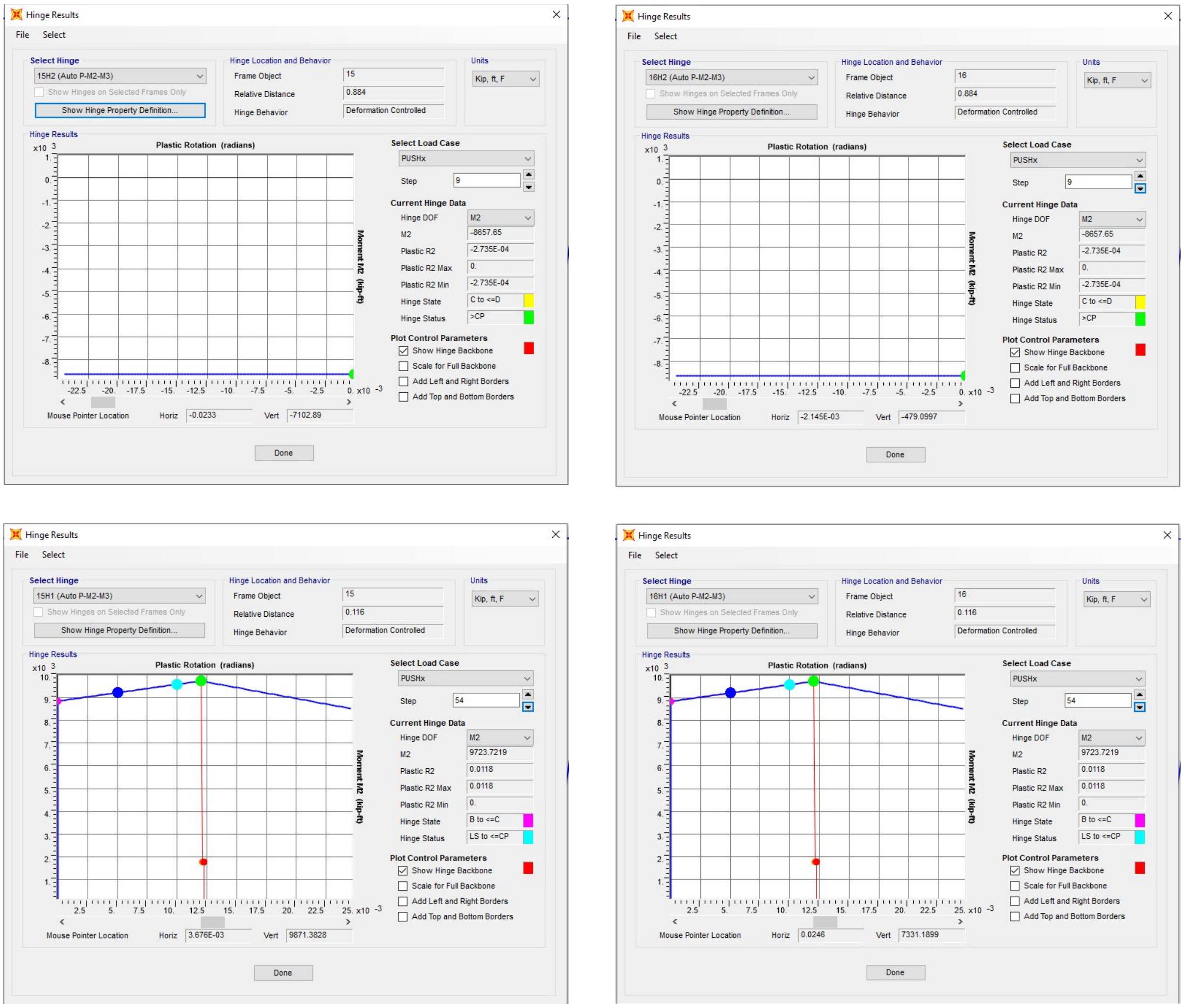

Image A 37: Hinges data and results at fully plastic hinge state (Step 54) of pushover analysis

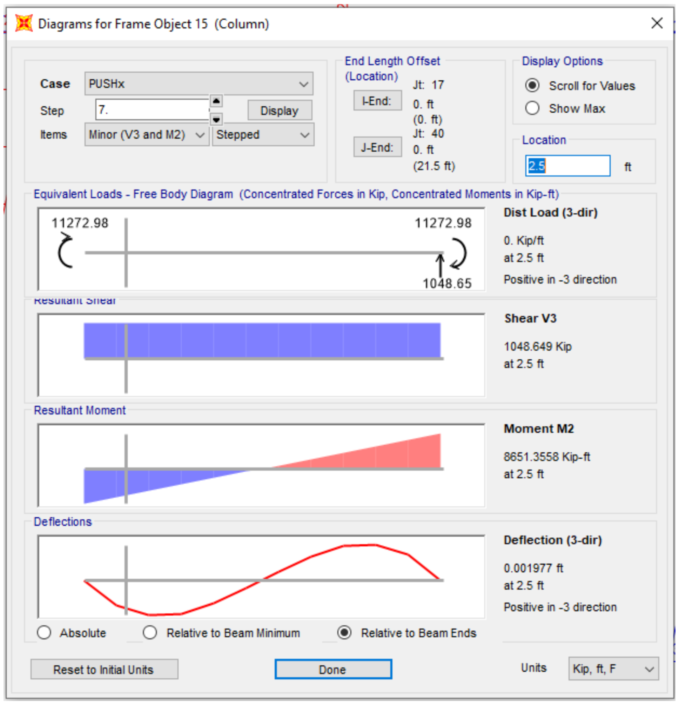

Image A 38: Shear, moment, and deflection at the beginning of hinge formation in the right column

Time History

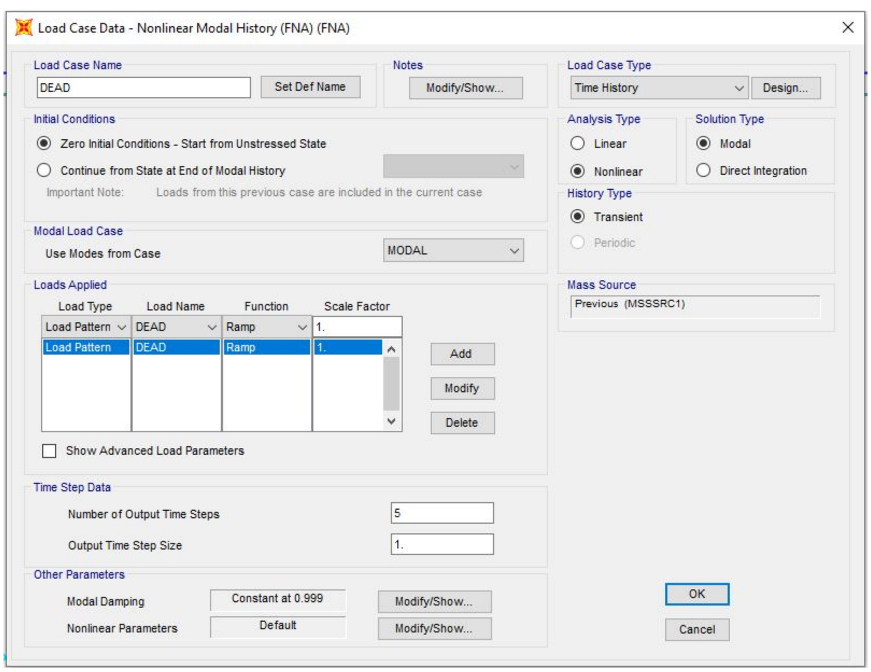

Image A 39: Non-linear dead load pattern defined for time history analyses

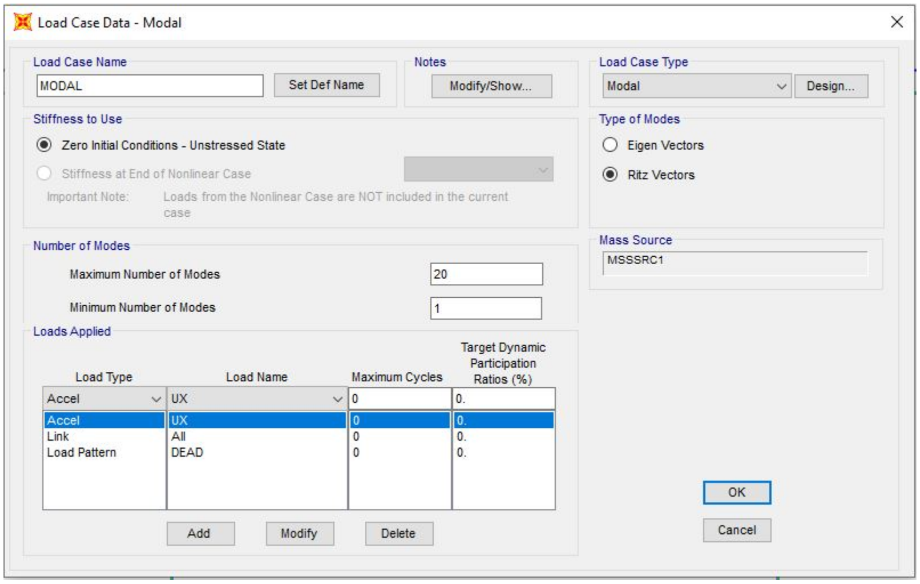

Image A 40: Modal load case defined for time history analyses

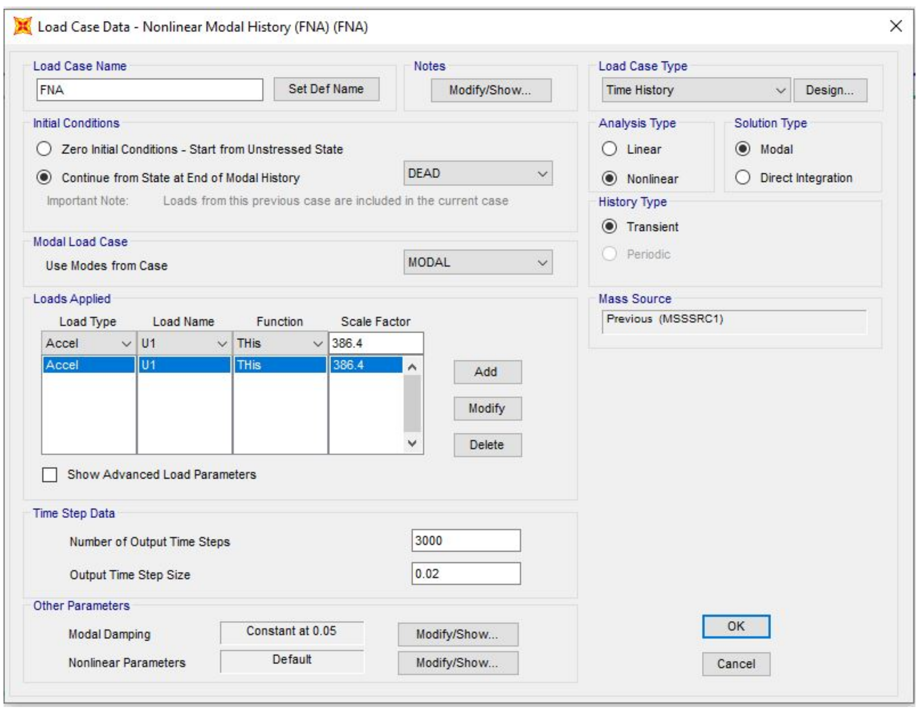

Image A 41: Non-linear time-history load case defined after dead load case

VITA

Hemant Raj Joshi, born and raised in Nepal, came to University of Mississippi to pursue Bachelor of Science in Civil Engineering in Department of Civil Engineering. He was the recipient of the Outstanding Senior Leadership Award. After completing his undergraduate, he continued his Master in Engineering Science with emphasis on Civil Engineering. During his master study, he researched on effectiveness of seismic bearings. After graduating from OleMiss, he is planning to gain some professional job experience in pursuit of becoming a professional engineer (PE).